UNIVERSITÀ DEGLI STUDI DI MILANO

Scuola di Dottorato in Fisica, Astrofisica e Fisica Applicata
Dipartimento di Fisica

Corso di Dottorato in Fisica, Astrofisica e Fisica Applicata
Ciclo XXXVII

On the control of open quantum batteries

Settore Scientifico Disciplinare FIS/03

Supervisore: Professor Marco G. GENONI

Coordinatore: Professor Aniello MENNELLA

Tesi di Dottorato di:
Daniele MORRONE

Anno Accademico 2023-2024

Commission of the final examination:

External Referee:
Prof. Giuliano BENENTI (Università degli Studi dell'Insubria, Italy)
Prof. Dario FERRARO (Università degli Studi di Genova, Italy)

External Member:
Prof. Giuliano BENENTI (Università degli Studi dell'Insubria, Italy)
Prof. Dario FERRARO (Università degli Studi di Genova, Italy)
Dr. Giacomo GUARNIERI (Università degli Studi di Pavia, Italy)

Internal Member:
Prof. Marco G. GENONI (Università degli Studi di Milano, Italy)

Final examination:

Date 14/03/2025

Università degli Studi di Milano, Dipartimento di Fisica, Milano, Italy

Cover illustration:

-

Internal illustrations:

Daniele MORRONE

Design:

Daniele MORRONE

MIUR subjects:

FIS/03 -

PACS:

03.67.-a
03.65.Yz
05.70.Ln

List of Publications

As of December 2024

Materials discussed in this thesis

Refereed publications

1. Daniele Morrone, Matteo A. C. Rossi, Andrea Smirne, and Marco G. Genoni. Charging a quantum battery in a non-Markovian environment: A collisional model approach. *Quantum Science and Technology*, 8(3):035007, May 2023
2. Daniele Morrone, Matteo A.C. Rossi, and Marco G. Genoni. Daemonic ergotropy in continuously monitored open quantum batteries. *Physical Review Applied*, 20(4):044073, October 2023

Publications in preparation

1. Daniele Morrone, Francesco Albarelli, Vittorio Giovannetti, and Marco G. Genoni. Daemonic work extraction via qnd-energy measurement. in preparation

Other materials

Refereed publications

1. 1 Daniele Morrone, N. Walter Talarico, Marco Cattaneo, and Matteo A. C. Rossi. Estimating Molecular Thermal Averages with the Quantum Equation of Motion and Informationally Complete Measurements. *Entropy*, 26(9):722, September 2024

Contents

List of Figures

Introduction

Motivation

Quantum batteries are a novel quantum technology designed to exploit quantum mechanical phenomena with the aim to outperform their classical counterpart. Classical thermal devices, with a history spanning centuries, have seen continuous innovation and theoretical development, driving their performance ever closer to their theoretical bounds. Batteries, as devices for storing work for later use, originated in the 19th century, with Alessandro Volta's pioneering work. Since then, battery technology has evolved through significant innovations, including lithium-ion technology and solid-state batteries.

In contrast, quantum batteries are a relatively new concept, with foundational studies emerging only in the past decade. While it remains uncertain whether scalable, competitive quantum batteries can be realized, the quantum scale offers both remarkable opportunities and significant challenges. The pursuit of quantum computing exemplifies this duality, with decades of effort leading to the current Noisy Intermediate Scale Quantum (NISQ) era. At this scale, noise and thermal fluctuations introduce errors but also highlight the potential for quantum computers to outperform classical ones in certain tasks through quantum specific algorithms. Quantum batteries may follow a similar trajectory, as their limitations and opportunities are carefully examined.

Research on quantum batteries focuses on addressing this two aspect brought by the quantum scale, by following two key directions. The first aims to identify scenarios where quantum effects improve performance and to determine optimal designs for leveraging these effects. The second addresses the challenges posed by noise, quantum fluctuations, and dissipation, which impact practical implementation. This thesis aspires to contribute to this growing body of knowledge by studying memory effects in dissipative quantum dynamics and developing active control techniques using quantum measurements to optimize work extraction protocols.

Thesis overview

This thesis is organized as follows:

Chapter 1: Introduction to the modern postulates of quantum mechanics
We set the stage by reviewing the fundamentals of quantum mechanics, starting from a modern formulation of its postulates and their role in establishing the mathematical framework of open quantum systems.

Chapter 2: Open Quantum systems
We present the theory of open quantum systems, describing how the interaction between a quantum system and its environment affect its dynamics. This chapter introduce the formalism of master equations and stochastic master equations for systems under continuous environmental measurement.

Chapter 3: Quantum batteries and work extraction from quantum systems
We provide a characterization of the process of extracting work from a quantum system consistent with the laws of thermodynamics and the framework of quantum mechanics. Moreover, Landauer's limit set the stage for configuring measurement as a thermodynamic process able to perform work at a certain cost. We characterize the role of measurement in this framework both in term of enhancement to the work extraction, and its energetic cost.

Chapter 4: Charging a quantum battery in a non-Markovian environment: a collisional model approach
We leverage a class of model known as collisional model to describe the interaction between a quantum battery and a non-Markovian environment. We provide evidence regarding the role of non-Markovianity in influencing the charging dynamics of quantum batteries.

Chapter 5: Daemonic ergotropy in continuously-monitored open quantum batteries.
The daemonic ergotropy is the working definition of maximum work extractable on average under the effect of a quantum measurement. We extend the definition of daemonic ergotropy to continuously-monitored open quantum systems, and provide boundaries condition to its minimum and maximum value. We analyze our result on a paradigmatic model of qubit quantum battery.

Chapter 6: Daemonic work extraction via non-ideal QND-energy measurment
We characterize the maximum extractable work via either unitary operations and thermal operations through a non-ideal QND-energy measurement. We characterize the energy cost of such protocol and describe the work gained from the protocol in terms of its cost and a cost-free variation. We provide evidence that under certain conditions, this variation can be positive.

CHAPTER 1

Introduction to the modern postulates of quantum mechanics

In this chapter, we review the fundamental tools of quantum mechanics, introduce its postulates, and establish the notation that will be used in later sections.

Quantum mechanics is intrinsically a mathematical framework designed to describe the inherent probabilistic nature of quantum systems. The building blocks for the theory are its postulates, that encode the necessary assumption required to be able to predict the behaviour of quantum systems.

Throughout this chapter, we will follow a modern characterization of quantum mechanics [6, 7], that will provide a minimal set of tools necessary for the discussions and analyses present in the rest of this thesis. For a more comprehensive and rigorous treatment of quantum mechanics we refer to [7, 8, 9].

The chapter is organized as follows: in Sec. 1.1 , we discuss the postulates of quantum mechanics in its standard formulation, which provide an exact description on the behaviour of closed quantum systems.

In Sec. 1.2, we discuss the most suitable tools to describe interacting or open systems.

In Sec. 1.3, we discuss the reason why the concepts introduced in the previous section do not constitute a new set of postulates and how open system can be thought as a part of a global closed system.

1.1 Closed quantum systems

1.1.1 States

As introduced, quantum mechanics is intrinsically probabilistic. This means that even when a system is prepared in a fully known state, the outcomes of experiments carry some degree of uncertainty. Consequently, the properties of a quantum system cannot all be deterministically known simultaneously, even if its state is deterministically known. Furthermore, the state itself may represent either a deterministic preparation (a pure state) or a statistical ensemble of possibilities (a mixed state). The first postulate of quantum mechanics defines the mathematical framework for describing these states.

The state of a quantum system is fully characterized by a unit vector in a separable Hilbert space $\mathcal{H}$. A Hilbert space is a vector space over the complex field $\mathbb{C}$, equipped with a scalar product satisfying the property

$$\langle \beta\psi | \alpha\phi \rangle = \beta^\star \alpha \langle \psi | \phi \rangle, \quad \forall |\psi\rangle, |\phi\rangle \in \mathcal{H}, \ \forall \alpha, \beta \in \mathbb{C}, \tag{1.1}$$

and is complete with respect to the norm induced by the scalar product. Separable means that $\mathcal{H}$ has a countable orthonormal basis.

Formally, a quantum state is not represented by a single vector in $\mathcal{H}$, but by a ray, an equivalence class of vectors that differ by a global phase factor. The term vector is commonly used to refer to its associated ray, and this convention will be followed throughout the thesis.

To describe closed systems, pure states expressed in terms of vector on a Hilbert space are enough, so the classical formulation of the first postulates it is done in terms of vector. However, it is useful to introduce the generalization to mixed state before discussing the other postulates. To generalize, we can describe quantum states using the density operator ρ, a more versatile mathematical object capable of representing both pure and mixed states.

To rigorously define the density operator, we introduce some preliminary concepts. The operators of interest in quantum mechanics are linear and bounded maps on $\mathcal{H}$, $\hat{A} : \mathcal{H} \to \mathcal{H}$. Operators that are also trace-class satisfy the condition

$$\mathrm{Tr}[\hat{A}] = \sum_j \langle e_j|\hat{A}|e_j\rangle < \infty, \tag{1.2}$$

where the sum is taken over the vectors $|e_j\rangle$ that form a complete orthonormal basis. The density operator ρ is a trace-class operator that represents a quantum state. It has the following properties:

- **Positivity**: $\rho \geq 0$, meaning all its eigenvalues are non-negative.
- **Normalization**: $\mathrm{Tr}[\rho] = 1$.
- **Purity**: $\mathrm{Tr}[\rho^2] \leq 1$.

When $\mathrm{Tr}[\rho^2] = 1$, the state is pure, and ρ reduces to a rank-1 projector (i.e., all eigenvalues are zero except for one). The quantity $\mathrm{Tr}[\rho^2]$, is called the purity of the state, and can be used to distinguish between pure ($\mathrm{Tr}[\rho^2] = 1$) and mixed states ($\mathrm{Tr}[\rho^2] < 1$). It is bounded as $\frac{1}{d} \leq \mathrm{Tr}\left[\rho^2\right] \leq 1$, where d is the dimension of the Hilbert space. the upper bound is satisfied for pure states and the lower bound is satisfied for the maximally mixed state $\rho = \frac{1}{d}\mathbb{I}_d$.

1.1.2 Dynamics

The second postulate of quantum mechanics describes how quantum states evolve, specifically addressing the dynamics of closed systems. In the most general formulation, it prescribes that the evolution of states for closed system is obtained by applying a unitary operator to the states:

$$|\psi'\rangle = \hat{U}|\psi\rangle, \tag{1.3}$$

or equivalently

$$\rho' = \hat{U}\rho\hat{U}^\dagger. \tag{1.4}$$

To be unitary, an operator has to satisfy $\hat{U}\hat{U}^\dagger = \mathbb{I}$, with $\hat{U}^\dagger$ being the adjoint of $\hat{U}$. [1] This formulation refrains from making assumptions about the full dynamical behavior of the system, providing only a prescription for relating the states of the system at two

[1] The adjoint of an operator $\hat{A}$ is the unique operator defined by $\langle\psi|\hat{A}\phi\rangle = \langle\hat{A}^\dagger\psi|\phi\rangle, \quad \forall|\psi\rangle, |\phi\rangle \in \mathcal{H}$.

specific points in time. For a more complete description of the dynamics, the postulate can be recast in differential form, where the states evolves according to the Schrodinger equation when written as a vector

$$i\hbar\frac{\mathrm{d}}{\mathrm{d}t}|\psi(t)\rangle = \hat{H}(t)|\psi(t)\rangle \tag{1.5}$$

and the Von Neumann equation when written as a density operator

$$i\hbar\frac{\mathrm{d}}{\mathrm{d}t}\rho(t) = \left[\hat{H}(t), \rho(t)\right]. \tag{1.6}$$

In the equations above

- $\hbar$ is the reduced Planck constant
- $\hat{H}$ is the operator acting as the generator of the dynamics. It is an Hermitian operator ($\hat{H} = \hat{H}^\dagger$) known as the Hamiltonian.
- $[\hat{A}, \hat{B}]$ is the commutator between the operator $\hat{A}$ and $\hat{B}$, defined as $[\hat{A}, \hat{B}] = \hat{A}\hat{B} - \hat{B}\hat{A}$.

For simplicity, we will adopt natural units throughout this thesis, setting $\hbar = 1$.

1.1.3 Measurement

The third postulate of quantum mechanics defines the process of measurement. In quantum mechanics, there are two fundamental aspects of the measurement process: the statistical distribution of outcomes and the effect of the measurement on the quantum state. Within the mathematical framework established by the postulates, measurements are associated with a collection of operators $\{\hat{M}_n\}$, where the index n denotes the possible measurement outcomes.

The most common type of measurement, which describes the effect of measurements on closed quantum systems, is the Projection-Valued Measure (PVM). In a PVM, the operators associated with the measure are projection operators $\hat{M}_n = \hat{P}_n$. These projectors satisfy the following properties:

- $\hat{P}_n\hat{P}_m = \delta_{n,m}\hat{P}_n$, ensuring that the operators $\hat{P}_n$ are idempotent and orthogonal.
- $\sum_k \hat{P}_k = \mathbb{I}$, indicating that the projectors form a resolution of the identity and span the Hilbert space, a requirement for attributing statistical meaning to measurement outcomes.

The measurement of a physical quantity is associated with a particular set of PVM projectors encoded in a Hermitian operator, called the observable. The observable $\hat{O}$ admits a spectral decomposition $\hat{O} = \sum_i o_i\hat{P}_i$, where the eigenvalues o_i represent a possible measurement outcomes and are guaranteed to be real due to the Hermiticity condition $\hat{O} = \hat{O}^\dagger$. In this formalism, each measurement outcome is associated with a real number o_i and a projection operator $\hat{P}_i$. These two elements allow us to describe both aspects of the measurement process.

When measuring the observable $\hat{O}$ on a system in a pure state $|\psi\rangle$, the probability of obtaining the outcome o_i is given by

$$p_i = \langle\psi|\hat{P}_i|\psi\rangle, \tag{1.7}$$

and the post-measurement state of the system is described by

$$|\psi_i\rangle = \frac{\hat{P}_i|\psi\rangle}{\sqrt{p_i}}, \tag{1.8}$$

where the denominator ensures proper normalization of the state.

If the state of the system is mixed and represented by a density operator ρ, these relations can be recast as:

$$p_i = \mathrm{Tr}\left[\rho\hat{P}_i\right], \tag{1.9}$$

$$\rho_i = \frac{\hat{P}_i\rho\hat{P}_i}{p_i}. \tag{1.10}$$

1.2 Composite quantum systems

In the previous sections we introduced the postulates of quantum mechanics, which provides the mathematical framework for describing closed quantum system. In this section we generalize the framework to describe composite quantum systems. We will separately address the three elements at the core of the postulates: states, dynamics and measurement.

1.2.1 Quantum states

Mixed states, introduced earlier in the context of state preparation, can also emerge naturally from the dynamics of interacting systems. While pure states (described by vectors) are commonly associated with closed-system dynamics, in the context of interacting systems density operators are used almost exclusively.

For two interacting quantum systems, each with its own Hilbert space $\mathcal{H}_A$,$\mathcal{H}_B$, the space of the composite system is described by their tensor product $\mathcal{H}_{AB} = \mathcal{H}_A \otimes \mathcal{H}_B$. The overall system's state ρ_{AB} lives in this composite space, and the reduced state of the subsystem A can be retrieved via the partial trace of the subsystem B as $\rho_A = \mathrm{Tr}_B\left[\rho_{AB}\right] = \sum_i \langle e_i|\rho_{AB}|e_i\rangle$, where the vectors $|e_i\rangle$ form a basis on $\mathcal{H}_B$. If the two subsystem are uncorrelated, the composite state factorize to $\rho_{AB} = \rho_A \otimes \rho_B$.

1.2.2 Dynamics

The dynamics of interacting systems are described by Completely Positive Trace-Preserving (CPTP) maps, rather than unitary operators. A CPTP map $\mathcal{E}$ must fulfill the following conditions:

- linearity: $\mathcal{E}[\sum_i p_i\rho_i] = \sum_i p_i\mathcal{E}[\rho_i]$
- completely positive: any extended map $\mathcal{E} \otimes \mathcal{I}_B$ must be positive on any extended space $\mathcal{H} \otimes \mathcal{H}_B$

- trace preserving: $\mathrm{Tr}\left[\mathcal{E}[\rho]\right] = \mathrm{Tr}\left[\rho\right]$.

CPTP map can be also written in Kraus form:

$$\mathcal{E}[\rho] = \sum_k \hat{K}_k \rho \hat{K}_k^\dagger \tag{1.11}$$

where the $\{\hat{K}_k\}$ are a set of operator satisfying the relation $\sum_k \hat{K}_k^\dagger \hat{K}_k = \mathbb{I}$. These properties are necessary to preserve the statistical interpretation of the density operator, and in particular the property of complete positivity help preserve the statistical interpretation for the density operator on a larger Hilbert space.

1.2.3 Measurements

For measurements, Positive Operator-Valued Measures (POVMs) generalize Projection-Valued Measures (PVMs). A POVM is a collection of positive operators $\{\hat{E}_n\}$ satisfying $\sum_n \hat{E}_n = \mathbb{I}$, without the restriction of being projectors.

To describe a post measurement state, it is also necessary to define a set of operators known as instruments satisfying the relation $\hat{E}_n = \hat{M}_n^\dagger \hat{M}_n$. It is evident that such set of operators are not unique for a given POVM. The post-measurement state when performing a given POVM depends on the way the POVM is applied, and different realization leads to different post measurement-states even when the outcome is the same. This degree of freedom is encoded in the freedom of choice for the set of operators that realize the POVM.

The probabilities of outcomes and the resulting post-measurement states are given by:

$$p_i = \mathrm{Tr}\left[\rho \hat{E}_i\right], \tag{1.12}$$

$$\rho_i = \frac{\hat{M}_i \rho \hat{M}_i^\dagger}{p_i}. \tag{1.13}$$

1.3 Global closed system

Mathematical tools such as POVM and CPTP maps do not constitute new postulates of quantum mechanics, nor are extension to the previous ones, but arise naturally from the existing postulates. By extending the Hilbert space of an interacting system as necessary, it is always possible to obtain a global system which is closed. In particular:

- It is always possible to find a "purification" for a mixed state: Given a system $\mathcal{H}_A$ in a mixed state ρ_A, then it is always possible to find a space $\mathcal{H}_B$ and a pure state $|\psi\rangle \in \mathcal{H}_A \otimes \mathcal{H}_B$ such that $\rho_A = \mathrm{Tr}_B\left[|\psi\rangle\langle\psi|\right]$. The vector $|\psi\rangle$ is called a purification of ρ_A

- Stinespring's dilation theorem affirm that if a system dynamics is described through a CPTP maps, then it is always possible to find an extension to its Hilbert space such that the dynamics of the composite system is unitary. To formalize, the effect of any CPTP map acting on a space $\mathcal{H}_A$ on a state ρ_A can be written as $\mathcal{E}[\rho_A] = \mathrm{Tr}_B\left[\hat{U}\left(\rho_A \otimes |\psi\rangle\langle\psi|\right)\hat{U}^\dagger\right]$, with $|\psi\rangle \in \mathcal{H}_B$.

- Naimark's dilation theorem affirm that a POVM can be realized as PVM on an extended Hilbert space. More specifically any POVM on $\mathcal{H}_A$ can be realized by applying an unitary operation on an extended Hilbert $\mathcal{H}_A \otimes \mathcal{H}_B$ space and performing a PVM on the ancillary system $\{\mathbb{I} \otimes \hat{P}_n\}$. The n-th outcome of the POVM can be obtained with probability $p_n = \mathrm{Tr}\left[\hat{U}\left(\rho_A \otimes |\psi\rangle\langle\psi|\right)\hat{U}^\dagger \left(\mathbb{I} \otimes \hat{P}_n\right)\right]$

These theorems allow to trace back the description of an interacting system to the description of a global closed system which is formalized in the postulates of quantum mechanics we have described in Sec. 1.1

CHAPTER 2

Open quantum systems

In this chapter we review the theory of open quantum systems.
The term "open systems" refers to systems whose dynamics is not isolated but instead influenced by interactions with external quantum systems. In this thesis, we will specifically use "open systems" to denote quantum systems that interact with an environment. We will classify the different kinds of environments as follows: we use the term reservoir for a system with an infinite number of degrees of freedom, where the frequencies of the reservoir modes form a continuum, while we will use the term heat bath for a reservoir in a state of thermal equilibrium.

The most well-understood class of open system dynamics exhibits Markovian behavior. Originally developed in the context of classical stochastic processes, the concept of Markovianity plays a critical role in open quantum systems, albeit with significant distinctions from its classical counterpart. A unique challenge in the quantum regime is the lack of a universally accepted definition of Markovianity. Instead, a hierarchy of weaker definitions are employed to characterize Markovian behavior [10, 11, 12].

For open quantum systems, the Markovian approximation is one of the central assumptions required to derive the GKSL master equation (named after Gorini, Kossakowski, Sudarshan, and Lindblad), commonly referred to as the Lindblad master equation [8, 13, 14]. This equation provides a framework to describe the dynamics of a wide class of systems. Outside the limits of this approximation, some results have been achieved, generally leading to a dynamics described by an integro-differential equation [15, 16, 17].

The dynamics of a system described by the Lindblad master equation are marked by a continuous leakage of information into the environment. By performing measurements on the environment, it becomes possible to retrieve partial information about the system and condition its dynamics accordingly. However, as this constitutes an indirect measurement, it is inherently inefficient, as not all lost information can be recovered. Consequently, the measurement exerts only a weak influence on the system.

When such weak measurements are performed continuously in time, they give rise to a stochastic process that produces random trajectories in the quantum state dynamics, known as quantum trajectories. Various experimental setups have successfully observed quantum trajectories, including superconducting qubits [18, 19, 20, 21], optomechanical systems [22, 23, 24] and hybrid [25] systems. Recently, feedback protocols able to cool mechanical oscillators have also been demonstrated [23, 26, 27]. The theoretical framework used to describe the dynamics of such quantum systems, which are influenced by the back-action of environmental monitoring, is called the stochastic master equation. In this framework, the differential equations that typically describe open quantum systems are augmented with stochastic terms to account for the randomness introduced by measurement processes.

Continuously-monitored open quantum systems [28, 29] have been extensively studied from a theoretical point of view, mainly for feedback-assisted quantum state engineering protocols [30, 31, 32, 33, 34, 35, 36, 37, 38, 39, 40, 41, 42, 43, 44, 45] and for quantum estimation purposes [46, 47, 48, 49, 50, 51, 52, 53, 54, 55, 56, 57, 58, 59, 60, 61, 62, 63]; more recently their quantum thermodynamics properties have been also analyzed, being a paradigmatic example of out-of-equilibrium quantum systems [64, 65, 66, 67, 68, 69, 70, 61, 71, 72, 73, 74, 75].

To explore these dynamics, we will exploit collisional models [76], a versatile class of models widely used in the study of open systems, especially in the context of quantum information [77], quantum optics [78] and quantum thermodynamics [79, 80, 81]. Collisional models not only can describe both Markovian and non-Markovian dynamics [82], but provide a framework to smoothly swap from the former to the latter. These models will serve as the foundation for deriving both the Lindblad master equation and the stochastic master equations that arise under continuous monitoring.

This chapter is structured as follows: In Sec. 2.1, we characterize Markovian dynamics, introduce collisional models in their Markovian formulation, and derive the GKSL master equation from both collisional models and a microscopic perspective.

In Sec. 2.2, we derive the stochastic master equations that describe quantum systems that are continuously monitored via either photo-detection and homodyne detection.

In Sec. 2.3, we further discuss Markovianity in the quantum regime and introduce measures of non-Markovianity.

In Sec. 2.4, we present a collisional model exhibiting non-Markovian behavior and derive an integro-differential master equation for its dynamics.

Finally, in Sec. 2.5, we provide a brief summary of this chapter.

2.1 Markovian dynamics

In this section, we derive the Master Equation (ME) that describes the dynamics of an open quantum system interacting with an environment under the Markovian approximation. We then extend this framework to show how the dynamics is described by a Stochastic Master Equation (SME) when the system is continuously monitored through measurements performed on the output field. The Lindblad ME is the most general form of a Markovian ME, provided the generator of the dynamics satisfies the dynamical semigroup property:

$$\mathcal{E}_{t_1+t_2} = \mathcal{E}_{t_1} \circ \mathcal{E}_{t_2}, \qquad t_1, t_2 \geq 0, \tag{2.1}$$

$$\mathcal{E}_0 = \mathcal{I} \tag{2.2}$$

where $\mathcal{E}_t$ is the dynamical map at time t and $\mathcal{I}$ is the identity map. This semigroup property serves as a working definition of Markovianity in the quantum regime.

To ensure the semigroup property holds, specific approximations are necessary, meaning that any microscopic derivation of the ME from a Hamiltonian starting point involves a set of assumptions. In all derivations, the Born approximation and the Markov approximation are always required.

- **Born Approximation:** Assumes that the joint density operator of the system and the environment can be factorized at all times, i.e., $\rho_{tot} \approx \rho_s(t) \otimes \rho_e$

- **Markov Approximation:** The environment's state remains unaffected by the system and, if in equilibrium, is assumed constant.

These approximations are typically valid when the environment's correlation functions decay much faster than the characteristic timescales of the system's dynamics. This separation of timescales ensures that the environment "forgets" its interaction with the system almost instantaneously, justifying the Markovian assumption.

While various derivations of the Lindblad ME exist under different physical assumptions, we will adopt the approach outlined in [83], which is inspired by collisional models (CM). These models offer significant insights into both the derivation of the ME and its stochastic counterpart, the SME. To begin with, we will characterize the Markovian collisional model, showing how simple assumptions about the evolution of the model naturally lead to a Lindblad ME.

2.1.1 Markovian collisional model

Before studying the dynamics of open systems from a standard physical setting (i.e., a microscopic model), we introduce the Markovian collisional model and derive the Lindblad ME.

Consider a system S interacting with a bath B_n, where the bath consists of a collection of n uncorrelated auxiliary systems. The model follows these key rules:

- The system and the bath constituents are initially in an uncorrelated state: $\tau_0 = \rho \otimes (\mu \otimes \mu \otimes \dots)$.
- The dynamics proceeds through ordered "collisions," i.e., short interactions between the system and a single auxiliary system in succession, with no couple of system interacting more than once.
- No interactions occur between auxiliary systems.

These conditions are sufficient to enforce Markovianity in the system's dynamics.

The dynamics is driven by the following unitary operator:

$$\hat{U}_n = e^{-i\left(\hat{H}_{0,n}+\hat{H}_{s,n}\right)\Delta t}, \tag{2.3}$$

where Δt is the duration of the collision, $\hat{H}_{0,n} = \omega_0 \hat{h}_s + \hat{H}_n$ is the free Hamiltonian of the system and the n-th ancilla, and $\hat{H}_{s,n} = g\hat{V}_{s,n}$ is the interaction Hamiltonian between the system and the n-th ancilla. After n collisions, the state of the system is given by

$$\rho_n = \mathrm{Tr}_{B_n}\left[\hat{U}_n(\rho_{n-1} \otimes \mu)\hat{U}_n^\dagger\right] = \mathcal{E}[\rho_{n-1}] = \mathcal{E}^n[\rho_0], \tag{2.4}$$

where the map $\Phi_n = \mathcal{E}^n$ satisfies the semigroup property as in Eq. (2.1).

To derive the Markovian ME, we expand $\hat{U}_n$ to second order in Δt and evaluate $\Delta\rho_n = \rho_{n+1} - \rho_n$. This yields:

$$\begin{aligned}\Delta\rho_n = &-i\left(\left[\hat{H}_s, \rho_n\right] + \mathrm{Tr}_{B_n}\left\{\left[\hat{H}_{s,n}, \rho_n \otimes \eta\right]\right\}\right)\Delta t \\ &+ \mathrm{Tr}_{B_n}\left\{\hat{H}_{s,n}(\rho_n \otimes \eta)\hat{H}_{s,n} - \frac{1}{2}\left[\hat{H}_{s,n}^2, \rho_n \otimes \eta\right]_+\right\}\Delta t^2,\end{aligned} \tag{2.5}$$

where $\left[\hat{A}, \hat{B}\right]_+ = \hat{A}\hat{B} + \hat{B}\hat{A}$, is the anticommutator. Defining the following quantities:

$$\hat{H}'_s = \mathrm{Tr}_{B_n}\left\{\hat{H}_{s,n}\eta\right\}, \tag{2.6}$$

$$\mathcal{D}[\hat{L}_{i,j}]\rho = \Gamma\left(\hat{L}_{i,j}\rho\hat{L}^\dagger_{i,j} - \frac{1}{2}\left[\hat{L}^\dagger_{i,j}\hat{L}_{i,j}, \rho\right]_+\right), \tag{2.7}$$

with $\Gamma = g^2\Delta t$ and $\hat{L}_{i,j} = \sqrt{p_j}\langle i|\hat{V}_{s,n}|j\rangle$, where p_j and $|i\rangle, |j\rangle$ are the eigenvalues and eigenvectors of the density operator μ, we arrive at the discrete Markovian ME:

$$\frac{\Delta\rho_n}{\Delta t} = -i\left[\hat{H}_s + \hat{H}'_s, \rho_n\right] + \sum_{i,j}\mathcal{D}[\hat{L}_{i,j}]\rho_n. \tag{2.8}$$

To obtain the Markovian ME in differential form, we take the continuous-time limit. In the discrete model, time is defined as $t = N\Delta t$. The limit is taken by fixing t and letting $N \to \infty$, so that $\Delta t \to 0$. Importantly, we require the rate Γ to remain finite in this limit, which necessitates a diverging coupling strength g.

To summarize, a collisional model is an open system model where the bath is composed of an infinite number of auxiliary systems, each interacting ("colliding") with the system S in an orderly fashion, following a specific collision scheme. To ensure Markovianity, and hence eliminate memory effects from the dynamics, additional rules are imposed. These rules act as the collisional model equivalent of the Born and Markov approximations. In the next subsection, we show how Markovian collisional models can emerge from microscopic settings.

2.1.2 The Markovian master equation

For this derivation, we consider a generic setting where a system S interacts with a bath of bosonic modes E, governed by the total Hamiltonian:

$$\hat{H} = \hat{H}_S + \hat{H}_E + \hat{H}_{SE}, \tag{2.9}$$

where $\hat{H}_S$ is the system Hamiltonian (left generic), and the other terms are specified as:

$$\hat{H}_E = \int_0^\infty \mathrm{d}\omega\, \omega\hat{b}^\dagger_\omega\hat{b}_\omega, \tag{2.10}$$

$$\hat{H}_{SE} = i\int_0^\infty \mathrm{d}\omega\sqrt{\frac{\kappa(\omega)}{2\pi}}\left(\hat{c}\hat{b}^\dagger_\omega - \hat{c}^\dagger\hat{b}_\omega\right), \tag{2.11}$$

where $\hat{c}$ is a generic system operator, and $\hat{b}_\omega$ are bath operators known as input modes satisfying the commutation relation:

$$[\hat{b}_\omega, \hat{b}^\dagger_{\omega'}] = \delta(\omega - \omega'). \tag{2.12}$$

In interaction picture with respect to $\hat{H}_0 = \hat{H}_S + \hat{H}_E$, we assume that the system operator $\hat{c}$ appearing in the interaction Hamiltonian (2.11) acquires a phase

$$\hat{c}(t) = \hat{c}e^{-i\omega_0(t-t_0)} \tag{2.13}$$

As a consequence, one can easily prove that the interaction Hamiltonian now reads

$$\hat{H}_{SE}(t) = i\sqrt{\kappa}\left(\hat{c}\hat{b}_t^\dagger - \hat{c}^\dagger\hat{b}_t\right). \tag{2.14}$$

where we defined time-dependent input modes:

$$\hat{b}_t = \frac{1}{\sqrt{2\pi}}\int_{\mathcal{W}} \mathrm{d}\omega\, \hat{b}_\omega e^{-i(\omega-\omega_0)(t-t_0)}. \tag{2.15}$$

In the equations above, ω_0 is the characteristic frequency of the system and t_0 is the initial time where the Schrödinger and interaction pictures coincide. For a Markovian dynamics, we assume the bath spectral density $\kappa(\omega)$ is constant over a bandwidth $\mathcal{W} = [\omega_0 - \theta, \omega_0 + \theta]$, i.e., $\kappa(\omega) = \kappa$ within $\mathcal{W}$ and zero outside.

This model can be interpreted as a continuous collisional model, with modes acting as auxiliary systems. To provide a more recognizable representation, we proceed by discretizing time to recover the familiar discrete collisional model derived above. For more detail on this procedure, we refer to [78]. We discretize time by setting $t = N\Delta t$, with discrete time steps $t_n = n\Delta t$. Using the Suzuki-Trotter formula, the unitary evolution operator is approximated as:

$$\hat{U}(t) = \lim_{N\to\infty} \hat{U}_N \cdots \hat{U}_1, \tag{2.16}$$

where each discrete step involves time-bin modes defined as:

$$\hat{b}_n = \frac{1}{\sqrt{\Delta t}}\int_{t_{n-1}}^{t_n} \mathrm{d}t'\hat{b}_{t'}. \tag{2.17}$$

The unitary operator for each step reads:

$$\hat{U}_n = e^{-i\sqrt{\kappa\Delta t}\left(\hat{c}\hat{b}_n^\dagger - \hat{c}^\dagger\hat{b}_n\right)}, \tag{2.18}$$

which describes discrete interactions between the system S and time-bin modes as auxiliary systems. From this discrete model, we can derive the ME by transitioning from discrete to continuous time as before.

To derive the continuous collisional model directly, we must address the commutator algebra of time-dependent modes, which is inconsistent with that of a harmonic oscillator. It is necessary to construct an operator describing the input mode that aligns with the harmonic oscillator's annihilation operator. This allows us to reinterpret the mode as such, enabling the environment to be described as a collection of harmonic oscillators, each serving as an auxiliary system in the collisional model. Effectively, for $\theta \gg \kappa$, $[\hat{b}_t, \hat{b}_{t'}^\dagger] = \delta(t-t')$, which is not well defined for $t = t'$. Conversely, the modes for the discrete time-bin modes defined in Eq. (2.17) serve as well-defined annihilation operator for an harmonic oscillator, satisfying the appropriate commutator algebra $\left[\hat{b}_n, \hat{b}_{n'}^\dagger\right] = \delta_{n,n'}$.

To construct the input mode for the time-continuous collisional model, we consider the infinitesimal equivalent of Eq. (2.17) by proceeding as follows. First, we integrate the modes over finite intervals:

$$\delta\hat{b}_t = \int_t^{t+\delta t} \mathrm{d}t'\hat{b}_{t'}, \tag{2.19}$$

leading to a finite commutator:

$$[\delta\hat{b}_t, \delta\hat{b}_t^\dagger] = \mathbb{I}\delta t. \tag{2.20}$$

In the limit $\delta t \to \mathrm{d}t$, we define properly normalized operators:

$$\mathrm{d}\hat{b}_t = \hat{b}_t \mathrm{d}t, \quad \hat{B}_t = \frac{1}{\sqrt{\mathrm{d}t}}\mathrm{d}\hat{b}_t. \tag{2.21}$$

With this new definition for the input modes, the commutator algebra

$$\left[\hat{B}_t, \hat{B}_t^\dagger\right] = \mathbb{I} \tag{2.22}$$

is compatible with that of annihilation operators of quantum harmonic oscillators, allowing us to define an Hilbert space associated with each mode, so that each mode can be reinterpreted as an auxiliary system for the collisional model.

The interaction Hamiltonian remains consistent, and we assume an initially uncorrelated state, that remain uncorrelated due to the separation of the timescales (Born-Markov approximation):

$$\tau(t) = \rho(t) \otimes \mu_t, \tag{2.23}$$

with $\mu_t = |0\rangle_{t\,t}\langle 0|$ for simplicity. We clarify here that the label t is used to refer to the time mode corresponding to the system $\{\hat{B}_t\}$. The state evolves over an infinitesimal time step via the unitary:

$$\hat{U}(t, t + \mathrm{d}t) = e^{-i\hat{H}_{SE}(t)\mathrm{d}t}. \tag{2.24}$$

We can expand $\hat{U}(t, t + \mathrm{d}t)$ to second order

$$\begin{aligned}\hat{U}(t, t + \mathrm{d}t) &\approx \mathbb{I} \otimes \mathbb{I} + \left(\hat{c} \otimes \hat{B}_t^\dagger - \hat{c}^\dagger \otimes \hat{B}_t\right)\sqrt{\kappa \mathrm{d}t} + \\ &+ \frac{1}{2}\left((\hat{c}^\dagger)^2 \otimes \hat{B}_t^2 + \hat{c}^2 \otimes (\hat{B}_t^\dagger)^2 - \hat{c}\hat{c}^\dagger \otimes \hat{B}_t^\dagger\hat{B}_t - \hat{c}^\dagger\hat{c} \otimes \hat{B}_t\hat{B}_t^\dagger\right)\kappa \mathrm{d}t\end{aligned} \tag{2.25}$$

to compute

$$\rho(t + \mathrm{d}t) = \mathrm{Tr}_{B_t}\left[\tau(t + \mathrm{d}t)\right], \tag{2.26}$$

where

$$\tau(t + \mathrm{d}t) = \hat{U}(t, t + \mathrm{d}t)(\rho(t) \otimes \mu_t)\hat{U}(t, t + \mathrm{d}t)^\dagger. \tag{2.27}$$

Performing the calculation yields:

$$\begin{aligned}\tau(t + \mathrm{d}t) = \rho(t) \otimes |0\rangle_{t\,t}\langle 0| &+ \sqrt{\kappa}\left(\hat{c}\rho(t) \otimes |1\rangle_{t\,t}\langle 0| + \rho\hat{c}^\dagger \otimes |0\rangle_{t\,t}\langle 0|\right)\sqrt{\mathrm{d}t} + \\ &+ \kappa\left(\hat{c}\rho(t)\hat{c}^\dagger \otimes |1\rangle_{t\,t}\langle 1|\right)\mathrm{d}t + \\ &+ \frac{\kappa}{2}\left(\sqrt{2}\hat{c}^2\rho(t) \otimes |2\rangle_{t\,t}\langle 0| - \hat{c}^\dagger\hat{c}\rho(t) \otimes |0\rangle_{t\,t}\langle 0| + \text{h.c.}\right)\mathrm{d}t,\end{aligned} \tag{2.28}$$

from which we can perform the trace over the environment

$$\rho(t+\mathrm{d}t) = \rho(t) + \kappa\hat{c}\rho(t)\hat{c}^\dagger\mathrm{d}t - \frac{\kappa}{2}\left[\hat{c}^\dagger\hat{c}, \rho(t)\right]_+ \mathrm{d}t. \tag{2.29}$$

Recalling the definition in Eq. 2.7, we can rewrite the equation in differential form as

$$\frac{\mathrm{d}\rho(t)}{\mathrm{d}t} = \kappa\mathcal{D}[\hat{c}]\rho(t) \tag{2.30}$$

where the Hamiltonian term is missing due to being in interaction picture.

2.2 Continuously monitored quantum systems and stochastic master equations

The derivation of the Lindblad ME from a collisional model provides a clear framework for describing Markovian dynamics of open quantum systems. However, the standard formulation involves tracing out the degrees of freedom of the environment, leading to an averaged evolution for the system. In scenarios where the environment is continuously monitored, the system's dynamics is conditioned on the measurement outcomes, resulting in stochastic trajectories rather than deterministic evolution.

This framework, often referred to as the stochastic master equation (SME) [28, 29, 84, 83], extends the Lindblad description by incorporating the effects of measurement-induced randomness. Depending on the type of measurement performed on the environment, different SMEs can be derived. For instance, photo-detection leads to quantum jump trajectories, while homodyne detection results in diffusive stochastic behavior.

In this section, we derive the SME using the collisional model as a starting point. By replacing the partial trace over environmental degrees of freedom with specific measurement operations, we outline the derivations for the two common cases of photo-detection and homodyne detection. This approach not only highlights the connection between measurement-based dynamics and open quantum system theory but also emphasizes the physical principles underlying the stochastic evolution of quantum states.

2.2.1 Photo-detection SME

For the case of continuous monitoring with a photo-detector, the auxiliary system is projected onto the Fock basis, $\{|n\rangle_t\,{}_t\langle n|\}$. Given the environment initially in the ground state, the only possible outcomes for an infinitesimal update are either photon emission $|1\rangle_t\,{}_t\langle 1|$ or no photon emission $|0\rangle_t\,{}_t\langle 0|$. The state updates are treated separately for these outcomes.

When no photon is emitted, the conditional density operator evolves as

$$\tilde{\rho}_0^c(t+\mathrm{d}t) = {}_t\langle 0|\,\tau(t+\mathrm{d}t)\,|0\rangle_t = \rho^c(t) - \frac{\kappa}{2}\left[\rho^c(t), \hat{c}^\dagger\hat{c}\right]_+ \mathrm{d}t, \tag{2.31}$$

with the probability of no emission given by

$$p_0(t+\mathrm{d}t) = \mathrm{Tr}\left[\rho_0^c(t+\mathrm{d}t)\right] = 1 - \kappa\langle\hat{c}^\dagger\hat{c}\rangle_t\mathrm{d}t, \tag{2.32}$$

where we used $\langle\hat{c}^\dagger\hat{c}\rangle_t = \mathrm{Tr}\left[\rho_c(t)\hat{c}\hat{c}^\dagger\right]$.

Using the outcome probability to normalize the state returns

$$\rho_0^c(t+\mathrm{d}t) = \rho^c(t) - \frac{\kappa}{2}\mathcal{H}\left[\hat{c}^\dagger\hat{c}\right]\rho^c(t)\mathrm{d}t. \tag{2.33}$$

where $\mathcal{H}[\hat{A}]\rho = \hat{A}\rho + \rho\hat{A}^\dagger - \langle \hat{A} + \hat{A}^\dagger \rangle \rho$.

Similarly for the case when a photon is detected, we obtain the following equation for the unnormalized state, the probability outcome and the normalized state

$$\tilde{\rho}_1^c(t + \mathrm{d}t) = \langle 1_{B_t} | \, \tau(t + \mathrm{d}t) \, | 1_{B_t} \rangle = \kappa \hat{c} \rho^c(t) \hat{c}^\dagger \mathrm{d}t, \tag{2.34}$$

$$p_1(t + \mathrm{d}t) = \mathrm{Tr}\left[\rho_1^c(t + \mathrm{d}t)\right] = \kappa \langle \hat{c}^\dagger \hat{c} \rangle_t \mathrm{d}t, \tag{2.35}$$

$$\rho_1^c(t + \mathrm{d}t) = \frac{\hat{c}\rho^c(t)\hat{c}^\dagger}{\langle \hat{c}^\dagger \hat{c} \rangle_t}. \tag{2.36}$$

The relations for the density operator conditioned by the two different outcome can be written as one by introducing a Poisson increment $\mathrm{d}N_t$. A Poisson process N_t is a stochastic process that models the occurrence of random events over time. It is characterized by a rate $\lambda(t)$, which represents the average number of events per unit time.

Over an infinitesimal time interval $\mathrm{d}t$, the probability of more than one event occurring is negligible, while the probability of a single event occurring is proportional to $\lambda(t)\mathrm{d}t$. Consequently, the infinitesimal increment $\mathrm{d}N_t$ can only take the values 0 or 1, with probabilities determined by the rate $\lambda(t)$.

The probability for a detection to occur in our setup is given by $\mathbb{E}\left[\mathrm{d}N_t\right] = p_1(t+\mathrm{d}t) = \kappa \langle \hat{c}^\dagger \hat{c} \rangle_t \mathrm{d}t$.

The equation for the updated conditioned density operator can now be rewritten as

$$\begin{aligned} \mathrm{d}\rho^c(t) &= \rho^c(t + \mathrm{d}t) - \rho^c(t) && (2.37) \\ &= \mathrm{d}N_t \left(\rho_1^c(t + \mathrm{d}t) - \rho^c(t)\right) + (1 - \mathrm{d}N_t)\left(\rho_0^c(t + \mathrm{d}t) - \rho^c(t)\right), && (2.38) \end{aligned}$$

which can be further simplified by discarding terms of order higher than $\mathrm{d}t$

$$\mathrm{d}\rho^c(t) = -\frac{\kappa}{2}\mathcal{H}[\hat{c}^\dagger \hat{c}]\rho^c \mathrm{d}t + \left(\frac{\hat{c}\rho^c(t)\hat{c}^\dagger}{\langle \hat{c}^\dagger \hat{c} \rangle_t} - \rho^c(t)\right)\mathrm{d}N_t. \tag{2.39}$$

When averaging over the conditional state, the unconditional state dynamics is again described by a Lindblad ME.

$$\mathbb{E}\left[\mathrm{d}\rho^c(t)\right] = \kappa \mathcal{D}[\hat{c}]\rho(t)\mathrm{d}t. \tag{2.40}$$

Averaging over all the trajectories coincide with discarding the outcome of the measurement, thus allowing to retrieve the state unconditioned by the their effect. The trajectories arising from the measurement are also said to constitute an unraveling of the unconditional state $\rho(t) = \mathbb{E}[\rho^c(t)]$.

In real-world scenarios, detection may not be perfect, with a certain portions of photon going undetected. We model this inefficiency in term of a probability $\eta \in [0, 1]$ of performing the measurement. This modifies the dynamics such that only a fraction η of photon events are registered, while the remaining fraction contributes to the non-selective evolution.

The SME for the process can be derived starting from the Lindblad ME and splitting the generator as

$$\frac{\mathrm{d}\rho(t)}{\mathrm{d}t} = \eta\kappa \mathcal{D}[\hat{c}]\rho(t) + (1 - \eta)\kappa \mathcal{D}[\hat{c}]\rho(t), \tag{2.41}$$

where now only the first term unravel due to the measurements. By proceeding as before, we can obtain the SME for inefficient photo-detection

$$\frac{\mathrm{d}\rho^c(t)}{\mathrm{d}t} = -\frac{\eta\kappa}{2}\mathcal{H}[\hat{c}^\dagger\hat{c}]\rho^c\mathrm{d}t + \left(\frac{\hat{c}\rho^c(t)\hat{c}^\dagger}{\langle\hat{c}^\dagger\hat{c}\rangle}_t - \rho^c(t)\right)\mathrm{d}N_t + (1-\eta)\kappa\mathcal{D}[\hat{c}]\rho^c(t). \tag{2.42}$$

It is important to notice, that efficient SMEs ($\eta = 1$) preserves the purity of the initial states, so if the initial state is pure, then the SME reduces to a Stochastic Schrödinger Equation (SSE). For a conditional state vector $|\psi^c(t)\rangle$, the SSE can be written as

$$\mathrm{d}\,|\psi^c(t)\rangle = \left[+\frac{\kappa}{2}\left(\langle\hat{c}^\dagger\hat{c}\rangle_t - \hat{c}^\dagger\hat{c}\right)\mathrm{d}t + \left(\frac{\hat{c}}{\sqrt{\langle\hat{c}^\dagger\hat{c}\rangle_t} - 1}\mathrm{d}N_t\right)\right]|\psi^c(t)\rangle\,, \tag{2.43}$$

where now $\langle\hat{c}^\dagger\hat{c}\rangle_t = \langle\psi^c(t)|\,\hat{c}^\dagger\hat{c}\,|\psi^c(t)\rangle$.

2.2.2 Homodyne SME

Homodyne detection involves measuring the environment by projecting it onto the unnormalized eigenstates $\{|x_\theta\rangle_t\,{}_t\langle x_\theta|\}$ of the quadrature operator

$$\hat{x}_\theta = \frac{1}{\sqrt{2}}\left(e^{i\theta}\hat{B}_t + e^{-i\theta}\hat{B}_t^\dagger\right). \tag{2.44}$$

Here, θ determines the measurement basis, allowing us to measure a particular combination of the annihilation and creation operators. The unnormalized conditional state after measurement is given by

$$\tilde{\rho}^c(t+\mathrm{d}t) = {}_t\langle x_\theta|\,\sigma(t+\mathrm{d}t)\,|x_\theta\rangle_t\,. \tag{2.45}$$

To proceed, we expand the unitary evolution operator $\hat{U}$ to $o(\sqrt{\kappa\mathrm{d}t})$, which is sufficient to recover the term up to order $o(\kappa\mathrm{d}t)$.

Noticeably, before the update the probability distribution for x_θ is a Gaussian with variance $\frac{1}{2}$ and zero mean $P_{x_\theta}(t) = |{}_t\langle x_\theta|0\rangle_t|^2 = \frac{1}{\sqrt{\pi}}e^{-x_\theta^2}$. We proceeds to explicitly compute the unnormalized state

$$\tilde{\rho}^c(t+\mathrm{d}t) = P_{x_\theta}(t)\left[\rho^c(t) + (\hat{c}\rho^c(t)e^{i\theta} + \rho^c(t)\hat{c}^\dagger e^{-i\theta})x_\theta\sqrt{2\kappa\mathrm{d}t}\right] + o(\sqrt{\kappa\mathrm{d}t}) \tag{2.46}$$

and the propability of the update

$$P_{x_\theta}(t+\mathrm{d}t) = \mathrm{Tr}\left[\tilde{\rho}^c(t+\mathrm{d}t)\right] \approx \frac{1}{\sqrt{\pi}}\exp\left\{-\left(x_\theta - \sqrt{\frac{\kappa\mathrm{d}t}{2}}\langle\hat{c}e^{i\theta} + \hat{c}^\dagger e^{-i\theta}\rangle_t\right)^2\right\}. \tag{2.47}$$

To interpret this result, we introduce a new stochastic increment $\mathrm{d}y_t$ and define the photocurrent $I(t)$, which relates directly to the measurement outcomes:

$$\mathrm{d}y_t = I(t)\mathrm{d}t = \sqrt{2\mathrm{d}t}x_\theta = \sqrt{\kappa}\langle\hat{c}e^{i\theta} + \hat{c}^\dagger e^{-i\theta}\rangle_t\mathrm{d}t + \mathrm{d}w_t, \tag{2.48}$$

where $\mathrm{d}w_t$ is a Gaussian random variable with variance $\mathrm{d}t$ and mean $\mathbb{E}\left[\mathrm{d}w_t\right] = 0$. The photocurrent itself can be written as

$$I(t) = \sqrt{\kappa}\langle \hat{c}e^{i\theta} + \hat{c}^\dagger e^{-i\theta}\rangle_t + \xi(t). \tag{2.49}$$

where $\xi(t) = \frac{\mathrm{d}w_t}{\mathrm{d}t}$ is a white noise term. Thus, the photocurrent is proportional to the measured quadrature plus some noise

The quantity $\mathrm{d}w_t$ is known as the Wiener increment. It represents the infinitesimal evolution of the corresponding continuous-time stochastic Wiener process. A key property of the Wiener increment, following Itô's lemma, is that $(\mathrm{d}w_t)^2 = \mathrm{d}t$. This imply that, while $\mathrm{d}w_t$ is a random variable, its square is deterministically equal to $\mathrm{d}t$.

The normalized state update can now be expressed compactly as

$$\mathrm{d}\rho^c(t) = \sqrt{\kappa}\mathcal{H}[\hat{c}e^{i\theta}]\rho^c(t)\mathrm{d}w_t + o(\sqrt{\kappa \mathrm{d}t}). \tag{2.50}$$

To recover higher order terms, it is enough to notice that the average over all possible outcome should return the Lindblad ME, similar as it was in the case of photo-detection where we obtained Eq. (2.40), and recalling that the Wiener increment has zero mean and that $\mathrm{d}w_t^2$ is deterministic because of the Itô's lemma, the SME for homodyne detection is trivially

$$\mathrm{d}\rho^c(t) = \kappa\mathcal{D}[\hat{c}]\rho^c(t)\mathrm{d}t + \sqrt{\kappa}\mathcal{H}[\hat{c}e^{i\theta}]\rho^c(t)\mathrm{d}w_t. \tag{2.51}$$

In the case of inefficient detection, we can once again use the method of splitting the ME in two part and only unravel the term proportional to η

$$\mathrm{d}\rho^c(t) = \kappa\mathcal{D}[\hat{c}]\rho^c(t)\mathrm{d}t + \sqrt{\eta\kappa}\mathcal{H}[\hat{c}e^{i\theta}]\rho^c(t)\mathrm{d}w_t. \tag{2.52}$$

An extension of this framework is heterodyne detection, where both quadratures of the field are measured simultaneously. This requires using two jump operators:

$$\hat{c}_1 = \frac{\hat{c}}{\sqrt{2}}, \quad \hat{c}_2 = \frac{i\hat{c}}{\sqrt{2}}, \tag{2.53}$$

which allow us to write the SME for heterodyne detection as:

$$\mathrm{d}\rho^c(t) = \kappa\mathcal{D}[\hat{c}]\rho^c(t)\mathrm{d}t + \sqrt{\frac{\kappa}{2}}\mathcal{H}[\hat{c}]\rho^c(t)\mathrm{d}w_t^{(1)} + \sqrt{\frac{\kappa}{2}}\mathcal{H}[i\hat{c}]\rho^c(t)\mathrm{d}w_t^{(2)}, \tag{2.54}$$

where $\mathrm{d}w_t^{(1)}$ and $\mathrm{d}w_t^{(2)}$ are uncorrelated Wiener increments corresponding to the two photocurrents

$$\mathrm{d}y_t^{(1)} = \sqrt{\eta/2}\,\langle \hat{c} + \hat{c}^\dagger\rangle_t\,\mathrm{d}t + \mathrm{d}W_t^{(1)} \tag{2.55}$$

$$\mathrm{d}y_t^{(2)} = \sqrt{\eta/2}\,\langle i\hat{c} - i\hat{c}^\dagger\rangle_t\,dt + \mathrm{d}W_t^{(2)}. \tag{2.56}$$

During the derivation of higher-order terms of the homodyne SME, it was assumed that the unconditional dynamics of the system correspond to a Lindblad ME. Equivalently, the homodyne SME can be regarded as an unraveling of the Lindblad ME. This property holds true for homodyne SMEs with any number of jump operators. Consequently, both the homodyne SME and the heterodyne SME satisfy the condition:

$$\mathbb{E}\left[\mathrm{d}\rho^c(t)\right] = \kappa\mathcal{D}[\hat{c}]\rho(t)\mathrm{d}t. \tag{2.57}$$

Similar to photodetection, the SMEs for homodyne and heterodyne detection with unit efficiency, starting from an initial pure state, reduce to a Stochastic Schrödinger Equation (SSE). The SSE for homodyne detection is given by:

$$\begin{aligned}\mathrm{d}\left|\psi^c(t)\right\rangle = \Bigg\{ & \left[-i\hat{H} - \frac{\kappa}{2}\left(\hat{c}^\dagger\hat{c} - \langle\hat{c}+\hat{c}^\dagger\rangle\hat{c} + \frac{\langle\hat{c}+\hat{c}^\dagger\rangle^2}{4}\right)\right]\mathrm{d}t \\ & + \sqrt{\kappa}\left(\hat{c} - \frac{\langle\hat{c}+\hat{c}^\dagger\rangle}{2}\right)\mathrm{d}\omega_t\Bigg\}\left|\psi^c(t)\right\rangle. \end{aligned} \tag{2.58}$$

2.3 Non-Markovianity

In quantum dynamics, the Markovian approximation assumes that a system's evolution is memoryless, meaning its future state depends solely on its current state. This simplification holds when the environment lacks long-lasting correlations or when the coupling between the system and the environment is weak. However, in many realistic scenarios, this assumption fails, leading to dynamics characterized by non-Markovian behavior.

Non-Markovianity refers to the presence of memory effects in a quantum system, where past interactions between the system and its environment influence its future evolution. These memory effects often arise in cases of strong system-environment coupling, structured reservoirs with finite size, or environments with slow relaxation times. Consequently, the system's dynamics deviate from those predicted by the widely used Lindblad ME.

We began this chapter by exploring the significance of Markovianity in open quantum systems and describing Markovian dynamics via the GKSL ME. In this section, we turn our attention to a deeper characterization of both Markovianity and non-Markovianity.

Classically, Markovianity is formally defined for a (discrete) stochastic process $\mathbf{X}_t$ with $t > 0$. The joint probability distribution of the random variables $\mathbf{X}$ up to a time t_n is given by

$$P(\mathbf{X}_{t_n}, \mathbf{X}_{t_{n-1}}, \ldots, \mathbf{X}_0). \tag{2.59}$$

Using Bayes' theorem, this can be rewritten as

$$P(\mathbf{X}_{t_n}, \mathbf{X}_{tn-1}, \ldots, \mathbf{X}_0) = P(\mathbf{X}_{t_n}|\mathbf{X}_{tn-1}, \ldots, \mathbf{X}_0)P(\mathbf{X}_{t_{n-1}}, \ldots, \mathbf{X}_0). \tag{2.60}$$

A stochastic process is said to be Markovian if it satisfies

$$P(\mathbf{X}_{t_n}|\mathbf{X}_{tn-1}, \ldots, \mathbf{X}_0) = P(\mathbf{X}_{t_n}|\mathbf{X}_{tn-1}), \tag{2.61}$$

which formalizes the idea that the future state of the process depends only on its present state.

For open quantum systems, however, this classical definition cannot be directly applied. While it is technically possible to define a joint probability distribution for measurement outcomes o_t of a given observable $\hat{O}$ at different times, such distributions do not fully characterize the underlying quantum stochastic process. Therefore, they do not allow us to infer all the relevant properties of the dynamics.

Alternative approaches to define Markovianity in quantum systems include methods based on dynamical maps or the nature of system-environment interactions. In the first approach, rooted in the concept of divisibility, Markovianity is defined through the semigroup property described by Eq. (2.1). This notion implies that the dynamics can be split at any intermediate time point, and the evolution beyond this point depends only on the system's state at the point itself. Memory effects from earlier times are not required. Dynamical maps that belong to this semigroup are an example of completely positive (CP)-divisible maps.

2.3.1 Measuring non-Markovianity

In Lindblad-like dynamics, information continuously flows only from the system to the environment, reflecting the memoryless nature of Markovian processes. In contrast, non-Markovian processes are characterized by an exchange of information, where some information initially lost to the environment returns to the system. This backflow of information provides a useful foundation for defining and measuring non-Markovianity.

One widely used approach [85] involves the trace distance, defined as

$$D(\rho^1, \rho^2) = \frac{1}{2}\|\rho^1 - \rho^2\| = \frac{1}{2}\,\mathrm{Tr}\left[\sqrt{(\rho^1 - \rho^2)^\dagger\,(\rho^1 - \rho^2)}\right]. \tag{2.62}$$

The trace distance $D(\rho^1, \rho^2)$ quantifies the distinguishability between two quantum states ρ^1 and ρ^2. It satisfies $D(\rho^1, \rho^2) = 0$ if the states are identical ($\rho^1 = \rho^2$) and $D(\rho^1, \rho^2) = 1$ if they are orthogonal. Importantly, completely positive trace-preserving (CPTP) maps are non-increasing with respect to the trace distance:

$$D(\mathcal{E}[\rho^1], \mathcal{E}[\rho^2]) \leq D(\rho^1, \rho^2). \tag{2.63}$$

This property ensures that, under Markovian dynamics, the distinguishability between any two states decreases monotonically over time.

A natural definition of Markovianity emerges: a quantum process is *Markovian* if the trace distance between all possible pairs of initial states decreases monotonically for all times. Conversely, any non-monotonic behavior of the trace distance indicates the presence of non-Markovianity.

To quantify the "degree" of non-Markovianity, one can sum over all intervals where the trace distance increases. This measure is proportional to the total backflow of information. Formally, we define:

$$\sigma_D(t) = \frac{\mathrm{d}}{\mathrm{d}t} D(\rho^1(t), \rho^2(t)), \tag{2.64}$$

and the measure of non-Markovianity as

$$\mathcal{N}_{BLP} = \max_{\rho^1, \rho^2} \int_{\sigma_D(t)>0} \mathrm{d}t\, \sigma_D(t). \tag{2.65}$$

The pair of states (ρ^1, ρ^2) that maximizes $\mathcal{N}$ are known as *optimal pairs*. An important simplification result is that these optimal pairs lie on the boundary of the state space and are orthogonal [86].

Another perspective on non-Markovianity arises from the so-called *geometrical measure* [87]. For any finite n-dimensional quantum system, a generic state ρ can be written as

$$\rho = \frac{1}{n}\left(\mathbb{1} + \sum_{\alpha=1}^{n^2-1} r_\alpha \hat{G}_\alpha\right), \tag{2.66}$$

where $r_\alpha \in \mathbb{R}$, and $\{\hat{G}_\alpha\}$ are the Hermitian traceless generators of $SU(n)$. For $n = 2$, these correspond to the Pauli matrices. The vector $\boldsymbol{r}$, with components $\{r_\alpha\}_{\alpha=1,\ldots,n^2-1}$, is called the *generalized Bloch vector*.

Under a quantum map $\mathcal{E}$, the dynamics of $\boldsymbol{r}$ becomes an affine transformation:

$$\boldsymbol{r}(t) = A(t)\boldsymbol{r}(0) + \boldsymbol{q}(t), \tag{2.67}$$

where $A(t)$ is a $(n^2 - 1) \times (n^2 - 1)$ real matrix, and $\boldsymbol{q}(t)$ is a real vector. The matrix elements of $A(t)$ are given by

$$A_{\alpha,\beta}(t) = \mathrm{Tr}\Big[\hat{G}_\alpha \mathcal{E}_t[\hat{G}_\beta]\Big], \tag{2.68}$$

and $A(t)$ typically includes rotations and contractions (or dilations) of the Bloch vector.

The set of accessible generalized Bloch vectors defines a volume $V(t)$ in state space. For Markovian dynamics, the volume of accessible states contracts monotonically due to the positive linear trace-preserving nature of the map. Specifically, the effect of the map on an infinitesimal volume element $\mathrm{d}^n V$ is given by

$$\mathrm{d}^n V(t) = |A(t)|\mathrm{d}^n V(0), \tag{2.69}$$

where $|A(t)|$ is the determinant of $A(t)$. A dilation occurs whenever $|A(t)| > 0$, signaling non-Markovian behavior.

Using $\sigma_A(t) = \frac{\mathrm{d}}{\mathrm{d}t}|A(t)|$, we define the geometrical measure of non-Markovianity as

$$\mathcal{N}_{geo} = \int_{\sigma_A(t)>0} \mathrm{d}t\, \sigma_A(t). \tag{2.70}$$

2.4 Non-Markovian collisional models

To showcase the behaviour of non-Markovian dynamics, we will discuss a non-Markovian formalization of collisional models.

There are a few ways in which it is possible to derive anon-Markovian collisional model. In here, we will display the non-Markovian collisional model obtained when ancilla-ancilla collision are allowed. Moreover, we will show a particular collisional model with ancilla-ancilla collision where a continuous time limit exists and it is possible to derive a integro-differential non-Markovian ME.

This non-Markovian collisional model can be derived from the Markovian case. We recall that, in the Markovian case, the evolution of the density operators is dictated by Eq. (2.4), a sequence of unitary operations and partial traces of the composite state of the model. To induce memory effect, we add an ancilla-ancilla collision at each step between the auxiliary system that collided at the previous step, and the auxiliary system that will collide at the successive step.

We introduce the following notation for simplicity: $\mathcal{U}[\sigma] = \hat{U}\sigma\hat{U}^\dagger$ and $\mathcal{T}_i = \mathrm{Tr}_i\,[\sigma]$. Here, the operator σ represents the system-environment composite state, as defined in Sec. 2.1.1, and Tr_i denotes the trace over the i-th auxiliary system's degree of freedom.

The dynamics of the collisional model with the new interaction take the form

$$\sigma_n = \mathcal{U}_{n-1}\mathcal{W}_{n,n-1}\sigma_{n-1} \tag{2.71}$$

To derive the non-Markovian collisional model that results in a non-Markovian ME in the continuous-time limit, we employ the incoherent partial swap as the ancilla-ancilla interaction, defined as:

$$\mathcal{W}_{n,n-1} = (1-p)\mathcal{I} + p\mathcal{S}_{n,n-1} \qquad n \geq 2, \tag{2.72}$$

where the operator $\hat{S}_{n,n-1}$ swaps the state of the n-th ancilla with that of the $(n-1)$-th ancilla.

The two limiting cases, $p = 0$ and $p = 1$, are particularly interesting. In the former case, the ancilla-ancilla interaction is the identity map, so the states of the two systems remain unchanged, and we recover the Markovian collisional model as before. In the latter case, if we denote with $\mathcal{F}$ the map of the collisional model with a perfect ancilla-ancilla swap ($p = 1$), and take advantage of the properties of the swap operator, we find that

$$\rho_n = \mathcal{F}_n\left[\rho_0\right] = \mathrm{Tr}_1\left[\hat{U}^n\rho \otimes \mu_1(\hat{U}^\dagger)^n\right]. \tag{2.73}$$

The structure of the equation above reinforces the idea that, by continuously swapping the state of the incoming auxiliary system with that of the previous one, the dynamics become equivalent to two systems continuously interacting. This ultimately results in a closed dynamics up to the time t_n.

To obtain a master equation for any value of $p \in [0, 1]$, we can proceed by induction from σ_0 to σ_n to compute the joint density matrix at the n-th step, obtaining

$$\sigma_n = (1-p)\sum_{j=1}^{n-1} p^{j-1}\mathcal{U}_n^j[\sigma_{n-j}] + p^{n-1}\mathcal{U}_n^n[\sigma_0]. \tag{2.74}$$

Tracing over the ancillas, we find the equivalent to the discrete ME for this collisional model

$$\rho_n = (1-p)\sum_{j=1}^{n-1} p^{j-1}\mathcal{F}_j[\rho_{n-j}] + p^{n-1}\mathcal{F}_n[\rho_0]. \tag{2.75}$$

From here it is possible to derive a continuous ME.

The limit is approached differently than in the Markovian case. In fact, it can be numerically verified that, as the collision time $\delta t \to 0$, the dynamics do not converge to a well-defined continuous-time limit. This can be understood as follows: The ancilla-ancilla interaction happens throughout a time-duration Δt, over which the two auxiliary systems are swapped with a swap probability p. If we keep fixed the value of p, while decreasing the time interval, we are actually increasing the frequency of swaps between ancillae, thus changing the dynamics. To keep the dynamics fixed while decreasing the time interval, we need to define a swap rate Γ to keep fixed while allowing p to change with the time interval.

Therefore, to obtain a continuous ME, we rewrite p as $p = e^{-\Gamma\Delta t}$, making its explicit dependence on the collision time clear. Then, in the limit $\Gamma\delta t \ll 1$, where $p \approx 1 - \Gamma\delta t$, we can derive

$$\frac{\mathrm{d}}{\mathrm{d}t}\rho = \Gamma\int_0^t \mathrm{d}t' e^{-\Gamma t'}\mathcal{F}(t')\left[\frac{\mathrm{d}}{\mathrm{d}t}\rho(t-t')\right] + e^{-\Gamma t}\frac{\mathrm{d}}{\mathrm{d}t}\mathcal{F}(t)[\rho_0] \tag{2.76}$$

2.5 Summary

- When a system is affected by its environment, its dynamics is no longer closed and unitary. Finding an equation to describe the dynamics of an open system is generally complicated.

  However, one such case where this is possible is when the system displays Markovian behavior. Under this condition, it is typically possible to derive a master equation for its dynamics, known as the Lindblad master equation.

- Information loss from the system into the environment can be retrieved by monitoring the outgoing field. In these cases, the backaction from the measurement affects the system, so its state will be described by a stochastic process.

  The case of photo-detection can be described through a Poisson process, while homodyne detection is described by a Wiener process. In both cases, a SME arises, whose average is the Lindblad master equation.

- While the Markovian approximation is extremely important for describing open quantum systems, Markovianity is a difficult concept to transpose to the quantum regime. Unlike the classical case, there are multiple weaker definitions of Markovianity in this regime, rather than a single, unified definition.

  Through these definitions, it is possible to characterize witnesses of non-Markovianity that allow us to measure and quantify the amount of memory in a specific dynamics.

- Collisional models are a versatile tool that allow us to display both Markov and non-Markov dynamics. A collisional model is a way to describe system-environment interactions in terms of short collisions between the system and a set of auxiliary systems acting as the environment.

  The collisional scheme for each model characterizes its properties, allowing us to derive either a Markovian or non-Markovian model by altering the scheme. In some cases, it is possible to take a limit for continuous time evolution, transitioning from dynamics described by discrete maps to a continuous-time master equation for the system.

CHAPTER 3

Quantum batteries and work extraction from quantum systems

The extension of thermodynamic concepts to the quantum regime began in the second half of the 20th century. A seminal contribution in this field was the work of Scovil and Schulz-DuBois [88], which established a parallel between quantum systems and thermal machines by modeling a three-level micromaser as a quantum heat engine.

This work laid the foundation for a framework for incorporating thermodynamic principles into quantum mechanics, which naturally includes generalizing the laws of thermodynamics to the quantum regime. Although certain aspects remain debated, early results on the first law in weakly coupled open systems were established in [89].

For the second law, development arose outside the scope of quantum mechanics. As the interest shifted from the thermodynamic behavior of macroscopic systems at equilibrium to microscopic systems out of equilibrium, this transition spurred the development of stochastic thermodynamics, a framework that rigorously examines thermodynamic quantities at the level of individual trajectories. Central to this field are the fluctuation theorems.

The first fluctuation theorem was introduced by Evans and collaborators [90], followed by rigorous proofs [91] and further generalizations [92, 93]. Prominent results include Crooks' fluctuation theorem [94] and the Jarzynski equality [95], which link nonequilibrium processes to equilibrium free energy differences.

Fluctuation theorems provide a detailed understanding of entropy production in small systems, demonstrating that while entropy production can be negative for individual realizations, its average always remains positive. These theorems quantify the likelihood of observing time-reversed processes relative to their forward counterparts, revealing an exponential suppression of such events. Importantly, the second law of thermodynamics emerges as a corollary of these results. Most importantly, these results also apply to quantum mechanics

Another significant research avenue concerns the energetic cost of information processing. Initiated by Landauer's principle [96], this work explores the connection between computation, energy dissipation, and heat generation. Landauer's ideas were later contextualized with Maxwell's demon and Szilard's engine [97], bridging thermodynamics and information theory. This interplay has since evolved into a unified framework, particularly in the quantum regime, where concepts like the thermodynamics of quantum measurements and information processing remain active areas of research [98, 99, 100, 101, 102, 103]. Key developments include the second law of information thermodynamics [104], which incorporates informational contributions to work, and its recent rigorous generalization [105].

In recent years, attention has turned to the potential of quantum systems as energy-storing devices, initiated by Alicki and Fannes [106]. Their work demonstrated how entanglement and other quantum effects can enhance the performance of energy storage and extraction. Significant progress has been made in exploiting collective quantum effects to boost charging power and efficiency [107, 108, 109, 110, 111].

However, considerable effort has also been devoted to understanding these processes in more realistic open-system settings, addressing challenges like decoherence, dissipation, and non-Markovian effects [5, 1, 112, 113, 114, 115, 116].

In this chapter, we will review these foundational concepts and introduce the quantities and relations necessary for the discussions in subsequent chapters. Our focus will be on defining work in the quantum regime, for both closed and open systems, and examining the impact of measurements on work extraction and energy costs.

This chapter is organized as follows: In Sec. 3.1,we provide a characterization of work extraction through different types of operations: unitary operations, typical of closed systems, and thermal operations, used when an environment is available to achieve a higher level of work extraction.

In Sec. 3.2, we provide the context that motivates the writing of this thesis, reviewing some important results on quantum batteries.

In Sec. 3.3, we explore the role of quantum measurement in enhancing work extraction through both unitary and thermal operations.

In Sec. 3.4, we justify the boost in work extraction by quantifying the expected work cost of measurement, contextualizing these results in terms of the laws of thermodynamics, especially the second law. Finally, we provide a general framework that allows the analysis of both the gain in work extraction and the work cost of measurement.

Finally, in Sec. 3.5, we provide a summary of the key concepts of this chapter.

3.1 Quantifying work extraction from quantum systems

In this section we will address the problem of quantifying the amount of extractable work from a quantum system. For our purpose, we will consider two slightly different contexts.

First, we will address how to quantify the amount of work we can extract from a closed system, and then we will extend to the case where the system can interact with a heat bath. It will be possible to notice, that while in the second case the interaction with an environment may lead to dissipation, in general protocols involving open system dynamics achieve an higher potential in terms of work extraction.

3.1.1 Work extraction from closed system

A fundamental consideration in studying work extraction from closed quantum systems is that they evolve through unitary operations, which are inherently non-dissipative. In this context, the first law of thermodynamics

$$\mathrm{d}E = đW + đQ \tag{3.1}$$

is simplified since $đQ = 0$.

As we are mostly concerned with extraction, from here on we will consider positive the work performed by the system. For a finite-size quantum system with Hamiltonian $\hat{H}_0$ and initially in a generic state ρ_0, the amount of work extracted through a unitary process $\hat{U}$ is

$$\mathcal{W}_U = E(\rho_0) - E(\hat{U}\rho_0\hat{U}^\dagger) \tag{3.2}$$

where $E(\rho) = \mathrm{Tr}\left[\hat{H}_0\rho\right]$.

To quantify how much work we can actually extract from the state ρ_0, formally, we would need to solve the following optimization problem

$$\mathcal{E}(\rho_0) = \max_{\hat{U}} \mathcal{W}_U, \tag{3.3}$$

where the quantity $\mathcal{E}$ that maximize the amount of work extracted through a unitary operation is known as "ergotropy" [117].

A key concept for understanding ergotropy is the notion of passive states. Formally, a passive state satisfies

$$\rho_p : \ \mathrm{Tr}\left[\rho_p\hat{H}_0\right] \leq \mathrm{Tr}\left[\hat{U}\rho_p\hat{U}^\dagger\hat{H}_0\right] \quad \forall\hat{U}, \tag{3.4}$$

so it represent a state of minimum energy for which no unitary can actually decrease its energy. Given a generic active state, there are two known contributions to the ergotropy [118]: a coherent contribution and an incoherent one.

The coherent part of the ergotropy is determined by the coherences of the state in the eigenbasis of the free Hamiltonian. The consumption of the coherences enables work extraction from the state; thus, unitary operations that reduce coherence determine the extraction of coherent ergotropy. The incoherent part, on the other hand, is obtained by minimizing the energy associated with the population distribution of the states.

Since unitary operations cannot alter the eigenvalues of the density operator, this minimization is achieved by rearranging the population such that the energy is minimized. Specifically, the highest eigenvalue aligns with the lowest energy eigenlevel of the Hamiltonian, and so forth.

From this characterization, it is evident that a passive state is diagonal in the energy eigenbasis, with its eigenvalues ordered accordingly, while an active state is characterized by either a population inversion along the diagonal or the presence of coherences.

It is evident then that the unitary operation that maximizes the work extraction is the unitary that send ρ_0 to its passive state. Since unitary operations preserve the eigenvalues of a density operator, we proceed as follows. Given the spectral decomposition of the state ρ_0

$$\rho_0 = \sum_j r_j \left|r_j\right\rangle\!\left\langle r_j\right|, \qquad r_1 \geq r_2 \geq \dots \tag{3.5}$$

and the spectral decomposition of the Hamiltonian $\hat{H}_0$

$$\hat{H}_0 = \sum_k \varepsilon_k \left|\varepsilon_k\right\rangle\!\left\langle\varepsilon_k\right|, \qquad \varepsilon_1 \leq \varepsilon_2 \leq \dots \tag{3.6}$$

where, without loss of generality, we set the lowest eigenvalue equal to zero, the corresponding passive state reads

$$\rho_p = \sum_j r_j \left|\varepsilon_j\right\rangle\!\left\langle\varepsilon_j\right|, \tag{3.7}$$

which can be obtain by applying the unitary operation

$$\hat{U} = \sum_j \left|\varepsilon_j\right\rangle\!\left\langle r_j\right|. \tag{3.8}$$

This allows us to directly compute Eq. (3.3) as

$$\mathcal{E}(\rho_0) = \sum_{j,k} r_j \varepsilon_k \left(|\langle r_j | \varepsilon_k \rangle|^2 - \delta_{j,k} \right). \tag{3.9}$$

It can also be useful to write the ergotropy in terms of the more familiar non equilibrium free energy $\mathcal{F}_\beta$

$$\mathcal{F}_\beta(\rho) = E(\rho) - \frac{1}{\beta} S(\rho), \tag{3.10}$$

where $S(\rho) = -\operatorname{Tr}[\rho \ln(\rho)]$ is the Von Neumann entropy. Because unitary operation preserve the entropy of the state, we can write

$$\begin{aligned}\mathcal{E}(\rho_0) &= E(\rho_0) - E(\rho_p) = E(\rho_0) + \frac{1}{\beta} S(\rho_0) - \frac{1}{\beta} S(\rho_0) - E(\rho_p) \\ &= \mathcal{F}_\beta(\rho_0) - \mathcal{F}_\beta(\rho_p),\end{aligned} \tag{3.11}$$

where we used $S(\rho_0) = S(\rho_p)$. In this equation, β is a free parameter with no particular physical interpretation.

In the particular case of a qubit, Eq. (3.9 can be further simplified. The ergotropy for a generic state ρ_0 can by written in term of the components of its Bloch vector $\langle \hat{\sigma}_i \rangle = \operatorname{Tr}[\rho_0 \hat{\sigma}_i]$

$$\mathcal{E}(\rho_0) = \frac{\omega_0}{2} \left(|\langle \hat{\boldsymbol{\sigma}} \rangle| + \langle \hat{\sigma}_z \rangle \right), \tag{3.12}$$

where we have defined the quantity $|\langle \hat{\boldsymbol{\sigma}} \rangle| = \sqrt{\langle \hat{\sigma}_x \rangle^2 + \langle \hat{\sigma}_y \rangle^2 + \langle \hat{\sigma}_z \rangle^2}$.

In the case of a qubit with Hamiltonian $\hat{H}_0 = (\omega_0/2)\hat{\sigma}_z$, which is commonly considered in the literature, we can further rewrite the formula above in terms of the energy and the purity. We recall that the purity of a qubit state is equal to

$$\mu(\rho) = \operatorname{Tr}\left[\rho^2\right] = \frac{1 + |\langle \hat{\boldsymbol{\sigma}} \rangle|^2}{2}, \tag{3.13}$$

so we can rewrite the ergotropy as

$$\mathcal{E}(\rho) = E(\rho) + \frac{\omega_0}{2} \sqrt{2\mu(\rho) - 1}. \tag{3.14}$$

We also point out that in general, a passive state is not completely passive, meaning that the n-fold product $\rho_p^{\otimes n}$ is not guaranteed to be a passive state with respect to the n-fold sum of its Hamiltonian. The only type of passive state that are also completely passive are the Gibbs state [119, 120, 121].

Gibbs states are a specific subset of passive states that satisfy additional conditions compared to other passive states. By definition, a Gibbs state minimizes energy while maintaining a fixed von Neumann entropy. Unitary operations also preserve the von Neumann entropy, but they form a subset of all entropy-preserving operations and, in particular, cannot alter the eigenvalues of the states to which they are applied. Entropy-preserving operations that allow eigenvalue rearrangement can further minimize energy by redistributing the eigenvalues to follow the Maxwell-Boltzmann distribution.

As systems grow in size, their spectral density approaches a continuum. In such cases, simply rearranging the eigenvalues can achieve the Maxwell-Boltzmann distribution, thereby further reducing the energy.

For smaller system, only relying on unitary operations does not allow the extraction of all the available work except in specific scenarios. Notable cases where all the work in a system can be extracted through unitary operations (and where the passive state the system reaches is effectively the Gibbs state) include:

- Systems initially in a pure state, where the associated passive state is trivially the ground state, allowing all the energy initially in the system to be extracted as work (a more detailed characterization of this statement will be provided in Chapter 5).
- Two-level systems, for which all passives states are thermal states.
- quantum harmonic oscillators in an initial Gaussian state

As we will discuss in the next section, however, there are other operations that can be employed to extract the remaining work in all other cases.

3.1.2 Work extraction with thermal operation

This subsection extends the previous framework by relaxing the requirement that the system remains closed, while retaining the condition $đQ = 0$.

By allowing a broader class of operations, the extractable work is expected to increase or, at the very least, remain unchanged. Introducing an auxiliary system enhances work extraction, with the heat bath being an optimal choice for such a system.

The class of operations that we will consider is known as thermal operations [113, 122, 123]. Thermal operations refer to energy preserving global unitary transformations that act jointly on a system and a heat bath.

Consider a system S with Hamiltonian $\hat{H}_s$ initially in the state ρ_0^S, and a heat bath in the Gibbs state $\rho_\beta^B = \exp\{-\beta H_e\}/Z$, with $Z = \mathrm{Tr}\left[\exp\{-\beta H_e\}\right]$, where β is the inverse temperature of the bath and $\hat{H}_b$ its free Hamiltonian. Since the bath is in a completely passive state, the work extractable from system S can be evaluated through the ergotropy of the composite system.

$$\begin{aligned}\mathcal{E}(\rho_0^S \otimes \rho_\beta^B) &= \mathcal{F}_\beta(\rho_0^S \otimes \rho_\beta^B) - \mathcal{F}_\beta((\rho_0^S \otimes \rho_\beta^B)_p) \\ &= \mathcal{F}_\beta(\rho_0^S \otimes \rho_\beta^B) - \mathcal{F}_\beta(\rho_\beta^S \otimes \rho_\beta^B) + \mathcal{F}_\beta(\rho_\beta^S \otimes \rho_\beta^B) - \mathcal{F}_\beta((\rho_0^S \otimes \rho_\beta^B)_p) \\ &= \frac{1}{\beta} S(\rho_0^S || \rho_\beta^S) - \frac{1}{\beta} S((\rho_0^S \otimes \rho_\beta^B)_p || \rho_\beta^S \otimes \rho_\beta^B) \\ &\leq \frac{1}{\beta} S(\rho_0^S || \rho_\beta^S) = \mathcal{F}_\beta(\rho_0^S) - \mathcal{F}_\beta(\rho_\beta^S),\end{aligned} \tag{3.15}$$

where

$$S(\rho|\tau) = \mathrm{Tr}\left[\rho\left(\ln\rho - \ln\tau\right)\right] \tag{3.16}$$

is the relative entropy. To distinguish the different definitions, we denote by $\mathcal{W}_\beta$ the work extracted from system S via thermal operations, which satisfies the following relation

$$\mathcal{W}_\beta(\rho_0^S) \leq -\Delta\mathcal{F}_\beta, \tag{3.17}$$

where we defined

$$\Delta\mathcal{F}_\beta = \mathcal{F}_\beta(\rho_\beta^S) - \mathcal{F}_\beta(\rho_0^S). \tag{3.18}$$

This bound, derived in this particular way in [113], is equivalent to the bound that in [124] was derived for a particular work extraction protocol. The protocol involves a sudden quantum quench, that is a change of the Hamiltonian $\hat{H}_s \to \hat{H}_{\rho_0^S} = -\frac{1}{\beta}\ln \rho_0^S$, followed by a quasistatic isothermal process during which the system is kept in contact with the bath, ultimately reaching ρ_β^S. The bound is saturated in the limit where the time corresponding to the second step of the protocol goes to infinity.

Interestingly, $\mathcal{W}_\beta$ has a minimum if one considers the heat bath at a temperature β^* corresponding to a thermal state with the same von Neumann entropy of the initial state of the system, that is for $\beta^* : \; S(\rho_0^S) = S(\rho_{\beta^*}^B)$. Notably, the work extracted via thermal operations serves as an upper bound for the ergotropy. Even at its minimum, $\mathcal{W}_\beta$ remains greater than or equal to the ergotropy, with equality occurring only when the eigenvalue distribution of the density operatorρ_0 follows a Maxwell-Boltzmann distribution.

Throughout the thesis, the generic term 'work', denoted as $\mathcal{W}$, will refer to either the ergotropy $\mathcal{E}$ or the work extracted through thermal operations $\mathcal{W}_\beta$, with the exception of when it is used as an upper bound, where naturally the definition of $\mathcal{W}_\beta$ will be assumed. In cases where the term 'work' pertains to classical driving, it is understood to follow the classical definition.

3.2 Quantum Batteries: Concepts and Progress

Since their conception in [106], quantum batteries have emerged as a vibrant area of research. This pioneering paper initiated the discussion on the role of quantum resources in charging quantum batteries, i.e., quantum systems functioning as energy storage devices. The enthusiasm surrounding quantum batteries has been driven by several motivations. Many researchers have focused on understanding whether quantum phenomena can lead to performance enhancements, determining optimal protocols for charging and discharging, exploring whether global operations are necessary or if local operations suffice, and investigating the relationship between uniquely quantum properties—such as quantum correlations—and the performance of such devices.

For others, quantum batteries serve as ideal testbeds to examine thermodynamic properties of quantum systems in various contexts, particularly in energy extraction. Thermodynamics in the quantum regime remains a relatively novel field with many unexplored concepts, and quantum batteries offer a promising platform for advancing this research. For example, as systems under scrutiny become smaller, thermal and quantum fluctuations play increasingly significant roles.

The role of fluctuations on work extraction is one active area of research. Some seminal results [125, 126, 127, 128, 129, 130] suggest trade-offs between maximum power, process efficiency, and the extent of fluctuations, even if violations are found under certain conditions [131].

Mitigating work fluctuation might still be a desirable in the context of quantum battery for a more stable work output, even at the cost of maximum power extraction. Some results in this direction includes [132, 111, 133].

Another motivation lies in understanding the role of measurement and its impact on thermodynamic frameworks, which we will explore in the next section. Studies of quantum batteries can deepen our understanding of thermodynamic quantities such as work, heat, and entropy generation, while also improving our ability to account for the energetics of other quantum devices, such as quantum computers.

Real-world quantum technologies are rarely isolated from external noise and dissipation, so quantum batteries in an open system setting are referred to as Open Quantum Batteries (OQB). Environmental interactions often lead to energy loss and decoherence, which is why research in open quantum batteries explores how to mitigate dissipative effects, optimize energy retention, and even utilize controlled dissipation as a resource for tasks such as charging or enhancing energy transfer.

Additionally, open quantum battery models provide a valuable framework for studying the interplay between quantum thermodynamics and non-equilibrium processes, shedding light on how open systems can still achieve high performance under realistic conditions.

Potential applications of quantum batteries remain an open question, with various hypotheses being proposed despite the nascent stage of this research. For instance, certain quantum technologies may require energy transfer mechanisms achievable only at energy or time scales accessible to quantum systems. These unique modalities could represent a distinct advantage of quantum batteries.

This section provides a brief overview of key milestones in the field. For a more extensive review, we refer to [134]. While ergotropy is a crucial metric for characterizing the performance of quantum batteries, other concepts such as power and efficiency also play important roles.

In the following subsections, we introduce these concepts, discuss quantum advantages offered by quantum batteries, examine the literature on OQB and analyze a particular model of OQB that will be useful in subsequent chapters. Finally, we discuss experimental implementation concerning quantum batteries.

3.2.1 Key figure of merits

The performance of quantum batteries can be evaluated using several metrics:

- **Ergotropy:** The maximum amount of work extractable from a quantum state via unitary operations, as defined in Eq. (3.3).

- **Capacity:** The maximum work that can be added to a quantum state through unitary operations is called the anti-ergotropy [135]. Formally, it is given by:

  $$\mathcal{A}(\rho_0) = \min_{\hat{U}} \mathcal{W}_U, \tag{3.19}$$

  where $\mathcal{W}_U$ represents the work associated with a unitary transformation. The *capacity* [136] of the battery, is defined as the difference between ergotropy and anti-ergotropy

  $$\mathcal{C}(\rho) = \mathcal{E}(\rho) - \mathcal{A}(\rho). \tag{3.20}$$

  and describes the the maximum amount of work passing through the battery during a charge-discharge loop.

- **Efficiency:** In open systems, efficiency is typically defined as the ratio of work gained by the battery to the total work input:

  $$\eta = \frac{\mathcal{E}}{\mathcal{W}_{\text{cl}}}, \tag{3.21}$$

  where $\mathcal{W}_{\text{cl}}$ is the classical work cost of driving the device [137]. While not fully capturing the amount of work performed during a protocol, the ratio

  $$R = \frac{\mathcal{E}}{E}, \tag{3.22}$$

is also considered in the literature as a measure of efficiency for the charging of open quantum batteries [5]. The value of R is directly related to the purity of the system's state. As will be shown in Chapter 5, pure states allow for the extraction of all their energy as ergotropy when the zero for the energy is set to the energy of the system's ground state, leading to the ratio achieving its upper bound ($R = 1$). For any mixed state, the ratio is lower. A notable example is the maximally mixed state, which maximizes the energy content while having zero ergotropy.

- **Power:** Power quantifies the rate of work extraction and can be expressed either instantaneously, $P(t) = \frac{\mathrm{d}}{\mathrm{d}t}\mathcal{W}(t)$, or as an average over a protocol duration, $\langle P\rangle_\tau = \mathcal{W}_\tau/\tau$.

3.2.2 Quantum Advantage

A significant focus of research has been identifying the quantum advantages of protocols that exploit quantum effects compared to purely classical ones. The pioneering work by Alicki and Fannes [106] suggested that optimal work extraction from a composite quantum battery (consisting of N cells) requires entangling operations.

Subsequent studies [138] demonstrated that optimal work extraction is possible without generating entanglement, provided that at least two-body operations are allowed. However, this comes at the cost of reduced power output due to longer trajectories in state space.

To quantify the advantage in power, the ratio between maximum quantum power and classical power is often considered [108]:

$$\Gamma = \frac{\langle P\rangle_q}{\langle P\rangle_c}. \tag{3.23}$$

Various studies have demonstrated scalable power advantages with quantum protocols, where power scales superextensively for different types of Hamiltonians [107, 108, 139, 140, 109, 141].

For example, in [142], it was shown that for a Hamiltonian with k-body interactions, the scaling is $\propto \gamma k$, where γ is independent of k and N. Models exhibiting superextensive scaling include the Dicke model model [109, 143], the Sachdev-Ye-Kitaev (SYK) model [144, 145], and spin chains [146, 147, 148].

In the Dicke model, investigated by Ferraro et al. [109] and experimentally demonstrated by Quach et al. [143], the power scaling of charging can be enhanced when Two-Level Systems (TLSs) are charged collectively (with all TLSs coupled to the same cavity) or in parallel (each TLS coupled to its own cavity). In the collective case, the scaling with the number of cells N is proportional to $\langle P\rangle_\tau \propto N\sqrt{N}$, whereas in the parallel case, the scaling is linear in N.

Similar superextensive scaling is observed in the SYK quantum battery model [144, 145], while in spin chain models, the scaling can reach up to N^2 [146].

Using a geometric approach, Julia-Farre et al. [110] derived an upper bound for maximum power:

$$P(t) \leq \sqrt{\Delta E_B^2(t) I_E(t)}, \tag{3.24}$$

where $\Delta E_B^2(t)$ is the variance of the battery Hamiltonian, and $I_E(t)$ is the Fisher information which relates to the speed of the charging process in energy eigenspace. They identified two contributions to $\Delta E_B^2(t)$: a diagonal term causing linear scaling and an entangling term that can produce superlinear scaling.

This distinction helps classify advantages as quantum (from entangling contributions to the variance $\Delta E_B^2(t)$) or collective (from the informational quantity $I_E(t)$). Using their framework, they demonstrated that the advantage in the SYK model is due to non-local correlations and is therefore of quantum origin, while the advantage in the Dicke model is collective.

As of today, an optimal model for quantum batteries is still not identified, with all models actually under scrutiny presenting their own advantages and limitations. The Dicke model and the spin chain that show a collective or quantum advantages face challenges to preserve their advantage in the thermodynamic limit ($N \to \infty$). If the cavity in the Dicke model scales in size such that the ratio N/V is kept constant, with V being the volume of the cavity, then the system does not display any superextensive scaling.

The collective advantage relies on the requisite that as the number of TLSs in the system increases, the size of the cavity remain fixed,which aligns well with typical experimental setups, given the significant size disparity between a cavity ($\sim cm$) and the atoms contained within it ($\sim \mu m$).

The limitations of spin chain in the thermodynamic limits are linked to the need for realizing entangling global unitary for an increasing number of sites. In the model proposed by [146], this could be achieved in the limit of strong nearest-neighbor interaction, leading to an effective Hamiltonian that realizes N-body interactions. However the perturbative nature of this Hamiltonian causes the effective interactions to vanish in the thermodynamic limit, resulting in a decline in power scaling as the system grows in size.

While the SYK model might appear to be an ideal framework for quantum batteries, supporting a quantum advantage in the thermodynamic limit, it should be noted that, among all the systems under investigation, no experimental platform capable of fully realizing this model currently exists.

At present, both the Dicke model [109] and the spin chain model [146] serve as valuable testbeds for exploring quantum advantage in finite-sized systems, outside the thermodynamic limit [143].

3.2.3 Open Quantum Batteries

From the ideal case of closed quantum systems, introducing an interaction with an environment in the dynamics of a quantum battery leads to a significantly different framework. This framework is characterized by both the detrimental effects of environmental interactions [137, 115, 5, 149] that can spurs idea in developing control strategies to counteract the impact of noise [150, 151, 152] , and the opportunities they present, such as leveraging the environment to assist charging [116, 153, 154], or conditioning the battery state via environmental measurements [2, 112].

More importantly, a realistic thermodynamic framework necessitates the inclusion of irreversible operations [155], as idealized reversible scenarios fail to capture key thermodynamic properties.

The study of open quantum batteries (OQB) interacting with Markovian environments has been extensive and remains one of the most comprehensively explored scenarios [5, 137, 156]. Open-system dynamics introduce dissipative effects such as decoherence and thermalization, which can hinder battery performance.

A considerable research effort has been devoted to mitigating environmental effects and stabilizing the charging process [153, 112, 157, 158].

Models of quantum battery charging typically fall into two categories:

- **Direct Environment Interaction:** The battery interacts directly with an environment, often with an initial charge or an applied drive.
- **Charger-Mediated Interaction:** The battery exchanges energy via an auxiliary system called a charger.

In the context of open quantum batteries, this distinction gains further importance as the charger mediates both the energy exchange and environmental effects.

A Markovian charged-mediated open quantum battery In [5], the authors investigate several charger-mediated open quantum battery models interacting with a Markovian environment. Among these, the qubit-qubit battery-charger model serves as an instructive case study and a benchmark for subsequent analyses.

The model involves a composite system where both the battery and charger are initially in their ground states.

The qubit B represents the quantum battery itself, with free Hamiltonian $\hat{H}_{B,0} = (\omega_0/2)\hat{\sigma}_z^{(B)}$, and it interacts with another qubit C that corresponds to the charger, via an energy-exchange interaction

$$\hat{H}_{BC} = g\left(\hat{\sigma}_-^{(B)}\hat{\sigma}_+^{(C)} + \hat{\sigma}_+^{(B)}\hat{\sigma}-^{(C)}\right), \qquad g \geq 0. \tag{3.25}$$

The Hamiltonian for the charger is the sum of two terms, $\hat{H}_C = \hat{H}_{C,0} + \hat{H}_{\mathsf{drive}}$, where $\hat{H}_{C,0} = (\omega_0/2)\hat{\sigma}_z^{(C)}$ is the free Hamiltonian of the charger, while

$$\hat{H}_{\mathsf{drive}} = \alpha\left(e^{-i\omega_0 t}\hat{\sigma}_+^{(C)} + e^{+i\omega_0 t}\hat{\sigma}_-^{(C)}\right), \qquad \alpha \geq 0 \tag{3.26}$$

represents the driving of the charger qubit, injecting energy in the system via a laser driving at frequency ω_0.

In [5], the charger is subjected to an amplitude damping due to the interaction with a memoryless environment at finite inverse temperature β, with dumping rate κ. By going to the interaction picture with respect to the Hamiltonian $\hat{H}_0 = \hat{H}_{B,0} + \hat{H}_{C,0}$, the dynamics of the battery and charger state is described by the Lindblad equation

$$\frac{d\rho}{dt} = -i[\hat{H}'_{BC}, \rho] + \kappa\,(N_b(\beta) + 1)\,\mathcal{D}[\hat{\sigma}_-^{(C)}]\rho + \kappa\,(N_b(\beta))\,\mathcal{D}[\hat{\sigma}_-^{(C)}]\rho\,, \tag{3.27}$$

where

$$\hat{H}'_{BC} = g\left(\hat{\sigma}_-^{(B)}\hat{\sigma}_+^{(C)} + \hat{\sigma}_+^{(B)}\hat{\sigma}_-^{(C)}\right) + \alpha\,\hat{\sigma}_x^{(C)}\,, \tag{3.28}$$

and N_b is the mean number of bath quanta at frequency ω_0 given by the Bose-Einstein distribution

$$N_b(\beta) = \frac{1}{\exp\{\beta^{-1}\omega_0\} - 1}. \tag{3.29}$$

Analytical integration of this equation yields expressions for figures of merit such as total energy and ergotropy of the battery. For instance, when the driving term is absent

($\alpha = 0$), energy can be deposited in the battery, but no ergotropy is generated:

$$E_B(\infty)\Big|_{\alpha=0} = \omega_0 N_f(\beta), \tag{3.30}$$

$$\mathcal{E}(\infty)\Big|_{\alpha=0} = 0, \tag{3.31}$$

where N_f is the average fermionic occupation number

$$N_f(\beta) = \frac{1}{\exp\{\beta^{-1}\omega_0\} + 1}. \tag{3.32}$$

In the zero-temperature regime with high damping ($\kappa \gg \alpha$) and specific parameter tuning ($\alpha = \sqrt{(\sqrt{2}+1)/2g} \approx 1.09g$), the system achieves maximum ergotropy:

$$\mathcal{E}_{max}(\infty) = \frac{\sqrt{2}-1}{2}\omega_0 \approx 0.207\omega_0. \tag{3.33}$$

3.2.4 Experimental Progress

While still in its infancy, the literature on quantum batteries includes some early experimental results. Various platforms have been leveraged to study the processes of charging and discharging quantum batteries, among which all quantum computing platforms are suitable for such experiments.

Superconducting circuit represents an an ideal platform to simulate the Tavis-Cummings (TC) model [159], as it has coherence lifetime long enough to experiment with different charging or discharging protocols, and can be scaled enough to verify eventual collective effects. One of the first examples of a physical realization of a quantum battery was presented in [160], which used a superconducting system as the platform. In this study, the battery model consisted of a single qutrit coupled to a single-mode cavity. As a single-cell battery, it did not allow for the study of quantum advantage or superextensive effects. However, it successfully demonstrated the experimental feasibility of charging and discharging protocols. Further studies on superconducting qubits were conducted on platforms like IBM Q, as reported in [161] and [162]. Of these, one [163] involve a protocol related to what will be discussed in Chapter. 5.

An important milestone in the field provided experimental proof of superextensive power in [143], where the authors used an optical cavity containing organic dye molecules acting as two-level systems (TLS). This setup offered a physical implementation of the Dicke model. By varying the dye concentration, the authors could adjust the number of battery cells in the system, enabling a demonstration of power scaling with the number of cells. Organic materials for such setups can be different, based on the desired properties of the system. In their experiment, the authors were able to study the charging protocol for the TLSs, and demonstrate the superextensive scaling, however, they were unable to show controlled discharge of the battery due to fast radiative emission.

A possible solution to address this issue can be achieved by designing an ensembles of TLS made of different materials. In a more recent work [164], the authors propose a QB based on the Dicke model with a multi-layer microcavity, with an absorption layer and an acceptor layer of dyes. The absorption layer is responsible for the absorption of light, while the acceptor layer is responsible for energy storage. Choosing the dye material appropriately, the authors results suggest that this configuration allow to greatly enhance the stored energy density and self-discharge time, while only minimally affecting charging power.

The Dicke model can be realized also through inorganic microcavities with semiconductor nanostructures such as quantum dots and quantum wells coupled to optical microcavities [165]. Semiconductor nanostructures display properties that are highly tunable by optical fields, which can be exploited to fine tune the light-matter interaction. This makes this kind of platform ideal for the implementation of precise charging and discharging protocols. A first experiment based on quantum dots is due to Wenniger and colleagues [166]. In their work, the authors were able to quantify the amount of work that could be extracted from the system and used to drive an external field.

To simulate spin chain system, platform such as nuclear spin can be leveraged. In a first endeavour, a QB has been realized by Joshi and colleagues [167], using nuclear spin located on central atoms, interacting with surrounding spins acting as the chargers. The authors used different molecules and were able to investigate different charging protocols and estimate the ergotropy of the system. Notably, as it was based on only a single spin, no collective effect could be investigated.

All of these implementations, while still limited in scale, represent significant progress and provide a foundation for future investigations, offering a first step toward validating theoretical predictions. Collective effect are still to be validated over most platform, as only a single experiment realized on an organic microcavity [143] were able to provide demonstration of superextensive scaling. Improvements in terms of designs, to increase the storage time, and develop controlled charging and discharging protocol are being proposed.

3.3 Daemonic work extraction

Informational thermodynamics explores the thermodynamic consequences of information processing [168, 169, 170, 171].

The field has its conceptual roots in Maxwell's demon, a thought experiment by James Clerk Maxwell, which posits that acquiring and utilizing information can have thermodynamic implications beyond the classical laws.

Maxwell proposed a thought experiment involving a sentient being, later referred to as the demon, capable of observing gas particles and acting based on their velocities. The setup consists of a box of gas divided into two compartments, with the demon controlling a gate between them. By selectively opening the gate for faster-than-average particles heading to one side and slower particles to the other, the demon could create a temperature gradient, seemingly violating the second law of thermodynamics.

Modern interpretations frame the demon's actions as measurements and feedback operations [124, 172, 173, 174], where it measures particle velocities and uses the outcomes to direct its actions.

The apparent paradox was resolved in the mid-20th century during the rise of information theory. Landauer's principle provided a physical basis, asserting that the erasure of information in an irreversible process generates a corresponding amount of heat [96]. This principle established a direct link between informational and thermodynamic irreversibility, establishing the physical role of information.

Experimental validation of Landauer's principle, previously impossible due to limitations in controlling microscopic systems, has emerged in recent decades. These experiments involved a single colloidal particle in a double well [175], trapped ultra-cold ion [176], and nuclear spins [177].

Following the idea behind Maxwell's demon, it is possible to enhance the extractable work from quantum system on which it is possible to perform measurements. In this section, we explore enhancement that can be achieved to the work extracted through either unitary or thermal operations.

Analytically, both the ergotropy and the work extractable from thermal operations are convex functionals. This means that if a state can be expressed as a convex combination—i.e., decomposing a mixed state into its components such as

$$\rho = \sum_a p_k \rho_k, \tag{3.34}$$

then the following inequalities hold:

$$\mathcal{E}(\rho) = \mathcal{E}(\sum_a p_k \rho_k) \leq \sum_k p_k \mathcal{E}(\rho_k), \tag{3.35}$$

$$\mathcal{W}_\beta(\rho) = \mathcal{W}_\beta(\sum_a p_k \rho_k) \leq \sum_k p_k \mathcal{W}_\beta(\rho_k). \tag{3.36}$$

According to these relations, on average, it is possible to extract more work from the individual states that compose the ensemble ρ than from the mixed state itself, by optimizing the extraction for each components instead of optimizing it for the average.

This property can be exploited in the context of quantum measurement. Quantum measurements directly influence the thermodynamics of a quantum system through two mechanisms: the back-action effect of the measurement and the informational processing aspect. Measurement back-action unravels the system's state into a convex combination of post-measurement states, where each component corresponds to a state conditioned on a specific measurement result.

Taking advantage of this enhancement is often considered a form of feedback control technique, as to extract more work the optimal extraction protocol must also be conditioned by the measurement outcome. This approach leverages the informational aspect of measurements, using the knowledge gained to tailor operations to each outcome.

This concept of extracting work by performing a measurement and utilizing the acquired information to optimize subsequent operations shares similarities with the functioning of Maxwell's demon.

The enhancement to the work extraction due to measurement has been interpreted in term of one of the known fundamental resource of quantum inforamtion theory: quantum correlations[178, 179, 180, 181, 182, 183, 184, 185, 186, 187].

In particular, correlations allow the acquisition of information to perform the feedback operation through indirect measurement. The role of correlation as a possible resource for work extraction is still debated, including in this context what role have classical correlations compared to quantum ones.

In the following we quantify the amount of work that can be extracted by indirect measurement and relates the gain obtained in term of the amount of correlations in the systems examined and their nature.

3.3.1 Daemonic ergotropy

The concept of measurement-enhanced ergotropy, or *daemonic ergotropy*, was introduced in [173] to describe the boost in work extraction enabled by correlations with auxiliary systems.

We consider the following setup. A bipartite system consists of a main system S with Hamiltonian $\hat{H}_s$, initially prepared in a joint state ρ^{SA} with an auxiliary system A. Without having access to the auxiliary system, the maximum amount of work that can be extracted from S is given by the ergotropy of its reduced density operator, i.e.,

$$\rho^S = \mathrm{Tr}_A\left[\rho^{SA}\right] \tag{3.37}$$

$$\mathcal{E}(\rho^S) = E(\rho^S) - \mathrm{Tr}\left[\hat{H}_s \hat{U}_{ext} \rho^S \hat{U}^\dagger_{ext}\right], \tag{3.38}$$

in accordance with what described in Sec. 3.1.1.

If it is possible to perform measurement on the auxiliary system, the result changes as follows. Applying a POVM $\{\Pi^A_a\}$ on the auxiliary system conditions the state of the system S accordingly, with the conditioned state given by

$$\rho^{S|a} = \frac{1}{p_a}\mathrm{Tr}_A\left[\rho^{SA}(\hat{\mathbb{1}}^S \otimes \hat{\Pi}^A_a)\right], \tag{3.39}$$

where

$$p_a = \mathrm{Tr}_{SA}[\varrho^{SA}(\hat{\mathbb{1}}^S \otimes \hat{\Pi}^A_a)] \tag{3.40}$$

is the probability to obtain the outcome a.

The ergotropy of the conditional state $\rho^{S|a}$ is expressed as:

$$\mathcal{E}(\rho^{S|a}) = E(\rho^{S|a}) - \mathrm{Tr}\left[\hat{H}_s \hat{U}_a \rho^{S|a} \hat{U}^\dagger_a\right], \tag{3.41}$$

where $\hat{U}_a$ is the unitary operation that optimizes work extraction for the measurement outcome a.

The daemonic ergotropy, defined as the average over all possible measurement outcomes, is given by:

$$\overline{\mathcal{E}}_{\{\Pi^A_a\}} = \sum_a p_a \mathcal{E}(\rho^{S|a}) \tag{3.42}$$

$$= E(\rho^S) - \sum_a p_a \,\mathrm{Tr}\left[\hat{H}_s \hat{U}_a \rho^{S|a} \hat{U}_a\right], \tag{3.43}$$

where we used the linearity of the trace to simplify the first term.

If we consider the spectral decomposition of $\hat{H}_s$ and $\rho^{S|a}$ as in Eqs. (3.5, 3.6), the daemonic ergotropy can also be expressed as:

$$\overline{\mathcal{E}}_{\{\Pi^A_a\}} = E(\rho^S) - \sum_a p_a \sum_k r^a_k \varepsilon_k. \tag{3.44}$$

Even when performing the measurement, if the extraction for each outcome is not optimized, so that at each realization $\hat{U}_a \to \hat{U}_{ext}$, only the ergotropy of the unconditional state will be extracted on average. Therefore the daemonic ergotropy becomes $\overline{\mathcal{E}}_{\{\Pi^A_a\}} = \mathcal{E}(\rho^S)$, leading to no effective boost to the work extraction.

It is useful to define the daemonic gain as

$$\Delta\overline{\mathcal{E}}_{\{\Pi^A_a\}} = \overline{\mathcal{E}}_{\{\Pi^A_a\}} - \mathcal{E}(\rho^S) \geq 0 \tag{3.45}$$

which represents the ergotropy gain due to the measurement. The positivity follows directly from the convexity of the ergotropy (3.35).

The equality is achieved only in the case when the initial state ρ^{SA} can be factorized

$$\rho^{SA} = \rho^S \otimes \rho^A, \tag{3.46}$$

while for any other case the daemonic ergotropy is always an improvement to the ergotropy.

This property will be instrumental in later chapters for deriving upper and lower bounds on the daemonic ergotropy. Specifically, it is bounded as

$$\mathcal{E}(\rho^S) \leq \Delta\overline{\mathcal{E}}_{\Pi_a^A} \leq E(\rho^S), \tag{3.47}$$

where the upper bound is achieved when ρ^{SA} is pure and the measurement is described by rank-1 projectors, as will be detailed in Chapter 5.

The positivity of the daemonic gain is one of the main results in [173]. Another result of the study classifies the daemonic gain $\Delta\overline{\mathcal{E}}_{\{\Pi_a^A\}}$ as a witness of quantum discord.

The quantum discord [188] $\mathcal{D}$ for the state ρ^{SA} of a bipartite system SA is defined as

$$\mathcal{D}(\rho^{SA}) = \mathcal{I}(\rho^{SA}) - \max_{\hat{\Phi}_a^S} \mathcal{J}(\rho^{SA}), \tag{3.48}$$

where:

- $\mathcal{I}(\rho^{SA}) = S(\rho^S) + S(\rho^A) - S(\rho^{SA})$ is the mutual information between S and A.
- the maximization is performed over all possible orthogonal measurements set $\hat{\Phi}_a^S$.
- $\mathcal{J}(\rho^{SA})$ is the quantum-classical mutual information that quantify the classical information contained in a quantum state and is defined as

$$\mathcal{J}(\rho^{SA}) = S(\rho^S) - \sum_a p_a S(\rho^{S|a}) \tag{3.49}$$

From its definition, it is evident that the quantum discord quantifies the non-classical portion of correlations contained in the system. The theorem proved in the work by Francica and colleagues [173] demonstrates that $\Delta\overline{\mathcal{E}}_{\{\Pi_a^A\}} = 0 \implies \mathcal{D}(\rho^{SA}) = 0$, that is non-zero discord is a sufficient condition for daemonic gain via any possible quantum measurement.

In general, the information acquired depends on the specific measurement performed. Consequently, strategies for identifying the optimal measurement to maximize the daemonic ergotropy are actively being developed [189].

3.3.2 Daemonic work extracted via thermal operations

Feedback protocols conditioned on measurement outcomes not only enhance the ergotropy of a system, but can also enhance work extraction under thermal operations. This process was characterized in [124].

Here we consider the same setup as in the previous section, but provide equivalent results for the mathematical framework describing work extracted through thermal operations.

If the maximum extractable work from the subsystem S is given by $\mathcal{W}_\beta(\rho^S)$, and we quantify the change in free energy due to a measurement with outcome a as

$$\Delta\mathcal{F}_\beta^{S|a} = \mathcal{F}_\beta(\rho^{S|a}) - \mathcal{F}_\beta(\rho^S), \tag{3.50}$$

then the total extractable work, conditioned on outcome a, is given by

$$\mathcal{W}(\rho^{S|a}) = \mathcal{W}_\beta(\rho^S) + \Delta\mathcal{F}_\beta^{S|a}. \tag{3.51}$$

The total work extracted, averaged over all outcomes, is:

$$\overline{\mathcal{W}}_{\{\hat{\Pi}_a^A\}} = \sum_a p_a \mathcal{W}(\rho^{S|a}) = \sum_a p_a \Delta\mathcal{F}_\beta^{S|a} + \mathcal{W}_\beta(\rho^S). \tag{3.52}$$

To take advantage of the enhancement, the protocol must be conditioned by the outcome of the measurement.

The extraction protocol adapts as follows: after obtaining outcome a, the Hamiltonian of S is quenched to $\hat{H}_{\rho^{S|a}} = \ln[\rho^{S|a}]/\beta$, followed by an isothermal quasistatic process where the Hamiltonian returns to $\hat{H}_S$.

As with the previous result concerning the daemonic gain, the convexity of the free energy as in Eq. (3.36) in this case also guarantees that

$$\Delta\overline{\mathcal{W}}_{\{\hat{\Pi}_a^A\}} = \overline{\mathcal{W}}_{\{\hat{\Pi}_a^A\}} - \mathcal{W}_\beta(\rho^S) \geq 0, \tag{3.53}$$

meaning that the gain due to measurement is always positive and, as in the previous case, the lower bound is achieved only for separable states.

An important result can be obtained if we explicitly evaluate the term $\sum_a p_a \Delta\mathcal{F}_\beta^{S|a}$,

$$\begin{aligned}\Delta\overline{\mathcal{W}}_{\{\hat{\Pi}_a^A\}} &= \sum_a p_a \Delta\mathcal{F}_\beta^{S|a} \\ &= \beta^{-1}\left(S(\rho^S) - \sum_a p_a S(\rho^{S|a})\right) \\ &= \beta^{-1}\mathcal{J}(\rho^{SA})\end{aligned} \tag{3.54}$$

where we applied the definition of $\mathcal{F}_\beta$ and used the linearity of the trace to simplify the term proportional to the energy.

In the last line we identified the quantity $\mathcal{J}$, which was previously defined as the QC-mutual information. Notably, only the classical part of the SA correlations contributes to enhancing the extractable work.

To interpret this result, we recall that the quantum discord quantifies the amount of correlations in a bipartite system that cannot be accessed by local measurements on one of the subsystems. This result further provides a classification on the nature of correlations required for the enhancement of work extraction.

3.4 Energetic cost of measurement

The thermodynamic implication of measuring and information were first introduced as a possible resolution to Maxwell's demon, with the interpretation that information processing, especially acquisition, comes at the cost of some irreversibility whenever the information acquired is later discarded, generating heat.

We previously showed that acquiring information leads to an enhancement in the extractable work upper bounded by $\beta^{-1}\mathcal{J}$. However, to ensure consistency with the second law of thermodynamics, this result must be contextualized within a broader thermodynamic framework.

As introduced, the second law can be derived from the fluctuation theorems, or from the Jarzynki equality [95, 190]:

$$\langle e^{\beta W} \rangle = e^{-\beta \Delta \mathcal{F}_\beta}. \tag{3.55}$$

Here, W represents the work done by the system during a non-equilibrium stochastic process, and $\Delta\mathcal{F}_\beta$ is the equilibrium free energy difference between the initial and final states of the system. This equation relates the work done by the system, averaged over many repetitions of the process, to the equilibrium free energy difference.

Applying Jensen's inequality to the Jarzynski equality yields:

$$\langle W \rangle \leq -\Delta \mathcal{F}_\beta, \tag{3.56}$$

which is the second law of thermodynamics for a microscopic setting.

Using Eq. (3.54) it is easy to show that the maximum work extracted on average in the setting discussed in the previous section is bounded as

$$\overline{\mathcal{W}}_{\{\Pi_a^A\}} \leq -\Delta \mathcal{F}_\beta + \beta^{-1}\mathcal{J}, \tag{3.57}$$

which seemingly allows for a violation of the second law on average.

The seminal work by Sagawa and Ueda [104] addressed this issue by explicitly quantifying the work cost of quantum measurement and subsequent information erasure. They derived an upper bound for extracted work that aligns with the equation above, establishing the second law of informational thermodynamics.

Interestingly, [104] found a measurement cost proportional to $\beta^{-1}\mathcal{J}$, consistent with independent results by [124]. This supports the conservation of work under ideal conditions, even in the context of information processing.

As [100] succinctly stated, "the energy cost of the measurement is the work value of the acquired information."

In this section, we review the results of [105], who rigorously validated the second law of informational thermodynamics under a generalized framework. Before doing that, we review the problem of Maxwell's demon and provide an abstract characterization of its elements that can be adapted to both the classical and quantum regimes.

3.4.1 Formal characterization of a Maxwell's demon

The fundamental constituents for the setup of Maxwell demon are the following:

- **Main system**: the system from which information is acquired and after the feedback operation is used to extract work. In the original formulation, a gas of particle in a box is the system under consideration. In modern formulations, both classical and quantum system can be used.
- **The detector**: it acquires information from the main system and stores it in the memory. In the quantum formulation of the problem the detector can consists of multiple elements: a system acting as a probe, a set of POVM enacting the measurements. Sometimes the memory is also considered part of the detecting apparatus

- **The memory**: The memory is a system that stores the information acquired from the detector. Based on its state after the measurement, feedback operations are performed on the system. To properly account for the energy costs of the whole process, the state of the memory, and all the rest of the controlling apparatus, must be restored to the initial state.

- **The demon**: It performs actions on the system based on the measurement outcome, effectively coordinating the measurement, feedback, and work extraction process. In modern formulations, it is abstractly represented by a conditional operation performed on the main system.

- **The heat bath**: it is used as a source of irreversibility. In the final steps of the process, it enables the erasure of the information from the memory. The increase in entropy due to the erasure ensures the overall consistency of the framework with the principles of thermodynamics.

By properly accounting for the energetic contributions of all components, a coherent thermodynamic picture emerges, illustrating the energetic value of information.

3.4.2 Universal validity of the second law of informational thermodynamics

In their work [105] the authors validate the second law of informational thermodynamics in a generalized framework. We will now introduce their results. To notice, in this section, we adopt the notation used in the work by Minagawa and colleagues [105], which may differ from the rest of the thesis. In Chapter 6, where these results are used, any differences in notation will be explicitly addressed. The setup considered by the authors consists of:

- a main system A, initially in an arbitrary state ρ_0^A, from which work will be extracted,

- a memory M, acting as a probe for system A, initially in an arbitrary state ρ_0^M,

- a classical record K, initially in the state $|0\rangle\langle 0|^K$,

- a heat bath B_1, initially in equilibrium, serving as an auxiliary system for the work extraction step,

- a second heat bath B_2, also in equilibrium, aiding in the memory erasure step.

Both heat baths are assumed to be in equilibrium at the same inverse temperature β. Initially, all subsystems are uncorrelated, and the composite state factorizes as:

$$\rho_0 = \gamma^{B_1} \otimes \rho_0^A \otimes \rho^M \otimes |0\rangle\langle 0|^K \otimes \gamma^{B_2} \tag{3.58}$$

The process proceeds through the following steps:

- **Measurement preparation** ($t = t_1$): A unitary interaction $\hat{U}$ couples the memory M and the main system A,

$$\rho_1 = \gamma^{B_1} \otimes \hat{U}(\rho_0^A \otimes \rho^M)\hat{U}^\dagger \otimes |0\rangle\langle 0|^K \otimes \gamma^{B_2}. \tag{3.59}$$

- **Read-out** ($t = t_2$): A POVM $\{\hat{M}_k^M\}$ is applied to the memory M, and the outcomes are recorded in the classical register K. The state becomes:

$$\rho_2 = \sum_k p_k \rho_{2,k}, \tag{3.60}$$

where

$$\rho_{2,k} = \gamma^{B_1} \otimes \rho_{2,k}^{AM} \otimes |k\rangle\langle k|^K \otimes \gamma^{B_2}. \tag{3.61}$$

with

$$\rho_{2,k}^{AM} = \frac{1}{p_k} \left(\mathbb{I}^A \otimes \hat{M}_k^M\right) \left(\hat{U}(\rho_0^A \otimes \rho^M)\hat{U}^\dagger\right) \left(\mathbb{I}^A \otimes \hat{M}_k^M\right) \tag{3.62}$$

and

$$p_k = \mathrm{Tr}\left[\left(\mathbb{I}^A \otimes \hat{M}_k^M\right) \left(\hat{U}(\rho_0^A \otimes \rho^M)\hat{U}^\dagger\right) \left(\mathbb{I}^A \otimes \hat{M}_k^M\right)\right]. \tag{3.63}$$

- **Work extraction** ($t = t_3$): A unitary

$$\hat{F} = \sum_k \hat{F}_k^{B_1 A} \otimes |k\rangle\langle k|^K \tag{3.64}$$

couples system A with the heat bath B_1 to extract work conditioned on the state of the memory $|k\rangle\langle k|$. The composite state becomes:

$$\rho_3 = \left(\hat{F} \otimes \mathbb{I}^{MB_2}\right) \rho_2 \left(\hat{F}^\dagger \otimes \mathbb{I}^{MB_2}\right) = \sum_k p_k \rho_{3,k}, \tag{3.65}$$

where

$$\rho_{3,k} = \rho_{3,k}^{B_1 AM} \otimes |k\rangle\langle k|^K \otimes \gamma^{B_2}. \tag{3.66}$$

and

$$\rho_{3,k}^{B_1 AM} = \left(\hat{F}_k^{B_1 A} \otimes \mathbb{I}^M\right) \left(\gamma^{B_1} \otimes \rho_{2,k}^{AM}\right) \left((\hat{F}_k^{B_1 A})^\dagger \otimes \mathbb{I}^M\right) \tag{3.67}$$

- **Erasure** ($t = t_4$): A unitary $\mathcal{V}$ acts on MK and B_2, resetting MK to its initial state:

$$\rho_4 = \left(\mathbb{I}^{B_1 A} \otimes \mathcal{V}^{MKB_2}\right)(\rho_3). \tag{3.68}$$

We specify that the operation $\hat{F}_k^{B_1 A}$ which implements the work extraction step can represent both a global unitary operation on the heat bath B_1 and the system A or a "pure" unitary acting only on A. In the latter case the operation is restricted to the for $\hat{F}^{B_1 A} = \mathbb{I}^{B_1} \otimes \hat{F}^A$. Both type of operations can therefore be analyzed in this framework.

Using this framework, the authors derived bounds for the extracted and injected work:

$$W_{\text{ext}}^A = -\Delta F_{0\to 4}^A + \beta^{-1}\left[I_{GO} - I(A:K)_{\rho_3} - S_{\text{irr}}^{B_1}\right], \tag{3.69}$$

$$W_{\text{in}}^{MK} = \beta^{-1}\Delta S_{0\to 2}^{AMK} + \beta^{-1}\left[I_{GO} + I(A:M|K)_{\rho_2} + S_{\text{irr}}^{B_2}\right] \tag{3.70}$$

The terms for the equations above are defined as follows:

- $\Delta F^A_{0\to 4} = \mathcal{F}_\beta(\rho^A_4) - \mathcal{F}_\beta(\rho^A_0)$, the free energy change
- $I_{GO} = S(\rho^A_0) - \sum_k p_k S(\rho^A_{2,k})$ is the Groenewold–Ozawa information gain [191, 192]
- $I(A:K)_{\rho_3} = S(\rho^A_3) - \sum_k p_k S(\rho^A_{3,k})$, is the Holevo information of the conditional states
- $S^{B_1}_{\text{irr}}$ is the irreversible entropy production associated with the extraction step defined as

$$S^{B_1}_{\text{irr}} = \sum_k p_k \Big(I(A:B_1)_{\rho_{3,k}} + S(\rho^{B_1}_{3,k} | \gamma^{B_1}) \Big) \geq 0 \tag{3.71}$$

- $\Delta S^{AMK}_{0\to 2} = S(\rho^{AMK}_2) - S(\rho^{AMK}_0)$, the difference in the Von Neumann entropy of the states
- $I(A:M|K)_{\rho_2} = \sum_k p_k \Big(S(\rho^A_{2,k}) + S(\rho^M_{2,k}) - S(\rho^{AM}_{2,k}) \Big)$ is the conditional mutual information
- $S^{B_2}_{\text{irr}}$ is the irreversible entropy production associated with the erasure step, defined as

$$S^{B_2}_{\text{irr}} = I(MK:B_2)_{\rho_4} + S(\rho^{B_2}_4 | \gamma^{B_2}) \geq 0 \tag{3.72}$$

These results generalize the second law of informational thermodynamics by Sagawa and Ueda, from which it can be easily recovered. Effectively, by discarding terms that are always positive or negative, universal bounds for work extraction and injection can be derived. Specifically, the work extracted is upper-bounded as:

$$W^A_{\text{ext}} \leq -\Delta F^A_{0\to 4} + \beta^{-1} I_{GO} \tag{3.73}$$

while the work injected is lower-bounded as:

$$W^{MK}_{\text{in}} \geq \beta^{-1} \left[\Delta S^{AMK}_{0\to 2} + I_{GO} \right]. \tag{3.74}$$

Eq. (3.73) is the upper bound for the work extracted and is a generalization of the second law of informational thermodynamics by Sagawa and Ueda [104] where instead of I_{GO}, the informational gain is quantified by the quantum-classical mutual information $\mathcal{J}$, as defined by Eq. (3.49).

We refer to [105] for a discussion on the type of protocol for which the two coincide. Here, we limit ourselves to pointing out that, while the quantum-classical mutual information is always positive, the Groenewold-Ozawa information gain is not guaranteed to be.

The bound in Eq. (3.73) can be saturated when $I(A:K)_{\rho_3} = S^{B_1}_{\text{irr}} = 0$. The irreversible entropy production $S^{B_1}_{\text{irr}}$ is trivially zero if the extraction protocol is pure unitary, but it is not a necessary condition for it to be zero. Conversely, a pure unitary is generally insufficient for the Holevo information $I(A:K)_{\rho_3}$ to vanish. For the latter to be zero, it is necessary that the entropy of all passive states is the same so that $S(\rho^A_{3,k} = S(\rho^A_{3,k'}),\ \forall\, k, k'$.

Since unitary operations do not change the entropy of a state, the requirement becomes that all post-measurement states must have the same entropy. This can indeed be achieved for specific protocols, but for general measurements, it is not the case.

So, while a thermal operation with zero irreversible entropy production can saturate the bound, the same cannot be generally achieved by a unitary operation.

Similarly, Eq. (3.74) provides the lower bound for the energy cost of the measurement protocol. Saturation of this bound requires $S_{\text{irr}}^{B_2} = 0$ and $I(A : M|K)_{\rho_2} = 0$. For $I(A : M|K)_{\rho_2} = 0$, the post-measurement composite state of AM must be factorized for all measurement outcomes, i.e., $\rho_{2,k}^{AM} = \rho_{2,k}^{A} \otimes \rho_{2,k}^{M}$. This condition depends on the instrument describing the POVM, and is satisfied by the "nuclear" or "measure-and-prepare" type [193].

3.5 Summary

- Work extraction from a closed quantum system is achieved through unitary operations. However, these operations face limitations, particularly in smaller systems. The maximum extractable work from a quantum system is termed ergotropy. As the size of the system increases and the Hamiltonian's eigenlevels become densely spaced, approaching a continuum, ergotropy converges to the classical definition of the difference in free energy.

  In general, this free energy difference serves as an upper bound to ergotropy. Remarkably, this upper bound can be achieved by employing thermal operations, which are global unitary transformations involving both the system and a heat bath.

- A quantum system designed to store energy is referred to as a quantum battery. The study of quantum batteries is relatively recent, with key performance metrics still under development. Research in this field primarily investigates whether quantum phenomena, such as entanglement, can enable these devices to outperform their classical counterparts.

  Current findings suggest that quantum effects may provide a performance advantage, particularly in the scaling of instantaneous power. Another critical focus is on mitigating dissipative effects and stabilizing stored energy in open quantum batteries, ensuring their practical viability.

- Information processing plays a significant role in altering the thermodynamic behavior of physical systems, especially in quantum mechanics, where measurement back-action strongly influences system dynamics. Both ergotropy and work extracted through thermal operations can be enhanced using feedback mechanisms based on measurement outcomes.

  To account for the increased work extraction enabled by such informational contributions, the thermodynamic laws must be modified. This necessity has led to the formulation of the second law of informational thermodynamics, recently extended and proven within a more general framework.

CHAPTER 4

Charging a quantum battery in a non-Markovian environment: a collisional model approach

As discussed in Sec. 3.2.3, in most of the study involving open quantum batteries, the dynamics induced by the environment is Markovian. The Markovian approximation is indeed a useful assumption that simplifies considerably the characterization of the dynamics, but in many circumstances one does need to go beyond it. For example, when the interaction of the system of interest with any further degree of freedom affecting its evolution is not weak or whenever the evolution of the environment takes place on a similar time scale as the one of the system, one should take memory effects into account, and is thus required to describe the dynamics through methods capable to account for non-Markovian behaviour, such as the models introduced in Sec. 2.4.

As regards OQBs, memory effects have been considered only in very few cases. In [115] the authors study the behaviour in time of the energy stored in a qubit coherently driven and whose dissipative dynamics is described via specific non-Markovian master equations, without however discussing the effect on the ergotropy, that is on the maximum amount of actual work extractable from the battery qubit. In [116] the dynamics of a system composed of a qubit-battery and a qubit-charger, with the second initially prepared in an excited state, is considered; there, both systems are interacting with two specific non-Markovian environments, where the initial excitation is eventually lost, and the analysis is focused on the time evolution of the ergotropy characterizing the battery. Finally, in [154] the charging and discharging of a qubit-battery is studied, and either a Markovian or non-Markovian environment plays the role of the charger.

In this chapter we rather consider the following model of an OQB, that has already been put forward in [5] and that is pictured in Fig. 4.1: two qubits, corresponding respectively to battery and charger, interact via an energy exchange Hamiltonian. The energy is injected into the system via a driving Hamiltonian applied to the charger. The charger qubit is also coupled to an environment that will cause decoherence and dissipation for the battery, leading eventually to the steady-state of the dynamics. At variance with [5], where the interaction with a memoryless environment was considered, we will here study the impact of an environment that can induce memory effects on the dynamics of the system.

For this purpose, we exploit as framework to study non-Markovianity the collisional models described in Sec. 2.4, which is defined by Eq. (2.75) in its time-discrete formulation and by Eq. (2.76) in its time-continuous formulation. We remark that CMs have already been employed as a tool for studying the behaviour of OQBs [158, 194, 195, 196, 197, 198, 199]. However in most of these works the stream of ancillas that constitutes the CM plays the role of the charger, except in [195] where it plays the role of the battery itself. In our model, as represented in Fig. 4.1, we instead exploit CMs in order to describe the dissipative environment interacting with the charger qubit.

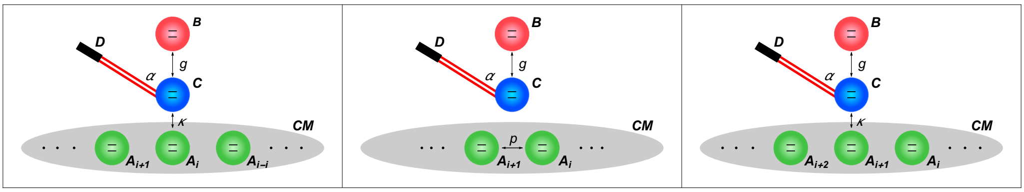

Figure 4.1: A collisional model of an OQB interacting with a non-Markovian environment: (left) two qubit systems representing a battery B (red qubit) and a charger C (blue qubit) interact between themselves for a discrete time δt via a energy-exchange Hamiltonian, with coupling constant g. At the same time, C is driven by an external laser (with frequency α) and interacts with the i-th environmental ancilla A_i, with coupling strength κ; (middle) before the next interaction between system and environment, the i-th and the $(i+1)$-th ancillas interact with each other via an incoherent partial-SWAP operation with probability p; (right) the interaction Hamiltonian is turned on for another time step δt and the charger is put in contact with the next ancillary system.

The structure of this chapter is as follows: in Sec. 4.1, we fix the microscopic details of the model we study. In Sec. 4.2, we present the results in the case of both a discrete-time and a continuous-time evolution, while in Sec. 4.1 the precise connection between non-Markovianity and ergotropy is investigated. Sec. 4.3 concludes the chapter with a final discussion and some outlooks of our work.

4.1 An open quantum battery, from Markovian to non-Markovian

In the following, we use the qubit model of OQB in a Markovian environment studied in [5] as a benchmark for our investigation, thereby fixing the microscopic details of the quantum battery under study.

In our case, the environment is modeled using the collisional model described in Sec. 2.4, where the ancilla-ancilla collision is represented by an incoherent partial swap with swap probability p. This setup captures both a Markovian environment ($p = 0$) and a strongly non-Markovian environment (p close to 1) in its limiting cases.

We already provided a description of the model discussed by Farina and colleagues in Sec. 3.2.3; here, we briefly recall it for convenience. Moreover, compared to the model in [5], our analysis is limited to the case where the environment is described by auxiliary systems in the ground state, corresponding to an environment at zero temperature.

The qubit B, with free Hamiltonian $\hat{H}_{B,0} = \omega_0(\hat{\sigma}_z^{(B)} + \mathbb{I}/2)$, interacts with another qubit C via an energy-exchange interaction

$$\hat{H}_{BC} = g\left(\hat{\sigma}_-^{(B)}\hat{\sigma}_+^{(C)} + \hat{\sigma}_+^{(B)}\hat{\sigma}-^{(C)}\right). \tag{4.1}$$

The Hamiltonian for the charger is the sum of two terms, $\hat{H}_C = \hat{H}_{C,0} + \hat{H}_{\mathsf{drive}}$, where $\hat{H}_{C,0} = \omega_0(\hat{\sigma}_z^{(C)} + \mathbb{I}/2)$ is the free Hamiltonian of the charger, while

$$\hat{H}_{\mathsf{drive}} = \alpha\left(e^{-i\omega_0 t}\hat{\sigma}_+^{(C)} + e^{+i\omega_0 t}\hat{\sigma}_-^{(C)}\right) \tag{4.2}$$

represents the driving of the charger qubit, injecting energy in the system via a laser driving at frequency ω_0.

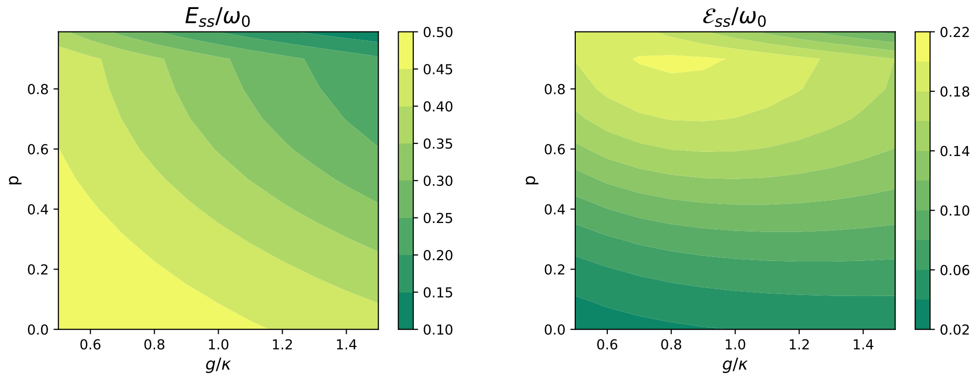

Figure 4.2: Steady-state value for the battery energy E_{ss}/ω_0 (left) and ergotropy $\mathcal{E}_{ss}/\omega_0$ (right) as functions of g/κ and p; with $\alpha = 0.9\kappa$ and $\gamma = 10^2\kappa$. While the energy is monotonously decreasing for both p and g increasing, the ergotropy displays a more complex behaviour. As a function of g, it has a maximum value for $\alpha \approx 1.09g$, which, for our choice of parameters, can be seen in the central area of the plot. As a function of p, it has a non-monotonous behaviour, increasing until it reaches a maximum value for $p \approx 0.9$ before starting to decrease.

By going to the interaction picture with respect to the Hamiltonian $\hat{H}_0 = \hat{H}_{B,0} + \hat{H}_{C,0}$, the effective Hamiltonian of the battery and charger is

$$\hat{H}'_{BC} = g\left(\hat{\sigma}_-^{(B)}\hat{\sigma}_+^{(C)} + \hat{\sigma}_+^{(B)}\hat{\sigma}-^{(C)}\right) + \alpha\,\hat{\sigma}_x^{(C)}\,. \tag{4.3}$$

We benchmark our results against the case of a purely Markovian environment where, as previously stated, the global maximum of the ergotropy is reached in the large-loss limit (i.e. for $\kappa \gg \alpha$), and by tuning driving and coupling such that $\alpha \approx 1.09g$, yielding [5]

$$\mathcal{E}_{\mathsf{max}} = \frac{\sqrt{2}-1}{2}\omega_0 \approx 0.207\omega_0\,. \tag{4.4}$$

In our analysis, we will consider the model discussed in [5] equivalent to ours in the case for $p = 0$, which is true in the continuous-time limit.

Here, we explore what happens beyond this regime by taking into account memory effects induced by the environment, first via a discrete-time collisional model, and then looking at the continuous-time limit.

As in [5] we focus on the steady-state properties of the battery, $\rho_{ss}^{(B)}$, evaluating the average energy, E_{ss}, and ergotropy, $\mathcal{E}_{ss}$.

4.2 Results

4.2.1 Discrete-time collisions

We first study the discrete-time collisional model where the open system consists of the two qubits representing the battery and the charger, with Hamiltonian $\hat{H}_S = \hat{H}'_{BC}$ as in Eq.(4.3), and the charger interacts with the ancillas describing the environment, via a

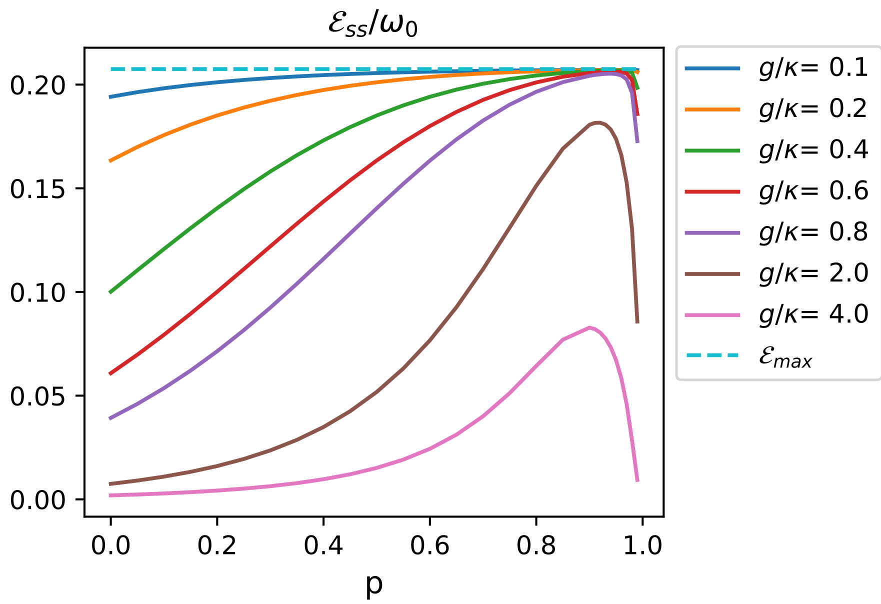

Figure 4.3: Steady-state ergotropy $\mathcal{E}_{ss}/\omega_0$ as function of p for different values of g/κ and fixing the coupling parameter such that $\alpha = 1.09g$ and $\gamma/\kappa = 10^2$. The value for the steady-state ergotropy is upper bounded by the maximum found in the memoryless case in the large-loss limit [5]. Indeed, for $p = 0$, the ergotropy is the higher the lower is g/κ, but when p increases, the ergotropy also starts to increase for all curves at different speed, with the curves further from the large-loss limit exhibiting the largest increment, all plateauing under the boundary condition. Therefore systems that are already in the optimal region of parameters display a mostly flat behaviour, while systems out of that region can achieve the maximum gain from a backflow of information due to the environment.

Hamiltonian that reads

$$\hat{V}_{s,a_i} = \sqrt{\frac{\kappa}{\delta t}} \left(\hat{\sigma}_+^{(C)} \hat{\sigma}_-^{(a_i)} + \hat{\sigma}_-^{(C)} \hat{\sigma}_+^{(a_i)} \right). \tag{4.5}$$

Each system-ancilla collision lasts for a time $\delta t = 1/\gamma$, leading to a unitary evolution of the form

$$\hat{U}_i = e^{-i(\hat{H}_s + \hat{H}_{a_i} + \hat{V}_{s,a_i})\delta t}, \tag{4.6}$$

and we introduce ancilla-ancilla interactions via the incoherent partial-swap map defined in Eqs. (2.72).

We now present our results for the steady state of the battery, focusing on the role of the parameter controlling the information backflow to the battery and the charger, that is the swap-probability p, as well as on the battery-charger coupling g and the driving constant α. We have considered collision rates γ much larger than the other frequencies characterizing the dynamics, so that by setting the swap probability $p = 0$ we (numerically) recover the continuous-time limit dynamics described by Eq. (3.27).

To characterize the battery charging properties in an environment with memory and beyond the large-loss limit, in Fig. 4.2 we plot the steady-state ergotropy and energy as a function of both p and g, by fixing the value of $\alpha = 0.9\kappa$.

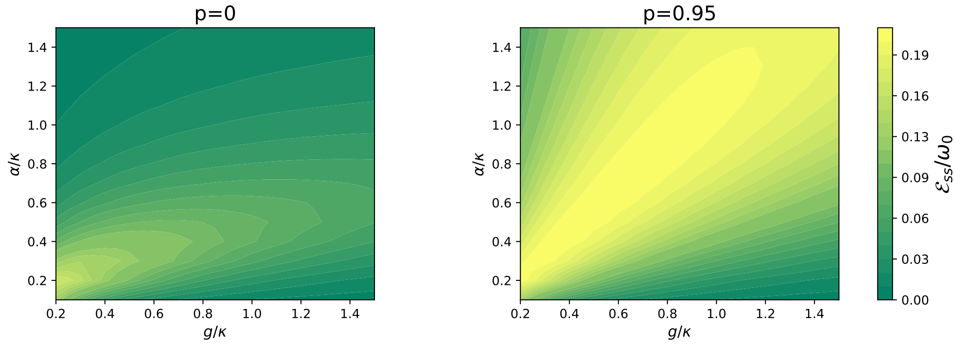

Figure 4.4: Steady-state ergotropy $\mathcal{E}_{ss}$ as function of α and g for fixed values of p (left: $p = 0$; right: $p = 0.95$); $\gamma = 10^2\kappa$. On the left, the steady-state ergotropy shows the same result obtained in [5], i.e., the ideal tuning condition to maximize the ergotropy exists in the large-loss limit, $\alpha \ll \kappa$, for a fixed ratio of α and g. On the right, the same plot realized for a higher value of p, shows how a backflow of information from the environment can extend the optimal tuning region also outside the large-loss limit.

We immediately notice a different behaviour between energy and ergotropy: in particular, while the former shows a generally decreasing behaviour with p, the ergotropy shows a non-monotonous behaviour as a function of both p and g. However, a noticeable optimal region of parameters can be identified, corresponding to $p \approx 0.9$ and $g \approx \alpha$, where the maximum amount of ergotropy is observed. This different behaviour emphasizes the necessity to use a measure of extractable work like the ergotropy as figure of merit for a quantum battery instead of simply evaluating its energy.

Indeed, for fixed values of α/κ and g/κ, increasing p can lead to an increase in the portion of the system maximum extractable energy, its ergotropy, while decreasing the maximum amount of average energy itself. As we remarked in Eq. (3.14), the ergotropy of a qubit can be expressed as a function of the energy and of the purity of the state. The previous observations clearly hint to the fact that the ergotropy enhancement due to the backflow of information from the environment corresponds to the generation of less mixed steady-states.

To further understand this improvement of the ergotropy due to memory effects, we compare the maximum of ergotropy in the region with $p > 0$ with the maximum achieved in the large-loss limit at $p = 0$.

In Fig. 4.3 we therefore show the behaviour of the steady-state ergotropy as a function of the memory parameter p, for different values of the coupling g, and by fixing the driving parameter α such that the optimal condition $\alpha = 1.09g$, identified for the large loss memoryless scenario [5], is satisfied.

We remark that in general, at each value of p, a different optimal tuning condition between α/κ and g/κ can be found. This tuning condition, as we will later describe, is generally close to the value at $p = 0$, and also the difference in the corresponding values of the ergotropy is negligible, as we have numerically verified for all the parameter regimes considered in our plots.

We observe that for small values of α and g, that is towards the large-loss limit, the behaviour of the ergotropy as a function of p is almost flat. Only for larger values of g and α we observe a more evident non-monotonous behaviour of the ergotropy as a function of p, and that an enhancement is observed with respect to the Markovian case

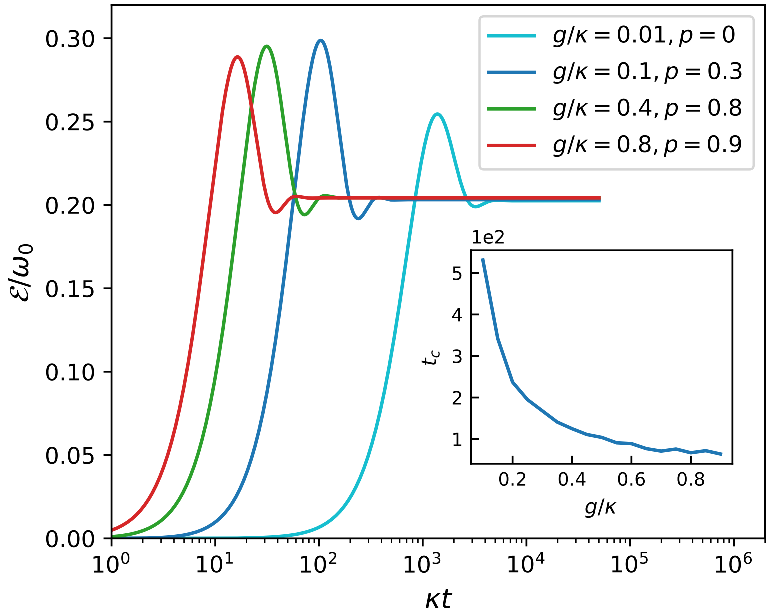

Figure 4.5: Ergotropy as a function of time for different combinations of parameters. For all curves with given values of g/κ and α/κ, the swap probability p has been chosen as the minimum needed to approximate $\mathcal{E}_{\max}$ within one percent of relative error. The inset shows the charging time t_c as a function of g/κ, where the other parameters are chosen following the same logic of the main plot (the charging time t_c is defined as the time necessary for the system to reach its steady state).

$p = 0$, reaching a maximum for a certain, relatively large, value of p.

The most remarkable result we observe in Fig. 4.3 is that the maximum amount of ergotropy $\mathcal{E}_{\max}$ derived in the memoryless case in the large-loss regime (see Eq. (4.4)) maximizes the ergotropy also in our collisional model with memory, but $\mathcal{E}_{\max}$ can be achieved also beyond the large-loss regime in the presence of large enough values of p. As we numerically checked, the maximum value of ergotropy is indeed reached in all the considered regimes via the same steady state, described by Bloch vector components $\langle\hat{\sigma}_x\rangle = -\sqrt{\sqrt{2}-1}$, $\langle\hat{\sigma}_y\rangle = 0$, $\langle\hat{\sigma}_z\rangle = \frac{1}{\sqrt{2}} - 1$.

Importantly, for any value of $g/\kappa \lesssim 1$, and for the right tuning condition between g and α, there is always a value of p for which the ergotropy approximates its maximum value, while this is no longer the case for larger values of g/κ.

We also observe that in our model only coherence contributes to ergotropy, and as a consequence its maximum possible value a priori could be $\omega_0/2$ [200]. However, we find $\mathcal{E}_{\max} < \omega_0/2$ irrespectively of the values of the parameters considered and of the memory properties of the environment, hinting to the fact that the optimal performance of the battery depends on the sole operatorial form of the interaction between battery and charger and between charger and environment.

We then further investigate the optimal tuning condition between α and g to achieve maximum ergotropy. In Fig. 4.4 we plot the steady-state ergotropy as a function of α and g, respectively, in the model without swap, $p = 0$, and for a large swap probability $p = 0.95$. In the former case, we observe as expected that the maximum of the ergotropy is obtained in the large-loss limit $\alpha \ll \kappa$ and for $\alpha = 1.09g$, as analytically demonstrated in [5].

On the other hand, in the case of a collisional model with memory, we now observe an extended region of parameters where one can find large values of the ergotropy, and in particular there exist a linear boundary between the parameters g/κ and α/κ along which the maximum value of the ergotropy can be found for a limited region of the plot, approximately identified by the condition $g/\kappa \lesssim 1$. We can thus conclude that the presence of memory effects allows us to obtain the maximum value of ergotropy $\mathcal{E}_{\mathsf{max}}$ for a larger region in the parameters space.

Besides the steady-state properties of the ergotropy of the battery, also its transient evolution can be indeed of interest, for example because the maximum value can be obtained on different timescales depending on the parameters fixing the dynamics.

In Fig. 4.5, we plot the ergotropy as a function of time for both the memoryless model in the large loss limit ($g/\kappa = 0.01$) and various combinations of the values for the swap probability p and for g/κ; in all these cases α/κ is determined by the optimal tuning condition that maximizes the steady state ergotropy. What is shown is that the various curves reach approximately the same asymptotic value $\mathcal{E}_{\mathsf{max}}$, but this happens the sooner the larger g/κ.

This shows that, if larger values of the coupling g are possible, an accurate choice of p can be done in order to speed up the dynamics and obtain the maximum amount of the ergotropy in a shorter time.

Indeed, one should keep in mind that too large values of p will eventually slow down the stabilization process, as in the limit $p \to 1$ one obtains a unitary dynamics. However a large enough value can still be chosen to approximate the maximum ergotropy at steady state and still speed up the dynamics.

For this reason the values of p leading to the curves in Fig. 4.5 correspond to the minimum value needed, at fixed g/κ, to approximate the maximum state ergotropy. In the inset we plot the time t_c that is required for these curves to reach their steady-state value as a function of g: we indeed observe how larger values of g monotonously lead to a faster charging time.

4.2.2 Continuous-time limit dynamics

As we described in Sec. 2.4, the considered collision-based model with memory leads to a well defined continuous-time limit if we introduce a memory rate Γ, allow the partial-swap probability to be dependent on the collision rate as $p = e^{-\Gamma/\gamma}$, and consider the regime $\Gamma \ll \gamma$. In fact under these conditions, the limit $1/\gamma = \delta t \to 0$ of the collision-based model is well described by the integro-differential ME (2.76), where the map $\mathcal{F}(t)$ also includes the effect of the driving Hamiltonian acting on the charger qubit and the charger-battery coupling Hamiltonian.

We have thus exploited our collisional model to simulate such integro-differential master equation, by considering the regime $\Gamma \ll \gamma$ and by fixing $\gamma/\kappa = 10^3$ (we have checked numerically that equivalent results are obtained by considering larger values of γ and thus approaching the continuous-time limit $\delta t \to 0$).

The results in terms of energy and ergotropy for the steady state of the dynamics are reported in Fig. 4.6. In particular, when compared to the discrete-time model where the energy decreases when increasing p, we observe that the energy has a minimum as a function of the memory rate Γ. On the other hand the ergotropy, which is our main figure of merit, monotonically increases with Γ.

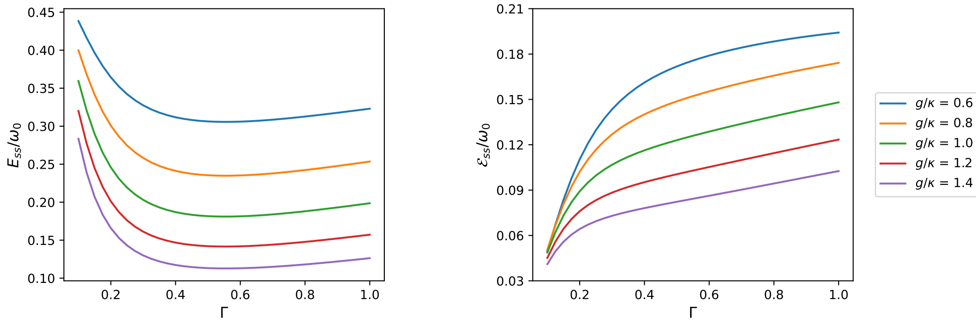

Figure 4.6: Steady-state energy E_{ss}/ω_0 (left) and ergotropy $\mathcal{E}_{ss}/\omega_0$ (right) for the continuous-time limit of the collision based model described by the ME (2.76) as a function of the memory rate Γ. Different curves correspond to different values of the coupling g. Other parameters are fixed as $\alpha = 0.9\kappa$ and $\gamma = 10^3\kappa$ (equivalent results are obtained as expected for larger values of γ, that is towards the continuous-time limit). As functions of the memory rate Γ, energy and ergotropy show opposite behaviours, with the energy decreasing to a minimum as Γ increases, while the ergotropy monotonously increases. In general, for higher values of Γ, more energy passed onto the system can no longer be recovered. This means, in this regime of parameters, that the backflow of information from the environment has a negative impact on the properties of the battery.

This result may seem in contradiction with what we have observed in the previous section for the discrete-time model, as it hints that ergotropy increases when one moves towards the Markovian regime, that is by increasing Γ. However we have to remind ourselves that in order to obtain a well-defined continuous limit, we are restricting to values of p very close to one; consequently, even if a one-to-one correspondence between the discrete- and continuous-time models cannot be properly defined due to the dependence between p, Γ and γ, what we observe in Fig. 4.6 approximately corresponds to the region in Fig. 4.2 where the ergotropy, after having reached its maximum, decreases when p takes large values and approaches one.

Until now, we have studied the steady state ergotropy for different values of the parameter p, which quantifies the probability of having collisions among the environmental ancillas, in turn inducing memory effects in the evolution of the battery and the charger as discussed in Sec. 2.4. On the other hand, to fully understand the role of non-Markovianity in the properties of the battery we need to quantify in an explicit way the amount of memory effects in the dynamics, i.e., to make use of a measure of non-Markovianity. In the next section, we make use of the geometrical measure of non-Markovianity introduced in Sec. 2.3 to interpret the results presented in this section.

4.2.3 Memory effects and steady state ergotropy

In the following we study the behaviour of the geometric non-Markovianity measure $\mathcal{N}_b$, by focusing on the discrete-time scenario. In particular, we evaluate the measure for both the composite system (battery plus charger) $\mathcal{N}_b^{(BC)}$ and for the battery subsystem only $\mathcal{N}_b^{(B)}$.

The non-Markovianity of the composite system, plotted in Fig. 4.7, follows the expected behaviour as it is monotonically increasing with the swap probability p, which in fact quantifies the memory of the environment affecting the composite system. We

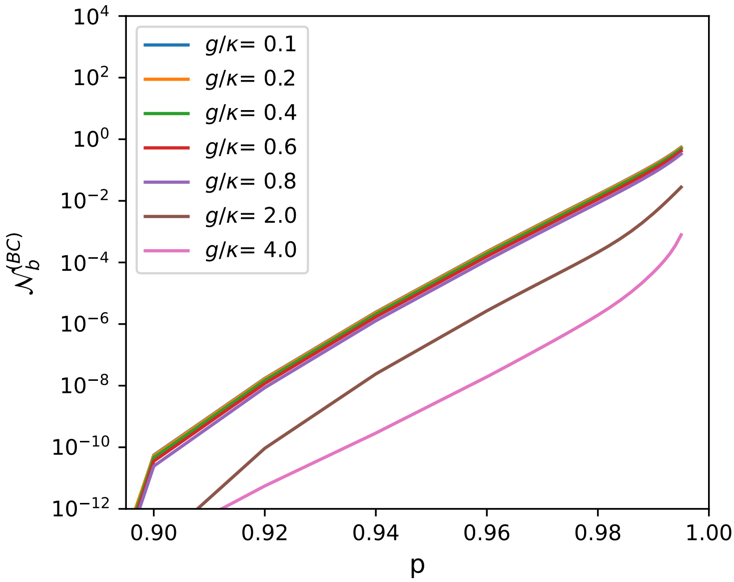

Figure 4.7: Geometrical measure $\mathcal{N}_b^{(BC)}$ for the composite system (charger + battery) as a function of p for different values of g. The other parameters are $\alpha = 1.09g$, $\gamma = 10^2\kappa$. As expected, the geometrical measure grows monotonously with p in the area shown. We remark that for smaller values of p, the measure of non-Markovianity is zero.

also observe that $\mathcal{N}_b^{(BC)}$ is equal to zero in a large region of values of p, the extension of which depends on the the different parameters involved in the dynamics.

If we rather focus on the battery subsystem only, the behaviour of the non-Markovianity measure $\mathcal{N}_b^{(B)}$ is rather different, as one can observe in Fig. 4.8. First, a non-zero value of non-Markovianity is obtained for a memoryless environment, that is for $p = 0$.

A Markovian dynamics of the joint system consisting of the battery and the charger, as fixed by the semigroup map in Eq. (2.4) (or the Lindblad equation (2.8) in the continuous case), can well induce a non-Markovian evolution of the battery only: the two-fold exchange of information between the battery and the charger qubits due to their coherent interaction will generally result in a repeated backflow of information to the battery, with large values of non-Markovianity.

Increasing the value of p the non-Markovianity of the battery has a non-monotonic behavior, which strongly depends on the ratio g/κ. For low values of g/κ ($g \lesssim 2\kappa$), $\mathcal{N}_b^{(B)}$ decreases and reaches zero at different values of the swap probability p, and then suddenly increases for $p \gtrsim 0.95$. For higher values of the ratio g/κ, $\mathcal{N}_b^{(B)}$ still decreases, but it no longer reaches zero.

An intuitive interpretation of this behaviour traces back to the fact that for values of p larger than zero the battery dynamics has two sources of memory. Besides the one already mentioned above originating directly in the coherent interaction with the charger, now there is also an information backflow from the environment, due to the ancilla-ancilla collisions.

As follows from the discussion in Sec. 2.4, the latter will store and give back memory about previous stages of the evolution, affecting in the first instance the charger, with which the ancillas directly interact, and then also the battery due to its interaction with the charger.

The overall behaviour of the battery dynamics depends on the interplay between these two sources of memory, so that the presence of a second source can reduce the impact of the memory effects induced by the charger observed in the case $p = 0$.

This effect strongly depends on the ratio of the two couplings g and κ, connecting respectively the charger with the battery, and the environment with the charger. For small values of this ratio, the environment is capable of affecting the battery dynamics enough to cancel out the information backflow from the charger, while for higher values of the ratio the impact of the memory from the environment on the non-Markovianity of the battery is weaker.

Note that there are values of p such that the joint battery-plus-charger dynamics is non-Markovian, while the reduced battery dynamics is Markovian, see Figs. 4.7 and 4.8; this is indeed in contrast with what happens commonly, that is, by enlarging the set of degrees of freedom one moves from non-Markovian to Markovian evolutions.

On the other hand, a similar phenomenon has been observed in [201] and exploited for quantum teleportation in [202], where non-local memory effects in the dephasing dynamics of two qubits – originating from the presence of initial correlations within the environment – affect the joint systen made by the two qubits, but neither of the two individually.

By comparing Fig. 4.3 and Fig. 4.8, we notice some significant correlations between $\mathcal{N}_b^{(B)}$ and $\mathcal{E}_{ss}$. The two have in general opposite behaviour, with one increasing while the other decreases. Even more, every time the steady state ergotropy approximate its absolute maximum $\mathcal{E}_{ss}$, the battery non-Markovianity $\mathcal{N}_b^{(B)}$ is equal to zero.

For small values of the ratio g/κ (e.g. $g/\kappa = \{0.1, 0.2\}$), the steady state ergotropy is approximately equal to $\mathcal{E}_{ss}$ for almost any value of p, and similarly $\mathcal{N}_b^{(B)}$ is zero for most values of p. Analogously, the range of values for which the curves referred to $g/\kappa = \{0.4, 0.6, 0.8\}$ approximate the maximum of steady state ergotropy corresponds to a region without memory effects in the battery dynamics.

We also notice how, differently, the curve with $g/\kappa = 2$ does not reach $\mathcal{E}_{ss}$ even though its value of $\mathcal{N}_b^{(B)}$ reaches zero for certain values of p.

We conclude that the absence of memory effects for the battery dynamics seems to be necessary, although not sufficient, to reach the maximum of steady state ergotropy in our model.

This is confirmed by the behaviour of $\mathcal{N}_b^{(B)}$ as a function of the ratio g/κ for the scenario described by the Lindblad master equation considered in [5] and that corresponds to our collisional model with no swap between ancillas ($p = 0$).

As shown in Fig. 4.9, the non-Markovianity measure is a monotonously increasing function of g/κ and it is equal to zero under a certain threshold; we thus observe that, also in this case, in the regime where one obtains the maximum ergotropy (the large loss limit, $g/\kappa \to 0$), the effective dynamics of the battery subsystem is in fact Markovian.

4.3 Conclusions

In this chapter, we studied the discrete-time and continuous-time dynamics of a quantum battery interacting with a collisional model that acts as the environment. Specifically, we described how a discrete-time collisional model is able to mimic an environment with memory by introducing an ancilla-ancilla partial swap interaction with a certain probability p.

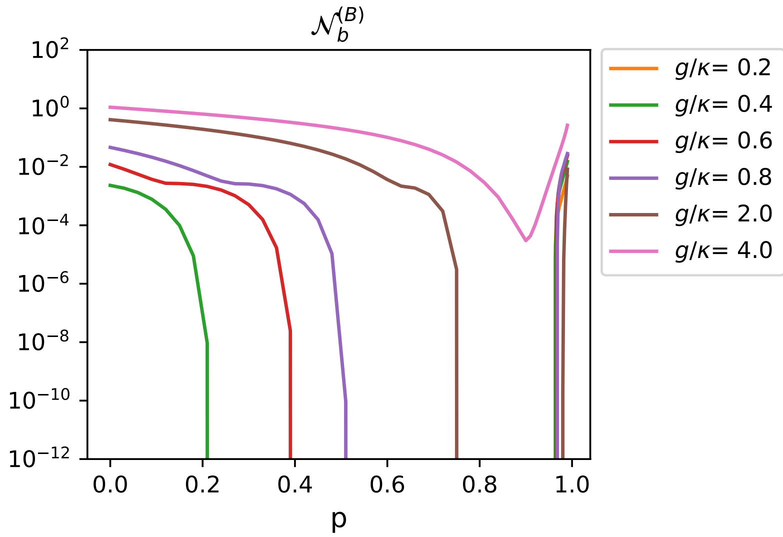

Figure 4.8: Geometrical measure for the battery subsystem $\mathcal{N}_b^{(B)}$ as a function of p for different values of g. The other parameters are: $\alpha = 1.09g$, $\gamma = 10^2\kappa$. At variance with the measure for the composite system, here $\mathcal{N}_b^{(B)}$ has a non-zero value for $p = 0$, due to the memory effects caused by the battery-charger coherent interaction, but as the backflow of information from the environment to the charger increases, the measure itself decreases. For values of the ratio g/κ small enough, $\mathcal{N}_b^{(B)}$ goes to zero for a given value of p, and it starts to increase only for very large values of p. For larger values of the ratio g/κ, $\mathcal{N}_b^{(B)}$ decreases to a finite minimum, without reaching zero. We remark that our numerical simulations show that towards the large-loss limit ($g/\kappa = \{0.1, 0.2\}$), $\mathcal{N}_b^{(B)}$ is zero except in the region of very large values of p.

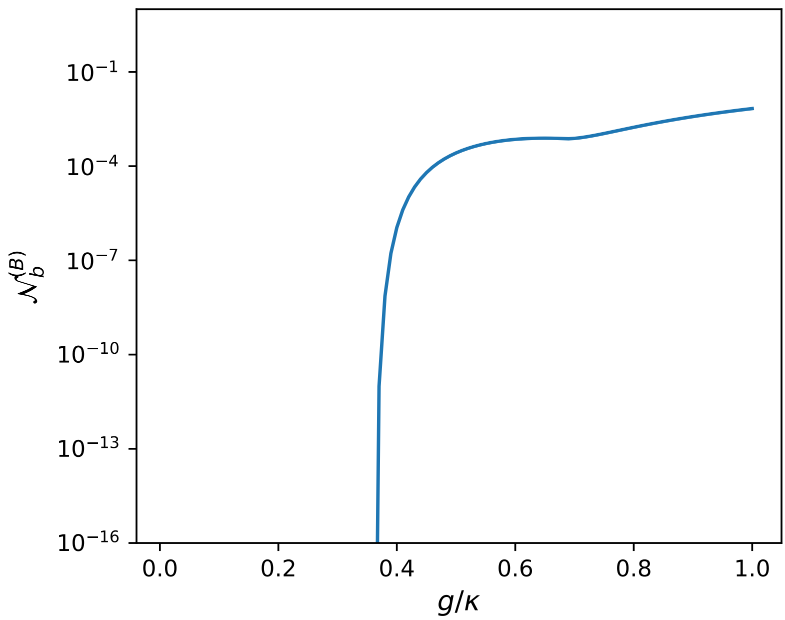

Figure 4.9: Geometrical measure for the battery subsystem $\mathcal{N}_b^{(B)}$ as a function of g/κ in the presence of a memoryless environment as discussed in [5]. For each value of g/κ, the driving α has been chosen in order to optimize the steady-state ergotropy.

It was therefore possible to explore the transition between a memoryless environment (obtained for $p = 0$) and an environment able to induce strong memory effects on the battery and the charger (for values of p approaching 1), while observing the properties of the corresponding steady states of the dynamics.

In particular, we observed a non-monotonic behaviour of the ergotropy as a function of the swap probability p, and the presence of a maximum for a large value of p, smaller than the limiting value $p = 1$.

As we also observed that energy decreases monotonically with p, we came to the conclusion that the ergotropy behaviour is mainly driven by the change in the steady-state purity.

We have also found that the maximum ergotropy achievable at steady state in all the different parameter regimes corresponds to the same value that was obtained with a Markovian environment in the strong dissipative regime, which suggests that the maximum ergotropy is fixed by the operatorial properties of the interaction, regardless of the features of the environment.

On the other hand, the presence of memory effects induced by the environment allows us to approach the maximum value of ergotropy in a broader region of the parameter space, and in a shorter amount of time, thus boosting the charging speed of the battery.

The behaviour observed in the discrete-time model is consistent with what we observe in the regime of parameters where the continuous-time limit exists, that is, for $p \approx 1$. Specifically, we observe that the ergotropy increases by increasing the memory rate Γ characterizing this dynamics, and thus by decreasing the capability of the environment to store information about the evolution of the system.

By using a definite measure of non-Markovianity, the geometrical measure, we investigated the amount of memory effects affecting the battery and the charge seen as a joint system, as well as the battery only. While the non-Markovianity of the joint system shows the expected monotonically increasing behavior as a function of the ancilla-ancilla collision parameter p, the non-Markovianity of the battery has a non-monotonic behavior as a function of p, possibly including regions where there are actually no memory effects, as quantified by the geometrical measure of non-Markovianity.

Remarkably, the maximum of the steady state ergotropy lies in regions of parameters where the battery dynamics is Markovian, as the combined effects of the memory due to, respectively, the direct coherent interaction with the charger and the backflow of information mediated by the ancilla-ancilla collisions cancel each other.

The work presented in this chapter is one of the first attempts in understanding the role of memory effects in quantum battery charging and is particularly suitable for a direct experimental implementation in the next future on actual quantum devices, as quantum collisional models have recently been demonstrated on different quantum simulation platforms [203, 204, 205].

We believe that our study paves the way to further research in this direction: it will be interesting and necessary to understand if the behaviour we have observed will be confirmed when considering quantum batteries with larger dimensionality, that is, going beyond the qubit case, and/or for other noise-models characterized by different forms of the coupling or by different sources of non-Markovianity. In the first instance, one could for example look at dephasing, where non-trivial thermodynamic behaviour has recently been found [206].

Concerning non-Markovianity, one could consider collisional models exhibiting information backflow with or without system-environment correlations [207]: it has been indeed shown how the two scenarios have an impact on thermodynamic properties, such as the entropy production rate [208]. These results suggest that it may be interesting to exploit these models in order to further study the actual relationship between ergotropy, decoherence, information backflow and system-environment correlations.

CHAPTER 5

Daemonic ergotropy in continuously-monitored open quantum batteries

The concept of daemonic ergotropy, as defined in Sec. 3.3.1, can be extended to the framework of open quantum systems by treating the environment as the auxiliary system in the measurement and leveraging the correlations that naturally arise during the dynamics.

Indeed, from a fundamental perspective, during its evolution, an open quantum system becomes correlated with its environment. Therefore, environmental measurements, such as those discussed in Sec. 2.2, which give rise to stochastic master equations, provide an ideal platform to investigate the properties of daemonic ergotropy, both for fundamental insights and potential practical applications in OQBs.

Adapting the notion of daemonic ergotropy to the framework of continuously-monitored open quantum systems enables experimental verification in platforms where environmental measurements are possible and single trajectories can be observed, such as superconducting qubits [18, 19, 20, 21] and optomechanical systems [22, 23, 24].

In this chapter, we investigate the general properties of daemonic ergotropy in open quantum systems. These results are valid for any unraveling that leads to dynamics described by a stochastic master equation, including non-Markovian dynamics or those driven by time-dependent Hamiltonians.

We demonstrate that the daemonic ergotropy of a continuously-monitored system can surpass the ergotropy of the unconditional state and, with perfectly efficient measurements, even reach the energy of the unconditional state. We also examine the performance of different measurement types with non-unit efficiency.

To verify these results, we analyze the simplest example of an OQB: a two-level atom driven by a classical field and spontaneously emitting photons into its electromagnetic environment. We describe the charging process of the battery, which starts from its ground state and is subjected to an external driving field while continuously monitored by its environment.

In this setup, the dissipative effects of the environment continuously subtract energy from the battery, while the back-action of the measurements on the battery enhances the work extractable from it, as discussed in Sec.3.3 and Sec.3.4.

The chapter is organized as follows: in Sec. 5.1 we recall the concept of daemonic ergotropy introduced in the previous chapters and present some preliminary results on this quantity.

In Sec. 5.2 we extend the concept of daemonic ergotropy to continuously-monitored open quantum systems, along with some general results that apply in this scenario.

In Sec. 5.3 we discuss these in a minimal example of an open quantum battery: a two level system driven by a classical field and whose spontaneous emitted photons are continuously monitored.

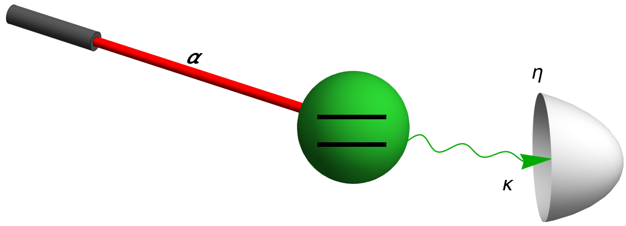

Figure 5.1: Pictorial representation of a continuously-monitored quantum battery: a coherent drive supplies energy with intensity α to a two-level atom (green) which is spontaneously emitting into its environment with rate κ. The emitted field is continuously monitored via a detector with efficiency η.

Finally, in Sec. 5.4, we give our conclusions and propose further outlooks.

5.1 Daemonic ergotropy

Before discussing the daemonic ergotropy in the context of an open quantum system, we prove a proposition concerning the daemonic ergotropy which has a more broad application and in here we state it in terms of the daemonic ergotropy for a generic bipartite system. We recall the definition of daemonic ergotropy as introduced in Sec. 3.3 for convenience.

Let us now consider a bipartite quantum state ϱ^{SA}, where the quantum system S represents our energy storing device, while A is an ancillary system. If the ancilla is discarded, the maximum amount of extractable work is simply equal to $\mathcal{E}(\varrho^S)$, with $\varrho^S = \text{Tr}_A[\varrho^{SA}]$.

We now assume that a measurement is performed on the ancilla, described by a positive operator-valued measurement (POVM) $\{\hat{\Pi}_a^A\}$. We can thus define the *daemonic ergotropy* as the average ergotropy of the corresponding conditional states [173]

$$\overline{\mathcal{E}}_{\{\hat{\Pi}_a^A\}} = \sum_a p_a \mathcal{E}(\varrho_a^S)\,, \tag{5.1}$$

where

$$p_a = \text{Tr}_{SA}[\varrho^{SA}(\hat{\mathbb{1}}^S \otimes \hat{\Pi}_a^A)] \tag{5.2}$$

$$\varrho_a^S = \text{Tr}_A[\varrho^{SA}(\hat{\mathbb{1}}^S \otimes \hat{\Pi}_a^A)]/p_a \tag{5.3}$$

denote respectively the probability and the conditional state corresponding to the measurement outcome a.

We also recall that the daemonic ergotropy satisfies the following properties. The ergotropy is a convex quantity in the quantum state ϱ [173, 189]; as a consequence, since $\varrho^S = \sum_a p_a \varrho_a^S$, one obtains that

$$\overline{\mathcal{E}}_{\{\hat{\Pi}_a^A\}} \geq \mathcal{E}(\varrho^S)\,, \tag{5.4}$$

that is the average work that may be extracted is increased thanks to the information obtained from the ancilla. Furthermore, the daemonic ergotropy can be rewritten as

$$\overline{\mathcal{E}}_{\{\hat{\Pi}_a^A\}} = E(\varrho^S) - \sum_a p_a \min_{\hat{U}_a} E(\hat{U}_a \varrho_a^S \hat{U}_a^\dagger)\,. \tag{5.5}$$

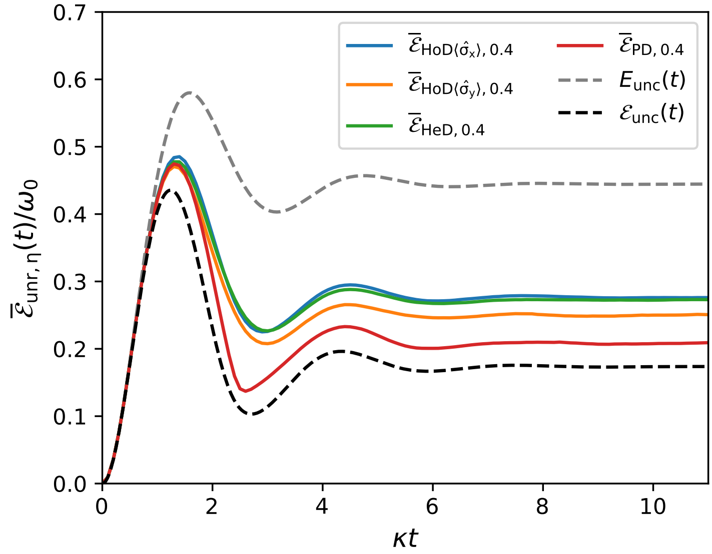

Figure 5.2: Daemonic ergotropies $\overline{\mathcal{E}}_{\mathrm{unr},\eta}(t)$ as a function of time for different unravellings (HoD with photocurrents monitoring either $\hat{\sigma_x}$ or $\hat{\sigma}_y$, HeD and PD) with $\alpha/\kappa = 1$, $\eta = 0.4$ and averaged over $n = 5 \times 10^4$ trajectories. Black and gray dashed lines correspond respectively to the ergotropy and energy of the unconditional state. The different daemonic ergotropies lie as expected between these two lines, with HeD and $\hat{\sigma}_x$-HoD giving the larger values of extractable work. The upper and the lower bounds would be saturated for all the unravellings in the case of respectively perfect monitoring ($\eta = 1$) and no-monitoring ($\eta = 0$).

we here present the first result of from our work via the following proposition.

Proposition 1. *Given a bipartite system system+ancilla prepared in an initial pure state $|\Psi\rangle^{SA}$, and assuming a projective (rank-one) measurement on the ancilla $\{\Pi_a^A = |\phi_a\rangle\langle\phi_a|\}$, then*

$$\overline{\mathcal{E}}_{\{\hat{\Pi}_a^A\}} = E(\varrho^S)\,, \tag{5.6}$$

that is, the daemonic ergotropy is equal to the energy of the reduced state of the system $\varrho^S = \mathrm{Tr}_A[\varrho^{SA}]$, independently of the measurement performed.

Proof. In order to prove this theorem, we first observe that the conditional state remains pure for any measurement outcome, i.e. $\varrho_a^S = |\xi_a\rangle\langle\xi_a|$, with

$$|\xi_a\rangle = \frac{1}{\sqrt{p_a}}\langle\phi_a|\Psi\rangle^{SA} \tag{5.7}$$

As a consequence one has

$$\begin{aligned}\overline{\mathcal{E}}_{\{\hat{\Pi}_a^A\}} &= \sum_a p_a \mathcal{E}(|\xi_a\rangle\langle\xi_a|) \\ &= \sum_a p_a E(|\xi_a\rangle\langle\xi_a|) = E(\varrho^S)\,, \end{aligned} \tag{5.8}$$

where we have exploited: i) the fact that the ergotropy of pure states is equal to their energy, ii) the linearity of the trace, and iii) the relationship $\varrho^S = \sum_a p_a |\xi_a\rangle\langle\xi_a|$. $\square$

The relation above has a straightforward interpretation: the amount of information we can extract through measurement, and consequently the ergotropy gained, depends on the choice of POVM applied. Ideally, to maximize the ergotropy, one should optimize the measurement protocol. Some studies have focused on identifying the optimal protocol [189]. Our result demonstrates that if a POVM can be applied efficiently, then all POVMs are equivalent in their ability to extract ergotropy.

5.2 Daemonic ergotropy in continuously-monitored open quantum systems

We start recalling the basic notions on continuously-monitored quantum systems and quantum trajectories [28, 29]. We assume that our quantum system is interacting with a Markovian environment such that its unconditional evolution is described by a master equation in Lindblad form

$$d\varrho_{\mathsf{unc}}(t)/dt = -i[\hat{H}_s(t), \varrho_{\mathsf{unc}}(t)] + \mathcal{D}[\hat{c}]\varrho_{\mathsf{unc}}(t)\,, \tag{5.9}$$

where $\hat{H}_s(t)$ denotes the Hamiltonian ruling the evolution of the system and $\mathcal{D}[\hat{c}]\varrho = \hat{c}\varrho\hat{c} - (\hat{c}^\dagger\hat{c}\varrho + \varrho\hat{c}^\dagger\hat{c})/2$ is the Lindbladian superoperator [1].

If one assumes that the environment is continuously monitored, the system evolution will be described by a stochastic master equation (SME) for the conditional state $\varrho_{\mathsf{c}}(t)$, as showed in Sec. 2.2. In general it is always true that

$$\varrho_{\mathsf{unc}}(t) = \sum_{\mathsf{traj}} p_{\mathsf{traj}}\, \varrho_{\mathsf{c}}(t), \tag{5.10}$$

where p_{traj} denotes the probability of each quantum trajectory $\varrho_{\mathsf{c}}(t)$.

Different measurement strategies will correspond to different unraveling of the unconditional master equation (5.9), that is to different SMEs for the conditional state $\varrho_{\mathsf{c}}(t)$ and, mathematically speaking, to different convex combinations for the unconditional state $\varrho_{\mathsf{unc}}(t)$.

We will later consider the most paradigmatic examples of such unravellings, corresponding to the scenarios where the environment is continuously-monitored via either photo-detection (PD), homodyne-detection (HoD) or heterodyne-detection (HeD).

The explicit formulas for the corresponding SMEs can be found in Sec. 2.2. Remarkably, while we here focus on Markovian open quantum systems described by a Lindblad master equation (5.9), all the results that follow apply whenever one can write the unconditional state as a mixture of trajectories as of (5.10), including monitored quantum systems exhibiting non-Markovian behaviour.

Besides the kind of detection performed on the environment, such unravellings are characterized by their measurement efficiency η, that comprehensively quantifies the portion of the environment that is accessible and the efficiency of the detector. In particular, we recall that for $\eta = 1$, that is when one assumes that the environment is fully accessible and measurable via a projective (rank-one) measurement, and for an initial pure

[1] We are here considering a single jump operator $\hat{c}$ describing the interaction between the system and a zero-temperature environment, but the formalism can be straightforwardly generalized to multiple jump operators and to generic thermal environments

state for the system, the stochastic master equation reduces to a stochastic Schrödinger equation, as the conditional state remains pure during the whole dynamics. The SSE for the photo-detection and homodyne detection are given in Eq. (2.43) and Eq. (2.58) respectively.

Proposition 2. *Given an open quantum system, whose charging process is described by a (possibly time-dependent) Hamiltonian $\hat{H}_s(t)$, and whose environment can be continuously monitored with efficiency η, the corresponding daemonic ergotropy*

$$\overline{\mathcal{E}}_{\mathsf{unr},\eta}(t) = \sum_a p_{\mathsf{traj}} \mathcal{E}(\varrho_{\mathsf{c}}(t)) \tag{5.11}$$

is bounded as

$$\mathcal{E}(\varrho_{\mathsf{unc}}(t)) \leq \overline{\mathcal{E}}_{\mathsf{unr},\eta}(t) \leq E(\varrho_{\mathsf{unc}}(t)) \,. \tag{5.12}$$

The upper bound can be achieved in the presence of Markovian environment, whenever the system is initially prepared in a pure state and the monitoring is performed with unit efficiency $\eta = 1$, independently of the kind of unravelling, i.e.

$$\overline{\mathcal{E}}_{\mathsf{unr},\eta=1}(t) = E(\varrho_{\mathsf{unc}}(t)).\,. \tag{5.13}$$

Proof. The first inequality in Eq. (5.12) is a generalization of Eq. (5.4), applied to (5.10). Similarly the upper bound is a consequence of Eq. (5.5), while the fact that the upper bound can be achieved for unravellings of pure states follows straightforwardly from Prop. 1. □

In the following, we show that as a corollary, the inequality above can be trivially extended to the case where ergotropies and energies are rescaled by the evolution time t, and thus in terms of figure of merits characterizing the charging power of the protocol.

5.2.1 Average power of continuously-monitored quantum batteries

Let us assume that the state of the quantum battery at the beginning of the charging process is initially in a pure state ($\varrho_0 = |\psi_0\rangle\langle\psi_0|$) , and a charging protocol evolve the system from a time $t = 0$ to $t = \tau$. We can use the definitions of energy (E), ergotropy ($\mathcal{E}$) and daemonic ergotropy ($\overline{\mathcal{E}}_{\{\hat{\Pi}_a^A\}}$) introduced in the manuscript, to define respectively the average power (P), the average ergotropic power ($\mathcal{P}$) and the average daemonic power ($\overline{\mathcal{P}}_{\{\hat{\Pi}_a^A\}}$) as follows:

$$P(\varrho(\tau)) = \frac{E(\varrho(\tau)) - E(\varrho_0)}{\tau} \tag{5.14}$$

$$\mathcal{P}(\varrho(\tau)) = \frac{\mathcal{E}(\varrho(\tau)) - E(\varrho_0)}{\tau} \tag{5.15}$$

$$\overline{\mathcal{P}}_{\{\hat{\Pi}_a^A\}}(\tau) = \frac{\overline{\mathcal{E}}_{\{\hat{\Pi}_a^A\}}(\varrho(\tau)) - E(\varrho_0)}{\tau} \tag{5.16}$$

We can thus formulate the following corollary, that can be easily proven starting from Prop. 2 of the manuscript.

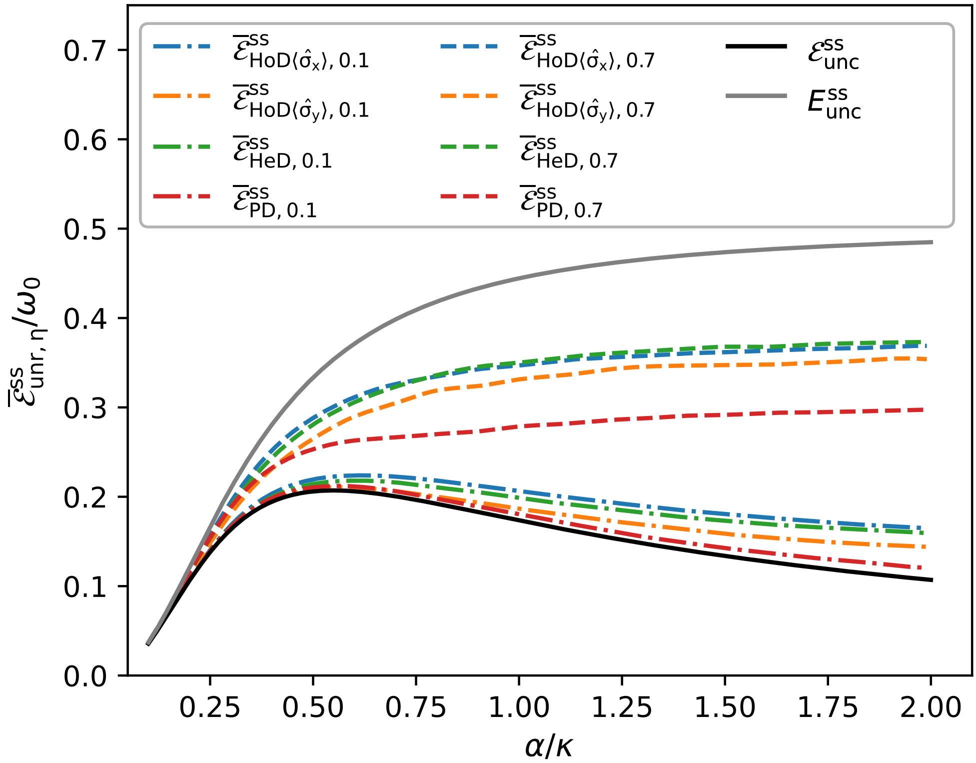

Figure 5.3: Steady-state daemonic ergotropy $\overline{\mathcal{E}}^{ss}_{unr,\eta}$ for the different unravellings (HoD with photocurrents monitoring either $\hat{\sigma}_x$ or $\hat{\sigma}_y$, HeD, PD) as a function of α and for $\eta = 0.1$ (dashed-dotted) and $\eta = 0.7$ (dashed) (number of trajectories $n = 5 \times 10^4$). Also in this case HeD and $\hat{\sigma}_x$-HoD yield the largest values. Black and gray solid lines correspond respectively to ergotropy and energy of the unconditional steady-state, that is to the lower and upper bound for the daemonic ergotropies, that would be obtained for respectively no-monitoring ($\eta = 0$) or perfect monitoring ($\eta = 1$).

Corollary 1. *Given an open quantum system, whose charging process is described by a (possibly time-dependent) Hamiltonian $\hat{H}_s(t)$, and whose environment can be continuously monitored with efficiency η, the corresponding average daemonic power $\overline{\mathcal{P}}_{\mathsf{unr},\eta}(t) = \sum_a p_{\mathsf{traj}} \mathcal{P}(\varrho_{\mathsf{c}}(t))$ is bounded as*

$$\mathcal{P}(\varrho_{\mathsf{unc}}(t)) \leq \overline{\mathcal{P}}_{\mathsf{unr},\eta}(t) \leq P(\varrho_{\mathsf{unc}}(t)) \,. \tag{5.17}$$

The upper bound can be achieved in the presence of Markovian environment, whenever the system is initially prepared in a pure state and the monitoring is performed with unit efficiency $\eta = 1$, independently of the kind of unravelling, i.e.

$$\overline{\mathcal{P}}_{\mathsf{unr},\eta=1}(t) = P(\varrho_{\mathsf{unc}}(t)) \,. \tag{5.18}$$

We have thus proved that, as expected, the extractable work and power can be increased in an open quantum system if one obtains some information by monitoring the environment.

Remarkably, the maximum daemonic ergotropy is equal to the unconditional energy and can be achieved via unit efficiency monitoring, independently of the measurement strategy. In the following we will rather investigate what happens in the more practical and experimentally relevant scenario of monitoring with non-unit efficiency or for initially mixed states, where a hierarchy between the different unravellings is established.

5.3 A continuously-monitored open quantum battery

We now consider the paradigmatic example of an OQB, that is a two-level atom characterized by a Hamiltonian $\hat{H}_0 = (\omega_0/2)(\hat{\sigma}_z + 1)$, driven by a resonant classical field of intensity α, which acts as a charger, and spontaneously emitting with rate κ (see Fig. 5.1). In interaction picture with respect to $\hat{H}_0$, the evolution of the system is described by a Markovian master equation of the form (5.9), where the Hamiltonian ruling the evolution and the jump operator respectively read $\hat{H}_s = \alpha\hat{\sigma}_x$ and $\hat{c} = \sqrt{\kappa}\sigma_-$, i.e.

$$\frac{d\varrho_{\mathsf{unc}}(t)}{dt} = -i\alpha[\hat{\sigma}_x, \varrho_{\mathsf{unc}}(t)] + \kappa\mathcal{D}[\hat{\sigma}_-]\varrho_{\mathsf{unc}}(t) \,. \tag{5.19}$$

An analytical solution can be obtained for $\varrho_{\mathsf{unc}}(t)$ and we report here the corresponding steady-state values of energy and ergotropy

$$E^{\mathsf{ss}}_{\mathsf{unc}}/\omega_0 = \frac{4\alpha^2}{8\alpha^2 + \kappa^2} \,, \tag{5.20}$$

$$\mathcal{E}^{\mathsf{ss}}_{\mathsf{unc}}/\omega_0 = \frac{\kappa}{2}\left(\frac{\sqrt{16\alpha^2 + \kappa^2} - \kappa}{8\alpha^2 + \kappa^2}\right) . \tag{5.21}$$

One observes that the steady state energy $E^{\mathsf{ss}}_{\mathsf{unc}}$ grows monotonically as a function of α/κ and asymptotically reaches the value $E^{\mathsf{ss}}_{\mathsf{unc,max}} = \omega_0/2$ in the limit of large driving. Oppositely, the steady-state ergotropy $\mathcal{E}^{\mathsf{ss}}_{\mathsf{unc}}$ presents a maximum at

$$\alpha/\kappa = \sqrt{(1+\sqrt{2})/8} \,, \tag{5.22}$$

where it reaches its peak value

$$\mathcal{E}^{\mathsf{ss}}_{\mathsf{unc,max}} = \omega_0(\sqrt{2} - 1)/2 \,. \tag{5.23}$$

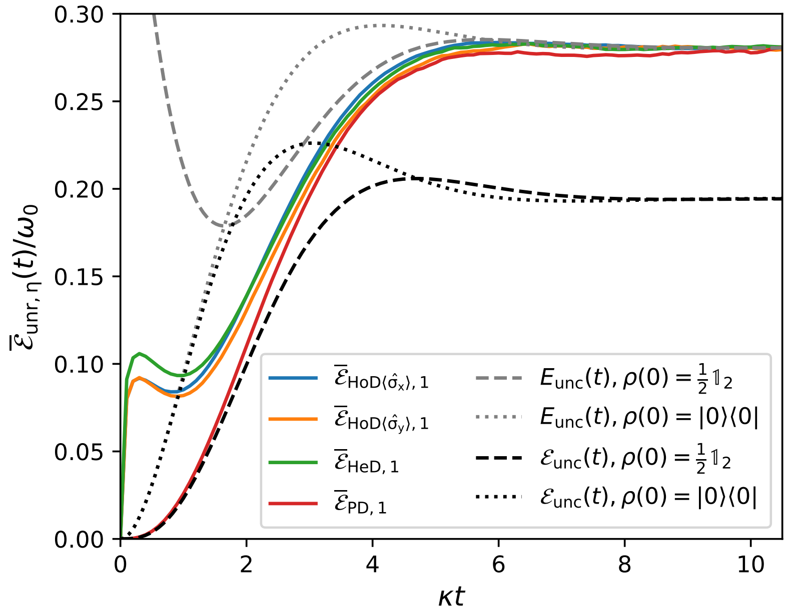

Figure 5.4: Daemonic ergotropy $\overline{\mathcal{E}}_{\mathrm{unr},\eta}(t)$ as a function of time for different unravellings (HoD with photocurrents monitoring either $\hat{\sigma_x}$ or $\hat{\sigma}_y$, HeD, PD) with $\alpha/\kappa = 0.4$, $\eta = 1$ and by considering the maximally mixed state $\rho_0 = \hat{\mathbb{1}}/2$ as initial state (number of trajectories $n = 5 \times 10^4$). Black and gray lines correspond respectively to ergotropy and energy of the unconditional state when initial states are the maximally mixed state (dashed) and the ground state (dotted).

If we now assume that a photo-counting detector is able to measure the spontaneously emitted photons with efficiency η, the dynamics of the conditional states $\varrho_{\mathrm{c}}(t)$ is described by a SME of the form (2.41); in particular the statistics of the corresponding Poissonian increment is univocally identified by its average value

$$\mathbb{E}[dN_t] = \eta\kappa\langle\hat{\sigma}_+\hat{\sigma}_-\rangle_t dt\,, \tag{5.24}$$

and thus depends on the average value of $\hat{\sigma}_z$ (we remind that $\hat{\sigma}_+\hat{\sigma}_- = (\hat{\sigma}_z + \hat{\mathbb{1}}_2)/2$).

If one rather considers a homodyne detection on the emitted field, one has a SME of the form (2.52), where in particular the continuous homodyne photo-current reads

$$dy_t = \sqrt{\eta\kappa}\langle\hat{\sigma}_- e^{i\phi} + \hat{\sigma}_+ e^{-i\phi}\rangle_t\, dt + dW_t\,, \tag{5.25}$$
$$= \sqrt{\eta\kappa}\langle\cos\phi\hat{\sigma}_x + \sin\phi\hat{\sigma}_y\rangle_t\, dt + dW_t\,, \tag{5.26}$$

where ϕ corresponds to the homodyne phase. In particular for $\phi = 0$ and $\phi = \pi/2$ one has photocurrents depending respectively to the average values of $\hat{\sigma}_x$ and $\hat{\sigma}_y$.

Heterodyne detection on the environment leads to a similar SME, as can be indeed thought and implemented as a double homodyne, measuring orthogonal quadratures with half efficiency. As a consequence one gets a SME of the form (2.54) where the two photocurrents depend on $\hat{\sigma}_x$ and $\hat{\sigma}_y$ as

$$dy_t^{(1)} = \sqrt{\frac{\eta\kappa}{2}}\langle\hat{\sigma}_x\rangle_t\,dt + dW_t^{(1)}\,, \tag{5.27}$$

$$dy_t^{(2)} = \sqrt{\frac{\eta\kappa}{2}}\langle\hat{\sigma}_y\rangle_t\,dt + dW_t^{(2)}\,. \tag{5.28}$$

We will denote with $\overline{\mathcal{E}}_{\mathsf{PD},\eta}$, $\overline{\mathcal{E}}_{\mathsf{HoD},\eta}$ and $\overline{\mathcal{E}}_{\mathsf{HeD},\eta}$ the daemonic ergotropies corresponding to continuous monitoring of the fluorescence field due to the atomic spontaneous emission via respectively PD, HoD and HeD with efficiency η.

According to Prop 2, we know that for unravellings of pure states with $\eta = 1$, one obtains $\overline{\mathcal{E}}_{\mathsf{unr},\eta=1}(t) = E(\varrho_{\mathsf{unc}}(t))$, that is, the energy of the unconditional state can be fully extracted via conditional unitary operations for all the possible detection strategies.

We first consider the situation where the system is initially prepared in the ground state $|0\rangle$, while the environment is not fully accessible and it is thus monitored with non-unit efficiency η. We have numerically solved the corresponding SMEs [209, 210] and evaluated the corresponding daemonic ergotropy by averaging over a large number of trajectories.

In this case we find that there is a hierarchy between the different unravellings: as one can observe in Fig. 5.2, for $\eta = 0.4$ and $\alpha = \kappa$, homodyne detection with photocurrent proportional to $\langle\hat{\sigma}_x\rangle_t$ (corresponding to $\phi = 0$) and heterodyne detection lead to the largest values of daemonic ergotropy, while photo-detection is the least performing strategy.

The results presented in this plot are quite general: in all our numerical simulations we find that, as regards HoD, $\overline{\mathcal{E}}_{\mathsf{HoD},\eta=1}(t)$ is maximized (minimized) for $\phi = 0$ ($\phi = \pi/2$), that is for a $\hat{\sigma}_x$-dependent ($\hat{\sigma}_y$-dependent) photocurrent.

Furthermore, in the whole range of parameters we have explored, $\hat{\sigma}_x$-HoD and HeD generally yield very similar values of daemonic ergotropy. The same behavior can be indeed observed if we focus on the steady-state properties as shown in Fig. 5.3, where steady-state daemonic ergotropies $\overline{\mathcal{E}}^{\mathsf{ss}}_{\mathsf{unr},\eta}$ for the different unravellings are plotted as a function of α and for two different values of η.

From the figure one can clearly observe the hierarchy existing between the different strategies, and how, by increasing the monitoring efficiency, the daemonic ergotropy can reach values, approaching the unconditional energy $E^{\mathsf{ss}}_{\mathsf{unc}}$ in the limit of $\eta = 1$.

Finally, in Fig. 5.4 we consider the other scenario where different unravellings lead to different daemonic ergotropies, that is when the environment is monitored with unit efficiency, but the initial state is mixed.

In particular, we consider the maximally mixed state $\varrho_0 = \hat{\mathbb{1}}/2$ as initial state and we plot $\overline{\mathcal{E}}_{\mathsf{unr},\eta}(t)$ as a function of time. We observe that at steady state all the unravellings lead to the same value of daemonic ergotropy, equal to the corresponding unconditional energy: the monitoring will eventually purify all the trajectories and thus one falls back into the scenario described in Prop. 2. However, different unravellings lead to a different purification speed, an effect that has been widely discussed in the literature [211, 212, 213, 214, 215, 216].

With respect to the scenarios described in these works, we here have a non-trivial system Hamiltonian $\hat{H}_s$ ruling the dynamics, and a fixed jump operator $\hat{c} = \sqrt{\kappa}\hat{\sigma}_-$, representing the interaction between system and environment. Remarkably, at small times we find that the purification speed of HeD and, in the second instance, HoD (almost independently on the phase ϕ) allows to achieve values of daemonic ergotropy evidently larger than the maximum daemonic ergotropy obtainable by starting from a ground state, whose upper bound (the unconditional energy represented as a dotted-gray line in Fig. 5.4) can be interpreted as the amount of energy injected into the system by the driving laser; we can thus conclude that in monitoring-enhanced battery charging protocols, the effects of purification may be more efficient than pure energy injection at small times.

On the other hand we also observe that PD still yields the lowest values of daemonic ergotropy in the transient leading to steady-state, and for small times the enhancement due to the monitoring respect to the unconditional ergotropy is almost negligible.

5.4 Conclusions

We have extended the concept of daemonic ergotropy to the open quantum system scenario, where some information leaking into the environment can be continuously monitored and exploited in order to enhance the work extraction protocol.

Our findings reveal that the daemonic ergotropy not only surpasses the unconditional state ergotropy, but can even reach its energy in the ideal scenario of unit efficiency detectors. We have then discussed the simplest, but practically relevant, example of an OQB, that is a two-level atom classically driven by an external field acting as a charger.

Our main results (Props.1,2) require very few assumptions compared to the ones implied in the model of OQB considered. In particular, they hold even for charging protocols with time-dependent Hamiltonian [217, 218], allowing one to further assess the performances of these protocols in the case of continuous monitoring and to envisage more efficient quantum feedback protocols.

Moreover, one can also consider trajectories describing continuously monitored open quantum systems in the presence of a non-Markovian environment; while the interpretation of unravellings of non-Markovian master equation in terms of monitoring is in general not guaranteed [219, 220, 221, 222, 223], our approach can be directly pursued in the non-Markovian setting by describing such quantum conditional dynamics via continuously measured collisional models [76, 1, 72].

A proof-of-principle experimental demonstration of our results can be readily pursued in a circuit-QED platform, where quantum trajectories corresponding to HeD of atom fluorescence have been recently observed [19, 20]. In general our results pave the way to further investigation on the relationship between measurement energy cost and work extraction in continuously-monitored quantum systems [224, 104, 172, 225, 100, 103, 124, 101], and on the design of a new generation of monitoring-enhanced and noise-resilient quantum batteries.

CHAPTER 6

Daemonic work extraction via non-ideal QND-energy measurement

As shown in Sec. 3.3, in quantum systems, the use of quantum measurements to extract work has been shown to enhance performance in proportion to the information acquired [173, 124, 2, 187]. In quantum thermodynamics, emerging technologies such as quantum heat engines and quantum batteries leverage these measurement-driven enhancements [1, 157]. However, while measurements improve device performance, the thermodynamic cost of measurement is often not accounted for in the analyses.

This cost has been associated with the cost of erasing the information obtained from the measurement, in agreement with Landauer's principle, leading to a work contribution from information to the second law of thermodynamics.

In this chapter, we address this gap by employing the framework of informational thermodynamics, as described in Sec. 3.4, to study work extraction from a quantum battery through a Quantum Non-Demolition (QND) energy measurement scheme.

We consider a generic quantum system as the battery, initially in an active state. Using a QND-energy measurement scheme as an extraction protocol, we aim to optimize the work extraction process while accounting for both the realistic costs and gains of measurement.

We first demonstrate how our protocol functions as a QND-energy measurement scheme, presenting its results in the ideal case. Subsequently, we characterize inefficiencies in the measurement protocol in terms of the temperature of the auxiliary system used to perform the POVM.

In our analysis, we separate the work gain from the protocol into two components: the work cost required to perform the measurement, as described by the framework proposed by Minagawa et al. [105], and an additional variation that accounts for the difference between the gain and the cost.

Our results show that for thermal operations, the daemonic gain is always less than or equal to the energy cost of the measurement. This implies that the second contribution serves as a measure of the protocol's inefficiency and quantifies the deviation of the gain from the cost.

For unitary operations, the gain can exceed the cost of the measurement. We interpret this difference as a "cost-free work variation," a quantity that can be either positive or negative, and in our framework, has a clear dependence on the temperature of the bath.

Furthermore, we discuss the extension of the framework to continuous measurement scenarios, modeling it through a collisional approach, following the example of Sec. 2.2. As a case study, we demonstrate our results for a quantum battery modeled as a two-level system.

This chapter is organized as follows: In Sec.6.1, we revisit the definition of daemonic ergotropy and present preliminary results that explore its informational content.

Sec.6.2 introduces our protocol for optimizing work extraction, we demonstrate it's interpretation as a non-ideal QND-energy measurement, discuss the role of the temperature as a model of measuring inefficiency, and characterize the maximum work achievable through thermal and unitary operations. We also contextualize the protocol's cost within the framework of the second law of informational thermodynamics.

In Sec.6.3, we demonstrate the application of our findings on a representative example of a qubit quantum battery.

Finally, in Sec.6.4, we summarize our conclusions.

6.1 The informational content of the daemonic ergotropy

In Sec. 3.3, we characterized the daemonic gain as a witness of quantum discord. However, calculations performed for the equivalent gain obtainable from unitary operations characterize it in terms of the quantum-classical mutual information, quantifying the classical amount of information gained from the measurement.

In this section, we analyze the daemonic gain in terms of its informational content, following an approach similar to the one adopted for thermal operations by Manzano and colleagues in [124].

We consider the same setup as in Sec. 3.3.1, involving a bipartite system SA initially prepared in a joint state ρ^{SA}. By performing the POVM $\{\Pi_a^A\}$ on the auxiliary system, the system S becomes conditioned on the measurement outcome according to Eq. (3.39), with the probability p_a of obtaining outcome a given by Eq. (3.40).

To recall, the daemonic gain, i.e., the gain obtained from measurement averaged over all outcomes, is defined as $\Delta\overline{\mathcal{E}}_{\{\Pi_a^A\}} = \overline{\mathcal{E}}_{\{\Pi_a^A\}} - \mathcal{E}(\rho^S)$, where the daemonic ergotropy is defined in Eq. (3.42). Using Eq. (3.11), we can rewrite the daemonic gain and perform calculations analogous to Eq. (3.54). This yields:

$$
\begin{aligned}
\Delta\overline{\mathcal{E}}_{\{\hat{\Pi}_a^A\}} &= \sum_a p_a \left[\mathcal{F}_\beta(\rho^{S|a}) - \mathcal{F}_\beta(\rho_p^{S|a}) - \mathcal{F}_\beta(\rho^S) + \mathcal{F}_\beta(\rho_p^S)\right] \\
&= \sum_a p_a \left[\Delta\mathcal{F}^{S|a} + \mathcal{F}_\beta(\rho_p^S) - \mathcal{F}_\beta(\rho_p^{S|a})\right] \\
&= \beta^{-1}\mathcal{J}(\rho^{SA}) + \left[\mathcal{F}_\beta(\rho_p^S) - \sum_a p_a \mathcal{F}_\beta(\rho_p^{S|a})\right]. \\
&= \beta^{-1}\mathcal{J}(\rho^{SA}) + \Delta\overline{\mathcal{F}}_p^S,
\end{aligned} \tag{6.1}
$$

where we define $\Delta\overline{\mathcal{F}}_p^S = \mathcal{F}_\beta(\rho_p^S) - \mathcal{F}_\beta(\rho_p^{S|a})$. This quantity encodes the average change in the free energy of the passive states before and after the measurement. We can easily think of relating this relation to Eq. (3.54), however a few distinction are noteworthy.

It is important to note that in the general setup without a directly involved environment, β is a free parameter with no physical interpretation and no operational meaning. Consequently, $\Delta\overline{\mathcal{E}}_{\{\hat{\Pi}_a^A\}}$ does not depend on the value of β.

Conversely, for thermal operations, β has a physical meaning determined by the temperature of the heat bath involved in work extraction. We discuss two particularly meaningful values of β that attributes some interpretation to the relation above:

- **Work cost interpretation**: While not directly involved in the work extraction process, the presence of a thermal bath is implicitly required for the measurement scheme. The information acquired through measurement must eventually be erased, dissipating heat in the bath as per Landauer's limit.

  If β is chosen such that $\beta^{-1}\mathcal{J}(\rho^{SA})$ represents the work cost of the measurement, the daemonic gain can be interpreted as the sum of two terms: the work cost associated with measurement (and the erasure of information) and a cost-free work variation arising from the free energy change in the passive states. The term $\Delta\overline{\mathcal{F}}_p^S$ encapsulates this cost-free variation.

- **Informational gain potential**: In the asymptotic limit of n-copies of ρ^S, as the energy spectrum of the system approach the continuum, the effects of unitary operations approach those of thermal operations, with $\beta = \beta^\star$, where $\beta^\star$ satisfies $S(\rho^S) = S(\rho^S_{\beta^\star})$.

  In this scenario, $\Delta\overline{\mathcal{F}}_p^S \to 0$. If β is chosen this way, we can interpret the first term with the informational work gain due to the measurement, and the second term encodes the effect on the work variation that arise due to the finite-size of the system and the restriction imposed by the action of the unitary operation.

Finally, we emphasize that $\Delta\overline{\mathcal{F}}_p^S$ can be positive or negative, meaning it may contribute either as a net gain or a net loss to work extraction.

We can further contextualize this results in light of those presented in [173], particularly the observation that the daemonic gain can serve as a witness for the absence of quantum discord. Recall that $\mathcal{J}(\rho^{SA})$ quantifies the classical information contained in the state, which does not contribute to quantum discord.

This relation is particularly clear in the scenario described above for the asymptotic limit of n-copies of ρ^S. As the system size increases and approaches the classical limit, $\Delta\overline{\mathcal{F}}_p^S$ vanishes, along with the purely quantum component of the correlations defined by the quantum discord.

Further studies investigating the relationship between quantum discord and daemonic gain would be valuable to elucidate a more explicit dependence between these quantities.

6.2 A QND-Energy measurement protocol for work extraction

In this section, we introduce the framework for our work extraction protocol. Contrarily to the previous section, in our settings, β will have an operational meaning, leading to an overall different situation.

The ideal QND-energy measurement protocol Before introducing our setup, we characterize the ideal case and demonstrate how it qualifies as a Quantum Non-Demolition (QND) measurement. The measurement component of the protocol involves two steps applied to a bipartite composite system SA, where S is the system being measured.

Crucially, S is not directly projected or altered in a way that destroys it, as happens in certain destructive measurements. For instance, photon detection requires its absorption by the detector, effectively destroying the photon. In contrast, in this QND scheme, the other component of the bipartite system, the auxiliary system A, is projected instead of S.

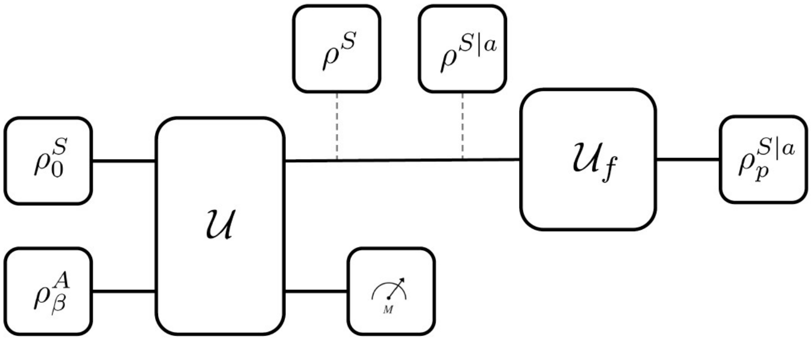

Figure 6.1: A schematic of the QND-energy measurement scheme considered in this chapter. A system S, initially in an active state ρ_0^S, interacts with an auxiliary system A, initially in a Gibbs state ρ_β^A, via a unitary operation $\hat{U}$. After performing a measurement on A through a POVM, work is extracted from S through either unitary or thermal operations.

In the ideal case, we assume that S is initially in an unknown state we wish to extract work from, while A starts in its ground state. The initial state of the composite system is thus given by:

$$\rho_0^{SA} = \rho_0^S \otimes \left|0^A\middle\rangle\!\middle\langle 0^A\right|, \tag{6.2}$$

where

$$\rho_0^S = \sum_{n,m} p_{n,m} \, |n\rangle\!\langle m| \tag{6.3}$$

represents a generic state of S expressed in the eigenbasis of the system's Hamiltonian $\hat{H}_0 = \sum_n \varepsilon_n \, |n\rangle\!\langle n|$.

The first step of the measurement process establishes a correlation between S and A by applying a unitary operation on the composite system. The unitary operator chosen is:

$$\hat{U}_{SA} = e^{-i\hat{H}_0 \otimes \hat{A}}, \tag{6.4}$$

with $\hat{A}$ defined such that it satisfies:

$$\hat{A} : |\psi_n\rangle = e^{-i\varepsilon_n \hat{A}}|0\rangle, \tag{6.5}$$

where the states $|\psi_n\rangle$ form a orthogonal basis on the Hilbert space of A.

Under this unitary evolution, the state of the system becomes:

$$\rho_1^{SA} = \hat{U}_{SA}(\rho_0^S \otimes \left|0^A\middle\rangle\!\middle\langle 0^A\right|)\hat{U}_{SA}^\dagger, \tag{6.6}$$

which expands as:

$$\rho_1^{SA} = \sum_{n,m} p_{n,m} \left(\left|n^S\middle\rangle\!\middle\langle m^S\right| \otimes \left|\psi_n^A\middle\rangle\!\middle\langle \psi_m^A\right| \right). \tag{6.7}$$

The second step of the measurement process involves projecting the auxiliary system A through a POVM. The specific unitary used ensures that the energy eigenstates of A are correlated with those of S. By performing a projective measurement on A, with the operators defined by the states $|\psi_n\rangle$, we indirectly project S onto its energy eigenspace. Applying the POVM $\{\mathbb{I} \otimes |\psi_k\rangle\langle\psi_k|\}$ results in the following state:

$$\rho_2^{SA} = \sum_k p_k \rho_{2,k}^{SA} = \sum_k p_k (|k^S\rangle\langle k^S| \otimes |\psi_k^A\rangle\langle\psi_k^A|), \tag{6.8}$$

For each outcome k, obtained with probability $p_k = p_{k,k}$, the state of S, after tracing out the degrees of freedom of A, becomes:

$$\rho_{2,k}^S = |k\rangle\langle k| \,. \tag{6.9}$$

Therefore, with this measurement protocol the state of S is conditioned as if an energy measurement were performed on it, yielding outcome k and projecting the state accordingly with the appropriate probability, all while performing the measurement solely on A.

The role of the temperature In our model, we assume access to a bath at an inverse temperature β. As shown in Secs. 2.1 and 2.2 through the derivation of the ME and SME through a collisional model, the interaction with the bath can be treated in term of a collisional model, where the bath is modeled as a stream of non-interacting input modes continuously refreshing.

Accordingly, we model the auxiliary system for our QND-energy measurement protocol as being in thermal equilibrium with a bath at inverse temperature β.

The temperature of the bath plays a crucial role in determining measurement efficiency. If the memory state of the auxiliary system is pure, the measurement becomes projective, and the system state S collapses to a pure state after the measurement.

Specifically, as shown above, for a given measurement outcome k, the system state S becomes $\rho_{2,k}^S = |k\rangle\langle k|$. In this case, even without prior knowledge of the initial state ρ_0^S, it is possible to apply an optimal unitary operation solely based on the measurement outcome k. This unitary operation, $U_k = |0\rangle\langle k|$, maps the state $|k\rangle$ to $|0\rangle$, thereby enabling the extraction of all available energy as useful work.

In the non-ideal case, where the auxiliary system is in a mixed state, the eigenstates of the main system and auxiliary system can no longer be perfectly correlated. Consequently, after the measurement, the system state S will not be pure. As the auxiliary system becomes increasingly mixed, the back-action effect on S weakens. This establishes the correlation between the temperature of the auxiliary system and the efficiency of the measurement, as claimed.

A non-ideal QND-energy measurement protocol for work extraction We now characterize the protocol we propose for extracting work through a QND-energy measurement. As represented in Fig. 6.1, we consider a main system S with free Hamiltonian $\hat{H}_0 = \sum_n \varepsilon_n |n\rangle\langle n|$, starting in an initially active state $\rho_0^S = \sum_{n,m} p_{n,m} |n\rangle\langle m|$. The auxiliary system A, acting as the Memory, has the same free Hamiltonian as the system S and is initially thermalized with a thermal bath B at inverse temperature β. Its state is given by the Gibbs state $\rho_\beta^A = e^{-\beta \hat{H}_0}/Z$, with $Z = \mathrm{tr}\left[e^{-\beta \hat{H}_0}\right]$. We assume that, at the start, the composite system state is factorized and equal to

$$\rho_0^{SAB} = \rho_0^S \otimes \rho_\beta^A \otimes \rho_\beta^B. \tag{6.10}$$

Our protocol consists of the following steps:

1. **Unitary evolution:** The system S and the auxiliary system A evolve unitarily, as in the ideal case, with the unitary being given by Eq. (6.4). Under the action of this unitary, the system state now evolves as

$$\rho_1^{SAB} = \hat{U}_{SA}(\rho_0^S \otimes \rho_\beta^A)\hat{U}_{SA}^\dagger \otimes \rho_\beta^B \tag{6.11}$$
$$= \sum_{n,m} p_{n,m} \left(|n^S\rangle\langle m^S| \otimes e^{-i\varepsilon_n \hat{A}} \rho_\beta^A e^{i\varepsilon_m \hat{A}^\dagger} \right) \otimes \rho_\beta^B. \tag{6.12}$$

2. **Energy measurement:** The energy measurement is performed on the auxiliary system, described by the set $\{\mathbb{I}\otimes|\psi_k\rangle\langle\psi_k|\}$. Due to the measurement, the state unravels into a convex combination

$$\rho_2^{SAB} = \sum_k p_k \rho_{2,k}^{SAB} \tag{6.13}$$

with

$$\rho_{2,k}^{SAB} = \left(\mathbb{I}^S \otimes |\psi_k^A\rangle\langle\psi_k^A|\right) \left(\rho_2^{SA}\right) \otimes \rho_\beta^B \tag{6.14}$$
$$= \rho_{2,k}^S \otimes |\psi_k^A\rangle\langle\psi_k^A| \otimes \rho_\beta^B. \tag{6.15}$$

3. **Work extraction:** Work is extracted from the system S by performing the optimal operation based on the measurement outcome. The extraction process is analyzed for both thermal and unitary operations, leading to different final passive states.

4. **Memory reset:** The auxiliary system A resets by thermalizing with the environment, returning its state to the Gibbs state

$$\rho_4^{AB} = \rho_\beta^A \otimes \rho_\beta^B \tag{6.16}$$

Before focusing on the extraction step, let us discuss some details of this protocol.

Work cost The work cost associated with the protocol can be evaluated from the generic bound introduced by Minagawa and colleagues [105], reported in Eq. 3.70. According to the relation, and assuming the idealization for which no entropy production is associated with the protocol, we can write the cost for our protocol as

$$\mathcal{W}_{\text{cost}} = \beta^{-1}(\Delta S_{2,0}^{SA} + \mathcal{J}_{GO}), \tag{6.17}$$

where $\Delta S_{2,0}^{SA} = S(\rho_2^{SA}) - S(\rho_0^{SA})$, and $\mathcal{J}_{GO}$ is the Groenewold-Ozawa informational gain.

Work extraction with thermal operation Let's now discuss the work extraction step, and evaluate the work gained from the the protocol when the extraction is being performed with thermal operation first. In this case, the passive state associated with all the trajectories is simply

$$\rho^S_{3,k} = \rho^S_\beta, \tag{6.18}$$

as when extracting work through thermal operation the final state reached by the system is the state in thermal equilibrium with the bath.

As done in Sec. 3.3.2, we can evaluate the work extracted for each trajectory and then average over them all. The work extracted from the state conditioned by the outcome k is given by

$$\mathcal{W}_\beta(\rho^S_{2,k}) = \mathcal{F}_\beta(\rho^S_{2,k}) - \mathcal{F}_\beta(\rho^S_{3,k}) = \mathcal{F}_\beta(\rho^S_{2,k}) - \mathcal{F}_\beta(\rho^S_\beta) \tag{6.19}$$

and the average work gained due to the protocol is

$$\begin{aligned}
\Delta\overline{\mathcal{W}}_{\{\Pi^A_a\}} &= \overline{\mathcal{W}}_{\{\Pi^A_a\}} - \mathcal{W}_\beta(\rho^S_0) = \sum_k p_k \mathcal{W}_\beta(\rho^S_{2,k}) - \mathcal{W}_\beta(\rho^S_0) \\
&= \sum_k p_k \mathcal{F}_\beta(\rho^S_{2,k}) - \mathcal{F}_\beta(\rho^S_\beta) - \mathcal{W}_\beta(\rho^S_0) \\
&= \mathcal{F}_\beta(\rho^S_0) - \mathcal{F}_\beta(\rho^S_0) + \sum_k p_k \mathcal{F}_\beta(\rho^S_{2,k}) - \mathcal{F}_\beta(\rho^S_\beta) - \mathcal{W}_\beta(\rho^S_0) \\
&= \sum_k p_k \left(E(\rho^S_{2,k}) - E(\rho^S_0)\right) + \beta^{-1}\left[S(\rho^S_0) - \sum_k p_k S(\rho^S_{2,k})\right] \\
&= \beta^{-1}\mathcal{J}_{GO},
\end{aligned} \tag{6.20}$$

where we used

- $\rho^S_1 = \sum_k p_k \rho^S_{2,k}$, the unconditional state is obtained by average over the state conditioned by the measurement
- $E(\rho^S_1) = E(\rho^S_0)$, due to the unitary being energy preserving
- $\mathcal{J}_{GO} = S(\rho^S_0) - \sum_k p_k S(\rho^S_{2,k})$, we substituted the Groenewold-Ozawa information gain.

Our result is in agreement with the upper bound for the work extraction from a measurement protocol under ideal condition, given in Eq. (3.73).

We highlight that the definition of work gain due to the protocol differs slightly from those introduced in previous chapters. Previously, the gain was defined as the average change in free energy due to the measurement, quantifying the difference in free energy between the state just before the measurement and the state immediately after, averaged over all outcomes.

This approach allowed us to leverage the convexity of the free energy, using the unraveling of the state to demonstrate that the gain is always positive. However, as previously mentioned, the Groenewold-Ozawa information gain can be negative, and consequently, so can the work gain resulting from the protocol, as in this time is defined as the average change in free energy due to all the steps of the protocol until the work extraction step.

The gain from the protocol is equal the cost whenever $\Delta S^{SA}_{2,0}$ is zero, which in general it isn't in our case. Therefore if we subtract the cost from the gain and write it as

$$\Delta\overline{\mathcal{W}}_{\{\Pi^A_a\}} = \mathcal{W}_{\text{cost}} + \mathcal{W}_{\text{free}}, \tag{6.21}$$

the term $\mathcal{W}_{\text{free}}$ would equal

$$\mathcal{W}_{\text{free}} = -\Delta S^{SA}_{2,0}. \tag{6.22}$$

As discussed by Minagawa and colleagues [105], while in general $\Delta S^{SA}_{2,0}$ can be negative, a sufficient condition for it to be non-negative is if the measurement applied to the memory is a PVM. As we perform a energy measurement on M, we conclude that it is not possible for the difference $\Delta\overline{\mathcal{W}}_{\{\Pi^A_a\}} - \mathcal{W}_{\text{cost}}$ to be positive.

Work extraction with unitary operation When extracting with unitary operation, the passive state associated with each trajectory will, in general, depend on the individual trajectory

$$\rho^S_{3,k} = \rho_{2,k,p}. \tag{6.23}$$

We can evaluate the change in ergotropy due to the protocol as:

$$\begin{aligned}
\Delta\overline{\mathcal{E}}_{\{\Pi^A_a\}} &= \sum_k p_k \mathcal{E}(\rho^S_{2,k}) - \mathcal{E}(\rho^S_0) \\
&= \sum_k p_k \left(\mathcal{F}_\beta(\rho^S_{2,k}) - \mathcal{F}_\beta(\rho^S_{2,k,p})\right) - \left(\mathcal{F}_\beta(\rho^S_0) - \mathcal{F}_\beta(\rho^S_{0,p})\right) \\
&= \sum_k p_k \left[\left(E(\rho^S_{2,k}) - E(\rho^S_0)\right) + \beta^{-1}\left(S(\rho^S_0) - S(\rho^S_{2,k})\right)\right] + \left(\mathcal{F}_\beta(\rho^S_{0,p}) - \sum_k p_k \mathcal{F}_\beta(\rho^S_{2,k,p})\right) \\
&= E(\rho^S_1) - E(\rho^S_0) + \beta^{-1}\mathcal{J}_{GO} + (\mathcal{F}_\beta(\rho^S_{0,p}) - \sum_k p_k \mathcal{F}_\beta(\rho^S_{2,k,p})) \\
&= \beta^{-1}\mathcal{J}_{GO} + \Delta\overline{\mathcal{F}}_{2,0,p}\ ,
\end{aligned} \tag{6.24}$$

where this time we defined the quantity $\overline{\mathcal{F}}_{2,0,p} = \mathcal{F}_\beta(\rho^S_{0,p}) - \sum_k p_k \mathcal{F}_\beta(\rho^S_{2,k,p})$, which quantify the average change in the residual free energy of the passive state before and after the protocol.

We recall that also in this case, the gain is defined as the change in ergotropy due to the protocol, and not due to the measurement, so it is not guaranteed to be positive or to satisfy the boundaries discussed in Chapter 5.

It is straightforward to show that the daemonic gain result for our protocol is compatible with the generic bound for work extraction established by Minagawa and colleagues. However, as it might be expected, it does not saturate this bound. As described in Sec. 3.4, it is generally not possible to saturate the bound with purely unitary operation, and the difference from the upper bound in our case is proportional to

$$\beta^{-1} I(S:K)_{\rho^S_3} = \beta^{-1}\left(S(\sum_k p_k \rho^S_{2,k,p}) - \sum_k p_k S(\rho^S_{2,p,k})\right). \tag{6.25}$$

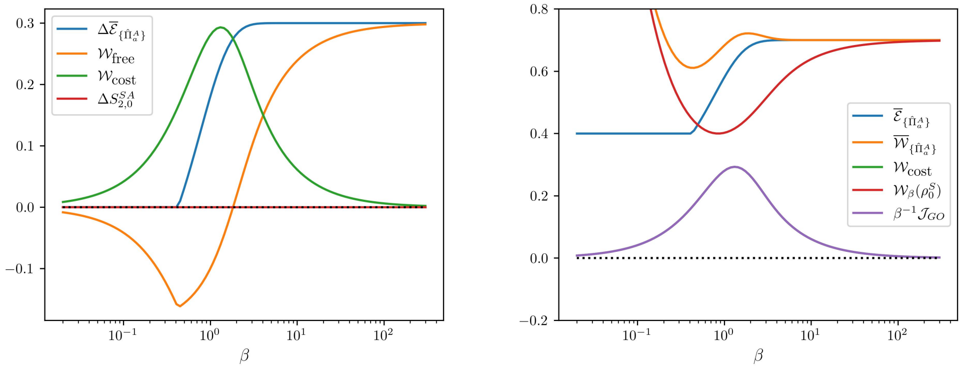

Figure 6.2: Plots of the results obtained from simulation with an initial state ρ_0^S given by Eq. 6.27, with $p = 0.7$. On the left: plot of the daemonic gain and its components in terms of work cost and cost-free work variation. The change in entropy is reported, which is shown to be always zero for all temperature. On the right: Plot of the daemonic ergotropy compared to the work extracted from thermal operations, both with and without applying the measurement protocol. The associated work cost and Groenewold-Ozawa information gain are also shown for reference. In this scenario the work cost is equal to the Groenewold-Ozawa information gain.

It is still possible to describe the daemonic gain in term of a work cost plus a cost free work variation as done in the previous section. Using the work cost evaluated for this protocol, we define the cost free work variation as

$$\begin{aligned}\Delta\overline{\mathcal{E}}_{\{\Pi_a^A\}} &= \Delta\overline{\mathcal{F}}_{2,0,p} + \beta^{-1}[\mathcal{J}_{GO} + \Delta S^{SA}_{2,0} + -\Delta S^{SA}_{2,0}] \\ &= \mathcal{W}_{\mathrm{cost}} + \Delta\overline{\mathcal{F}}_{2,0,p} - \beta^{-1}\left[\Delta S^{SA}_{2,0}\right] = \mathcal{W}_{\mathrm{cost}} + \mathcal{W}_{\mathrm{free}},\end{aligned} \tag{6.26}$$

where $\mathcal{W}_{\mathrm{free}} = \Delta\overline{\mathcal{F}}_{2,0,p} - \beta^{-1}\left[\Delta S^{SA}_{2,0}\right]$. As in the previous case, and contrarily to the gain evaluated for thermal operation, the cost free work variation can be either positive or negative.

6.3 A QND-energy measurement protocol for extracting work from a qubit quantum battery

In this section, we apply the results derived earlier to a paradigmatic example of a qubit quantum battery to optimize work extraction and evaluate the convenience of our proposed protocol. Specifically, we consider numerical simulations of the protocol implemented on a system S, modeled as a two-level system with Hamiltonian $\hat{H}_0 = \omega_0(\hat{\sigma}_z + 1)/2$, and initialized in arbitrary states. In particular, for this analysis we will discuss results obtained with initial states for S that are incoherent, generated as

$$\rho_0^S = p\,|1\rangle\langle 1| + (1-p)\,|0\rangle\langle 0| \tag{6.27}$$

or coherent, generated as

$$\rho_0^S = p\,|+\rangle\langle +| + (1-p)\,|-\rangle\langle -|\,, \tag{6.28}$$

with $|+\rangle, |-\rangle$ being the eigenstates of $\hat{\sigma_x}$, both for some particular choice of p. The memory M also consists of a qubit with Hamiltonian $\hat{H}_0$, initially in a thermal state at inverse temperature β. The memory operator $\hat{A}$, satisfying the relation in Eq. (6.5), is chosen as $\hat{A} = \pi\hat{\sigma}_x/2$. This particular choice is so that the basis $|\psi_n\rangle$ correspond to the energy eigenbasis of A.

In Figure 6.2, we present the results for an initial state of S that is diagonal in the energy eigenbasis. Specifically, we plot the results for ρ_0^S, as defined in Eq. 6.27, with $p = 0.7$.

Our simulations explore various values of p, both above and below $p = 0.5$, which serves as a cutoff between active and passive states. For all cases, the behavior of the quantities of interest remains similar, except for $p = 0.5$, which exhibits a subtle difference that we will highlight.

In the left panel, we plot the daemonic gain and its two components: the work cost of the measurement, $\mathcal{W}_{\text{cost}}$, and the cost-free work variation, $\mathcal{W}_{\text{free}}$. Additionally, we include $\beta^{-1}\Delta S_{2,0}^{SA}$, which is found to be zero at all temperatures in this scenario. Consequently, the work cost $\mathcal{W}_{\text{cost}}$ is equal to the Groenewold-Ozawa information gain.

The daemonic gain is a monotonic function of β, bounded by $\Delta\overline{\mathcal{E}}_{\{\Pi_a^A\}} = E(\rho_0^S) - \mathcal{E}(\rho_0^S)$ as $\beta \to \infty$ and $\Delta\overline{\mathcal{E}}_{\{\Pi_a^A\}} = 0$ as $\beta \to 0$. Surprisingly, in this particular case where the initial state is diagonal in the energy eigenbasis, the daemonic ergotropy satisfy the same boundaries discussed in Chapter 5, while the daemonic gain preserves its positivity.

The work cost of the measurement is always positive, peaking at a finite value of β and vanishing at the extremes. This behavior arises because, while significant information is accessible as $\beta \to \infty$, the associated work cost is suppressed as $1/\beta$. Conversely, as $\beta \to 0$, the information content of the measurement, quantified by $\mathcal{J}_{GO}$, diminishes to zero.

The cost-free work variation, $\mathcal{W}_{\text{free}}$, is maximized at low temperatures ($\beta \to \infty$) and decreases as the temperature increases, becoming negative at a finite value of β. For all studied cases except $p = 0.5$, there exists a threshold temperature above which $\mathcal{W}_{\text{free}}$ becomes negative. For $p = 0.5$, however, the cost-free work variation remains positive across all temperatures.

For the daemonic ergotropy, this protocol therefore achieves a net gain whenever $\mathcal{W}_{\text{free}}$ is positive, which is verified at low temperature, while if one's interested resides in purely maximize the work extraction regardless of its cost, the daemonic gain is higher than zero for a larger range of temperatures. In this scenario there is no real drawback to apply this protocol as in any case the gain never becomes negative.

In the right panel, we compare the daemonic ergotropy obtained using this protocol to the work extractable through thermal operations, with and without applying the measurement protocol. For reference, the Groenewold-Ozawa information gain, representing the work gain enabled by the protocol, is also shown.

The work extractable from thermal operations exhibits a minimum at $\beta^\star$, where $\beta^\star$ satisfies $S(\rho_0^S) = S(\rho_{\beta^\star}^S)$. At other β values, additional work can be extracted by exploiting the temperature difference between the system and the bath. As $\beta \to \infty$, the extractable work for all extraction methods converges to the upper bound of the daemonic ergotropy, determined by the initial energy of the system. In this regime, the work gain from the protocol vanishes, and the extractable work coincides with the system's initial energy.

In this specific case, as $\beta^{-1}\Delta S_{2,0}^{SA} = 0$ for all temperatures, the work gain for thermal operations corresponds exactly to the measurement cost, demonstrating that the protocol achieves maximum efficiency with no dissipative terms.

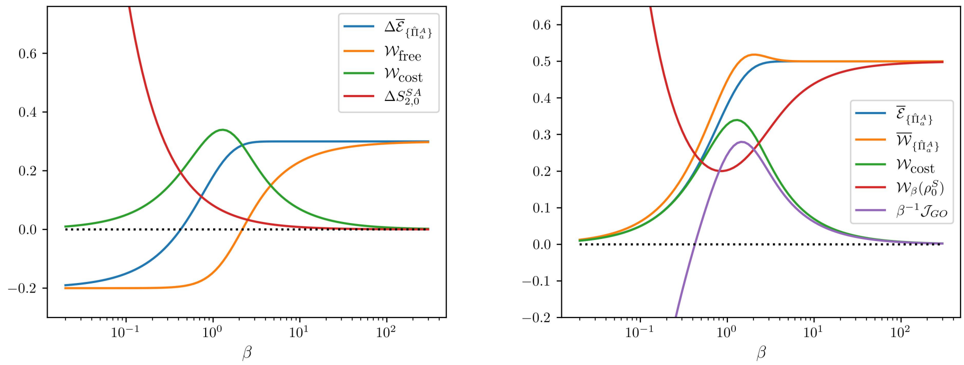

Figure 6.3: On the left: plot of the daemonic gain and its components in terms of work cost and cost-free work variation for an initial state ρ_0^S given by Eq. 6.28, with $p = 0.7$. On the right: Plot of the daemonic ergotropy compared to the work extracted from thermal operations, both with and without applying the measurement protocol. The associated work cost and Groenewold-Ozawa information gain are also shown for reference.

At lower β, thermal operations significantly outperform unitary operations. In this regime, as the gain from the protocol approaches zero, there is no substantial difference between the two thermal extraction protocols (with and without the measurement scheme).

Between these extremes, when the protocol's gain is near its peak, the daemonic ergotropy significantly outperforms thermal operations without the measurement protocol. When the measurement protocol is included, thermal operations naturally provide an upper bound for the daemonic ergotropy.

Over a finite range of β, the daemonic ergotropy exceeds the work achievable via thermal operations and approaches the measurement-enhanced work extracted from thermal operations at low temperatures.

The results of simulations with an initially coherent state are presented in Fig. 6.3. Since the behaviors of all studied quantities are similar across cases, we again show results for a single value of $p = 0.7$. In both panels, the same metrics as in the previous case are plotted.

In the left panel, we observe that, unlike the incoherent case, $\Delta S_{2,0}^{SA}$ is no longer zero for all temperatures; instead, it decreases exponentially as β increases. This implies that for an initially coherent state, the cost of the protocol is no longer equal to the Groenewold-Ozawa information gain, leading to a lower overall efficiency. For example, in the case of thermal operation, this implies that the cost of performing the measures is no longer equal to the gain.

Another difference in the left panel is that the Groenewold-Ozawa information gain becomes negative at lower β. In this regime, the work extracted through this protocol when using either unitary or thermal operation is lower than the work extracted without applying the protocol. Interestingly, the behavior of the work extracted via measurement enhanced thermal operation in this regime resembles that of the daemonic ergotropy, no longer increasing as the temperature of the bath increases.

Overall, for an initially coherent state, the differences between high and low β are significant. At high β, the protocol can be applied efficiently as a tool for work extraction.

At low β, however, it has a detrimental effect on the work extraction process.

6.4 Conclusion

In this chapter, we studied a QND-energy measurement protocol for enhancing work extraction from a quantum battery. As a preliminary step, we characterized the daemonic gain in terms of the informational content of classical correlations within a generic bipartite system. These correlations were quantified using the quantum-classical mutual information. Through this analysis, we established a framework that decomposes the daemonic gain into two components: the measurement cost and a cost-free work variation, while also elucidating its connection to quantum correlations.

We contextualized the proposed extraction protocol within the framework of Landauer's principle, properly accounting for both the gain and the work cost associated with the measurement process. Importantly, we demonstrated that our protocol is efficient by proving that it saturates the work extraction bound established by Minagawa and colleagues [105] when employing thermal operations, which are necessary to achieve this bound.

However, thermal operations are challenging to implement experimentally, in contrast to unitary operations. We further showed that work extraction via unitary operations is also efficient, even if formally they do not saturate the bound by Minagawa and colleagues [105], and for this case, we quantified the deviation from the upper bound. This deviation arises solely from the inability of the passive state, in general, to achieve uniformity across all trajectories. We extended the characterization of the daemonic gain to this scenario, confirming that it can still be expressed as the sum of the measurement cost and the cost-free work variation.

To validate our findings, we applied the results to the paradigmatic example of a qubit quantum battery initialized in arbitrary states. In particular we investigated our results in the cases where the initial states where either diagonal or non-diagonal in the energy eigenbasis. Our analysis revealed that these two cases give raises to completely different scenarios.

In both cases, the cost-free work variation is maximized when interacting with a zero-temperature bath, from which it gradually decreases as the temperature increases and the efficiency of the measurement diminishes. Notably, the daemonic ergotropy demonstrates its ability to outperform thermal operations for finite values of β and remains comparable to measurement-enhanced thermal operations over a broad range of low temperatures. In this region, the conditional mutual information resulting from the measurement—i.e., the factor that prevents the daemonic ergotropy from saturating Minagawa's upper bound—has negligible values, showing that our protocol optimize work extraction through unitary operations.

At higher temperatures, the scenario differs. For an incoherent initial state, the protocol becomes ineffective. The information gained from the measurement as it becomes more inefficient goes to zero, therefor the work gained also goes to zero. Surprisingly, it never becomes negative, achieving less work extracted than it was possible without the protocol.

Differently, if the initial state is coherent, when the measurement is highly inefficient, the protocol becomes counterproductive, as the information gained fails to offset the cost of generating correlations between the battery and the memory. In such cases, it is more effective to extract work directly without performing the measurement.

A proof-of-principle demonstration of our results could be realized on a circuit-QED platform. Additionally, digital quantum computers offer a promising avenue for simulating and validating our findings [163].

Conclusion and outlooks

In this PhD dissertation, we presented our contributions to the field of open quantum batteries. Our results are centered on two primary objectives in this area of research: (1) characterizing and understanding the influence of noise on open quantum batteries, and (2) developing optimal control techniques to enhance battery performance through the use of quantum measurement.

In Chapter 1, we reviewed fundamentals concepts from quantum mechanics. We introduced the postulates of quantum mechanics in its standard formulation, which describe how a closed quantum system behaves. We further described the tools used to describe open quantum systems and showed how these tools can be considered as resulting from an extension of the standard postulates.

In Chapter 2, we characterize the behaviour of open quantum system, in our case defined as quantum system interacting with a reservoir or a heat bath. We show that in the Markovian regime, the dynamics of the system is described by a a differential equation known as the GKSL master equation, while in the non-Markovian regime the dynamics is known to be described an integro-differential master equation. For continuously monitored quantum system, the back-action effect of the measurement leads to a stochastic dynamics unravelling in trajectories of which properties are determined by a stochastic master equation.

In Chapter 3, We summarize concept from quantum thermodynamics that are useful for the rest of the thesis. In particular, we determine the amount of work that can be extracted from a quantum system through either thermal operation or unitary operation. We define the daemonic ergotropy as the amount of work that can be extracted from a quantum system, on average, when the system can be measured, and studied it's equivalent quantity when the final extraction step is performed through a thermal operation. We characterize the improvement in work extraction in terms of additional work performed through the measurement, and show that it correlates with concept from Maxwell's demon, where a feedback operation (the extraction process conditioned on the outcome of the measurement) allow to further extract work by making use of the acquired information. We characterize the cost of the measurement through Landauer's limit and the second law of informational thermodynamics. We finally provide a review of some important results concerning the quantum batteries in both closed and open system settings. We include a description of experimental works on the arguments and a discussion on the major challenges for future experimental works.

In Chapter 4, we studied the dynamics of an open quantum battery using a collisional model capable of introducing memory effects in its dynamics. We observed that an increase in memory effects in the battery dynamics generally reduces the capacity to extract work, as quantified by the ergotropy of the steady state. However, the interplay between different sources of memory effects revealed non-linear behavior. Specifically, memory effects induced by the environment could mitigate pre-existing memory effects within the battery's dynamics, thereby improving its performance. We concluded that environmental memory effects may play a non-trivial role in enhancing battery performance, particularly in charger-mediated interactions.

In Chapter 5, we extended the concept of daemonic ergotropy to continuously monitored open quantum systems. We established upper and lower bounds for the daemonic ergotropy of an unraveling in terms of the energy and ergotropy of the corresponding unconditional state. Additionally, we derived corollaries to these bounds, which extended the analysis to the daemonic power, i.e., the average rate of change of the daemonic ergotropy. These results provide a theoretical foundation for evaluating work extraction in continuously monitored quantum systems.

In Chapter 6, we proposed a protocol for QND-energy measurement, including its application in non-ideal regimes, and analyzed the work gain and energy cost associated with the protocol. For thermal operations, we demonstrated that the extractable work saturates the bounds established in [105], confirming the optimality of the proposed protocol. For unitary operations, while the upper bounds could not be saturated, we quantified the deviation from the bounds and showed that this deviation becomes arbitrarily small for efficient measurements as the temperature of the bath, which models measurement inefficiency, approaches zero. In both cases, we characterized the gain from the protocol in terms of its cost and a cost-free energy variation. Notably, for thermal operations, the cost-free variation is always non-positive, while for unitary operations, it can be positive if the measurement efficiency exceeds a certain threshold, i.e., if the temperature is sufficiently low.

In conclusion, this dissertation advances our understanding of open quantum batteries, particularly in terms of the influence of noise and the development of measurement-based control strategies to enhance performance. However, many open questions remain, and further research is needed to fully understand the potential of quantum batteries. In the following, we provide some future directions towards which our effort could be directed to achieve such result.

Outlooks

While significant progress has been made in studying the influence of environmental interactions on quantum battery dynamics under the Markovian approximation, much less attention has been given to non-Markovian regimes. Our results in this context are among the first contributions of this type. Future research could apply similar methodologies to investigate other types of noise, such as decoherence, and their effects on quantum battery performance. The results characterizing daemonic ergotropy in terms of correlations in bipartite systems suggest that system-environment correlation buildup plays a critical role in dissipation processes. As proposed in this dissertation, further studies could use collisional models that explicitly allows for such analysis. Moreover, while the stabilization of quantum battery charge in an open system setting is an ongoing area of research, it would be valuable to study work extraction during transient dynamics, focusing on specific time intervals that optimize figures of merit such as ergotropy or average charging power. In terms of quantum measurement, our findings provide a basis for further development of measurement-based control strategies, particularly by incorporating cost considerations into performance evaluations. Extending the QND-energy measurement protocol to the framework of continuous measurement could offer new insights into the cost-performance trade-offs in this context. Furthermore, trade-offs between maximum power and power stability, as suggested in [126], are expected to apply to daemonic ergotropy. However, a comprehensive characterization of work distribution for extraction protocols involving measurement is currently lacking in the literature and presents a promising avenue for future work.

From an experimental perspective, the results presented in this thesis on measurement enhanced work extraction are experimentally feasible within certain limitations. While generic thermal operations are notoriously challenging to implement, in part due to difficulties in reconciling their theoretical definition with experimental constraints [226], alternative pathways exist. For instance, efficient thermal operations can be implemented by leveraging the adiabatic theorem [227] enabling work extraction via quasistatic dynamics, albeit at the cost of reduced power output. In contrast, as demonstrated in Chapter 6, measurement protocols augmented by unitary operations can match the efficiency of thermal operations in specific regimes, offering a viable alternative for fully extracting work from quantum systems without relying on environmental interactions.

Recent proposals for elementary thermal operations (ETOs) [228], a simplified subset of thermal operations, may further bridge the gap between theory and experiment. However, a systematic comparison of their performance relative to both thermal and unitary operations in the context of daemonic work extraction remains an open question. A faithful implementation of our protocols based on thermal operations may be experimentally challenging, so a pragmatic compromise involves leveraging techniques such as quasistatic dynamics, shortcuts to adiabaticity, ETOs, or quantum adiabatic brachistochrones [229]. Although these methods may not saturate the theoretical upper bounds for daemonic work extraction, they are expected to outperform protocols lacking the feedback mechanisms. A comprehensive comparison of measurement enhanced work extraction with experimentally realizable discharging protocols remains a critical direction for future work.

Notably, unitary operations face fewer practical hurdles than thermal operations. Recent proof-of-principle experiments, such as those on the IBM Quantum platform [163], have successfully demonstrated the feedback mechanism. The measurement scheme proposed in Chapter 6 (see Sec. 6.4) is readily implementable across multiple experimental platforms. Further simplifications arise when our protocol is implemented through continuous measurement of the energy eigenbasis: the inherent purification effect drives the system toward a Hamiltonian eigenstate over time, obviating the need for complex feedback control. From the photocurrent, the collapse trajectory can be inferred, enabling effective feedback with a finite set of operations.

Bibliography

[1] Daniele Morrone, Matteo A. C. Rossi, Andrea Smirne, and Marco G. Genoni. Charging a quantum battery in a non-Markovian environment: A collisional model approach. *Quantum Science and Technology*, 8(3):035007, May 2023.

[2] Daniele Morrone, Matteo A.C. Rossi, and Marco G. Genoni. Daemonic ergotropy in continuously monitored open quantum batteries. *Physical Review Applied*, 20(4):044073, October 2023.

[3] Daniele Morrone, Francesco Albarelli, Vittorio Giovannetti, and Marco G. Genoni. Daemonic work extraction via qnd-energy measurement. in preparation.

[4] Daniele Morrone, N. Walter Talarico, Marco Cattaneo, and Matteo A. C. Rossi. Estimating Molecular Thermal Averages with the Quantum Equation of Motion and Informationally Complete Measurements. *Entropy*, 26(9):722, September 2024.

[5] Donato Farina, Gian Marcello Andolina, Andrea Mari, Marco Polini, and Vittorio Giovannetti. Charger-mediated energy transfer for quantum batteries: An open system approach. *Physical Review B*, 99(3):035421, January 2019.

[6] Michael A. Nielsen and Isaac L. Chuang. *Quantum Computation and Quantum Information: 10th Anniversary Edition*. Cambridge University Press, Cambridge, 2010.

[7] Matteo G. A. Paris. The modern tools of quantum mechanics (A tutorial on quantum states, measurements, and operations). *The European Physical Journal Special Topics*, 203(1):61–86, April 2012.

[8] H. P. Breuer and F. Petruccione. *The Theory of Open Quantum Systems*. Oxford University Press, 2002.

[9] Teiko Heinosaari and Mário Ziman. *The Mathematical Language of Quantum Theory: From Uncertainty to Entanglement*. Cambridge University Press, Cambridge, 2011.

[10] Li Li, Michael J. W. Hall, and Howard M. Wiseman. Concepts of quantum non-Markovianity: A hierarchy. *Physics Reports*, 759:1–51, October 2018.

[11] Ángel Rivas, Susana F. Huelga, and Martin B. Plenio. Quantum non-Markovianity: Characterization, quantification and detection. *Reports on Progress in Physics*, 77(9):094001, August 2014.

[12] Heinz-Peter Breuer, Elsi-Mari Laine, Jyrki Piilo, and Bassano Vacchini. Colloquium: Non-Markovian dynamics in open quantum systems. *Reviews of Modern Physics*, 88(2):021002, April 2016.

[13] G. Lindblad. On the generators of quantum dynamical semigroups. *Communications in Mathematical Physics*, 48(2):119–130, June 1976.

[14] Vittorio Gorini, Andrzej Kossakowski, and E. C. G. Sudarshan. Completely positive dynamical semigroups of N-level systems. *Journal of Mathematical Physics*, 17(5):821–825, May 1976.

[15] Adrián A. Budini. Stochastic representation of a class of non-Markovian completely positive evolutions. *Physical Review A*, 69(4):042107, April 2004.

[16] P. Kaer, T. R. Nielsen, P. Lodahl, A.-P. Jauho, and J. Mørk. Non-Markovian Model of Photon-Assisted Dephasing by Electron-Phonon Interactions in a Coupled Quantum-Dot–Cavity System. *Physical Review Letters*, 104(15):157401, April 2010.

[17] Jin-Shi Xu, Chuan-Feng Li, Cheng-Jie Zhang, Xiao-Ye Xu, Yong-Sheng Zhang, and Guang-Can Guo. Experimental investigation of the non-Markovian dynamics of classical and quantum correlations. *Physical Review A*, 82(4):042328, October 2010.

[18] K. W. Murch, S. J. Weber, C. Macklin, and I. Siddiqi. Observing single quantum trajectories of a superconducting quantum bit. *Nature*, 502(7470):211–214, October 2013.

[19] P. Campagne-Ibarcq, P. Six, L. Bretheau, A. Sarlette, M. Mirrahimi, P. Rouchon, and B. Huard. Observing Quantum State Diffusion by Heterodyne Detection of Fluorescence. *Physical Review X*, 6(1):011002, January 2016.

[20] Q. Ficheux, S. Jezouin, Z. Leghtas, and B. Huard. Dynamics of a qubit while simultaneously monitoring its relaxation and dephasing. *Nature Communications*, 9(1):1926, May 2018.

[21] Z. K. Minev, S. O. Mundhada, S. Shankar, P. Reinhold, R. Gutiérrez-Jáuregui, R. J. Schoelkopf, M. Mirrahimi, H. J. Carmichael, and M. H. Devoret. To catch and reverse a quantum jump mid-flight. *Nature*, 570(7760):200–204, June 2019.

[22] Witlef Wieczorek, Sebastian G. Hofer, Jason Hoelscher-Obermaier, Ralf Riedinger, Klemens Hammerer, and Markus Aspelmeyer. Optimal State Estimation for Cavity Optomechanical Systems. *Physical Review Letters*, 114(22):223601, June 2015.

[23] Massimiliano Rossi, David Mason, Junxin Chen, Yeghishe Tsaturyan, and Albert Schliesser. Measurement-based quantum control of mechanical motion. *Nature*, 563(7729):53–58, November 2018.

[24] David Mason, Junxin Chen, Massimiliano Rossi, Yeghishe Tsaturyan, and Albert Schliesser. Continuous force and displacement measurement below the standard quantum limit. *Nature Physics*, 15(8):745–749, August 2019.

[25] Rodrigo A. Thomas, Michał Parniak, Christoffer Østfeldt, Christoffer B. Møller, Christian Bærentsen, Yeghishe Tsaturyan, Albert Schliesser, Jürgen Appel, Emil Zeuthen, and Eugene S. Polzik. Entanglement between distant macroscopic mechanical and spin systems. *Nature Physics*, 17(2):228–233, February 2021.

[26] Lorenzo Magrini, Philipp Rosenzweig, Constanze Bach, Andreas Deutschmann-Olek, Sebastian G. Hofer, Sungkun Hong, Nikolai Kiesel, Andreas Kugi, and Markus Aspelmeyer. Real-time optimal quantum control of mechanical motion at room temperature. *Nature*, 595(7867):373–377, July 2021.

[27] Felix Tebbenjohanns, M. Luisa Mattana, Massimiliano Rossi, Martin Frimmer, and Lukas Novotny. Quantum control of a nanoparticle optically levitated in cryogenic free space. *Nature*, 595(7867):378–382, July 2021.

[28] Howard M. Wiseman and Gerard J. Milburn. *Quantum Measurement and Control*. Cambridge University Press, November 2009.

[29] Kurt Jacobs. *Quantum Measurement Theory and Its Applications*. Cambridge University Press, Cambridge, 2014.

[30] H. M. Wiseman and G. J. Milburn. Quantum theory of optical feedback via homodyne detection. *Physical Review Letters*, 70(5):548–551, February 1993.

[31] H. M. Wiseman. Quantum theory of continuous feedback. *Physical Review A*, 49(3):2133–2150, March 1994.

[32] A. C. Doherty and K. Jacobs. Feedback control of quantum systems using continuous state estimation. *Physical Review A*, 60(4):2700–2711, October 1999.

[33] L. K. Thomsen, S. Mancini, and H. M. Wiseman. Spin squeezing via quantum feedback. *Physical Review A*, 65(6):061801, June 2002.

[34] Alessio Serafini and Stefano Mancini. Determination of Maximal Gaussian Entanglement Achievable by Feedback-Controlled Dynamics. *Physical Review Letters*, 104(22):220501, June 2010.

[35] A. Szorkovszky, A. C. Doherty, G. I. Harris, and W. P. Bowen. Mechanical Squeezing via Parametric Amplification and Weak Measurement. *Physical Review Letters*, 107(21):213603, November 2011.

[36] Marco G. Genoni, Stefano Mancini, and Alessio Serafini. Optimal feedback control of linear quantum systems in the presence of thermal noise. *Physical Review A*, 87(4):042333, April 2013.

[37] Marco G. Genoni, Jinglei Zhang, James Millen, Peter F. Barker, and Alessio Serafini. Quantum cooling and squeezing of a levitating nanosphere via time-continuous measurements. *New Journal of Physics*, 17(7):073019, July 2015.

[38] Sebastian G. Hofer and Klemens Hammerer. Entanglement-enhanced time-continuous quantum control in optomechanics. *Physical Review A*, 91(3):033822, March 2015.

[39] Leigh Martin, Felix Motzoi, Hanhan Li, Mohan Sarovar, and K. Birgitta Whaley. Deterministic generation of remote entanglement with active quantum feedback. *Physical Review A*, 92(6):062321, December 2015.

[40] Matteo Brunelli, Daniel Malz, and Andreas Nunnenkamp. Conditional Dynamics of Optomechanical Two-Tone Backaction-Evading Measurements. *Physical Review Letters*, 123(9):093602, August 2019.

[41] Yuxiao Jiang, Xiyue Wang, Leigh Martin, and K. Birgitta Whaley. Optimality of feedback control for qubit purification under inefficient measurement. *Physical Review A*, 102(2):022612, August 2020.

[42] Song Zhang, Leigh S. Martin, and K. Birgitta Whaley. Locally optimal measurement-based quantum feedback with application to multiqubit entanglement generation. *Physical Review A*, 102(6):062418, December 2020.

[43] Antonio Di Giovanni, Matteo Brunelli, and Marco G. Genoni. Unconditional mechanical squeezing via backaction-evading measurements and nonoptimal feedback control. *Physical Review A*, 103(2):022614, February 2021.

[44] Alessandro Candeloro, Claudia Benedetti, Marco G. Genoni, and Matteo G. A. Paris. Feedback-Assisted Quantum Search by Continuous-Time Quantum Walks. *Advanced Quantum Technologies*, 6(1):2200093, 2023.

[45] Frederik Werner Isaksen and Ulrik Lund Andersen. Mechanical cooling and squeezing using optimal control. *Physical Review A*, 107(2):023512, February 2023.

[46] H. Mabuchi. Dynamical identification of open quantum systems. *Quantum and Semiclassical Optics: Journal of the European Optical Society Part B*, 8(6):1103, December 1996.

[47] Jay Gambetta and H. M. Wiseman. State and dynamical parameter estimation for open quantum systems. *Physical Review A*, 64(4):042105, September 2001.

[48] JM Geremia, John K. Stockton, Andrew C. Doherty, and Hideo Mabuchi. Quantum Kalman Filtering and the Heisenberg Limit in Atomic Magnetometry. *Physical Review Letters*, 91(25):250801, December 2003.

[49] Mădălin Guţă, Bas Janssens, and Jonas Kahn. Optimal Estimation of Qubit States with Continuous Time Measurements. *Communications in Mathematical Physics*, 277(1):127–160, January 2008.

[50] Mankei Tsang. Optimal waveform estimation for classical and quantum systems via time-symmetric smoothing. ii. applications to atomic magnetometry and hardy's paradox. *Phys. Rev. A*, 81:013824, Jan 2010.

[51] Mankei Tsang, Howard M. Wiseman, and Carlton M. Caves. Fundamental Quantum Limit to Waveform Estimation. *Physical Review Letters*, 106(9):090401, March 2011.

[52] Mankei Tsang. Quantum metrology with open dynamical systems. *New Journal of Physics*, 15(7):073005, July 2013.

[53] Søren Gammelmark and Klaus Mølmer. Bayesian parameter inference from continuously monitored quantum systems. *Physical Review A*, 87(3):032115, March 2013.

[54] Søren Gammelmark and Klaus Mølmer. Fisher Information and the Quantum Cram\'er-Rao Sensitivity Limit of Continuous Measurements. *Physical Review Letters*, 112(17):170401, April 2014.

[55] P. Six, Ph. Campagne-Ibarcq, L. Bretheau, B. Huard, and P. Rouchon. Parameter estimation from measurements along quantum trajectories. In *2015 54th IEEE Conference on Decision and Control (CDC)*, pages 7742–7748, December 2015.

[56] Catalin Catana, Luc Bouten, and Mădălin Guţă. Fisher informations and local asymptotic normality for continuous-time quantum Markov processes. *Journal of Physics A: Mathematical and Theoretical*, 48(36):365301, August 2015.

[57] Alexander Holm Kiilerich and Klaus Mølmer. Bayesian parameter estimation by continuous homodyne detection. *Physical Review A*, 94(3):032103, September 2016.

[58] Jason F. Ralph, Simon Maskell, and Kurt Jacobs. Multiparameter estimation along quantum trajectories with sequential Monte Carlo methods. *Physical Review A*, 96(5):052306, November 2017.

[59] Marco G. Genoni. Cram\'er-Rao bound for time-continuous measurements in linear Gaussian quantum systems. *Physical Review A*, 95(1):012116, January 2017.

[60] Francesco Albarelli, Matteo A. C. Rossi, Matteo G. A. Paris, and Marco G. Genoni. Ultimate limits for quantum magnetometry via time-continuous measurements. *New Journal of Physics*, 19(12):123011, December 2017.

[61] Massimiliano Rossi, Luca Mancino, Gabriel T. Landi, Mauro Paternostro, Albert Schliesser, and Alessio Belenchia. Experimental Assessment of Entropy Production in a Continuously Measured Mechanical Resonator. *Physical Review Letters*, 125(8):080601, August 2020.

[62] Theodoros Ilias, Dayou Yang, Susana F. Huelga, and Martin B. Plenio. Criticality-Enhanced Quantum Sensing via Continuous Measurement. *PRX Quantum*, 3(1):010354, March 2022.

[63] Dayou Yang, Susana F. Huelga, and Martin B. Plenio. Efficient Information Retrieval for Sensing via Continuous Measurement. *Physical Review X*, 13(3):031012, July 2023.

[64] Cyril Elouard and M. Hamed Mohammady. Work, Heat and Entropy Production Along Quantum Trajectories. In Felix Binder, Luis A. Correa, Christian

Gogolin, Janet Anders, and Gerardo Adesso, editors, *Thermodynamics in the Quantum Regime: Fundamental Aspects and New Directions*, Fundamental Theories of Physics, pages 363–393. Springer International Publishing, Cham, 2018.

[65] Gonzalo Manzano and Roberta Zambrini. Quantum thermodynamics under continuous monitoring: A general framework. *AVS Quantum Science*, 4(2):025302, May 2022.

[66] Juan P. Garrahan and Igor Lesanovsky. Thermodynamics of Quantum Jump Trajectories. *Physical Review Letters*, 104(16):160601, April 2010.

[67] Juan P. Garrahan, Andrew D. Armour, and Igor Lesanovsky. Quantum trajectory phase transitions in the micromaser. *Physical Review E*, 84(2):021115, August 2011.

[68] Juan P. Garrahan and Mădălin Guţă. Catching and reversing quantum jumps and thermodynamics of quantum trajectories. *Physical Review A*, 98(5):052137, November 2018.

[69] Dario Cilluffo, Salvatore Lorenzo, G. Massimo Palma, and Francesco Ciccarello. Quantum jump statistics with a shifted jump operator in a chiral waveguide. *Journal of Statistical Mechanics: Theory and Experiment*, 2019(10):104004, October 2019.

[70] Alessio Belenchia, Luca Mancino, Gabriel T. Landi, and Mauro Paternostro. Entropy production in continuously measured Gaussian quantum systems. *npj Quantum Information*, 6(1):1–7, December 2020.

[71] Gabriel T. Landi and Mauro Paternostro. Irreversible entropy production: From classical to quantum. *Reviews of Modern Physics*, 93(3):035008, September 2021.

[72] Gabriel T. Landi, Mauro Paternostro, and Alessio Belenchia. Informational Steady States and Conditional Entropy Production in Continuously Monitored Systems. *PRX Quantum*, 3(1):010303, January 2022.

[73] Bibek Bhandari and Andrew N. Jordan. Continuous measurement boosted adiabatic quantum thermal machines. *Physical Review Research*, 4(3):033103, August 2022.

[74] Kagan Yanik, Bibek Bhandari, Sreenath K. Manikandan, and Andrew N. Jordan. Thermodynamics of quantum measurement and Maxwell's demon's arrow of time. *Physical Review A*, 106(4):042221, October 2022.

[75] Bibek Bhandari, Robert Czupryniak, Paolo Andrea Erdman, and Andrew N. Jordan. Measurement-Based Quantum Thermal Machines with Feedback Control. *Entropy*, 25(2):204, February 2023.

[76] Francesco Ciccarello, Salvatore Lorenzo, Vittorio Giovannetti, and G. Massimo Palma. Quantum collision models: Open system dynamics from repeated interactions. *Physics Reports*, 954:1–70, April 2022.

[77] Barış Çakmak, Steve Campbell, Bassano Vacchini, Özgür E. Müstecaplıoğlu, and Mauro Paternostro. Robust multipartite entanglement generation via a collision model. *Physical Review A*, 99(1):012319, January 2019.

[78] Francesco Ciccarello. Collision models in quantum optics. *Quantum Measurements and Quantum Metrology*, 4(1), December 2017.

[79] Giacomo Guarnieri, Daniele Morrone, Barış Çakmak, Francesco Plastina, and Steve Campbell. Non-equilibrium steady-states of memoryless quantum collision models. *Physics Letters A*, 384(24):126576, August 2020.

[80] Stella Seah, Stefan Nimmrichter, Daniel Grimmer, Jader P. Santos, Valerio Scarani, and Gabriel T. Landi. Collisional Quantum Thermometry. *Physical Review Letters*, 123(18):180602, October 2019.

[81] Vahid Shaghaghi, G. Massimo Palma, and Giuliano Benenti. Extracting work

from random collisions: A model of a quantum heat engine. *Physical Review E*, 105(3):034101, March 2022.

[82] Steve Campbell, Francesco Ciccarello, G. Massimo Palma, and Bassano Vacchini. System-environment correlations and Markovian embedding of quantum non-Markovian dynamics. *Physical Review A*, 98(1):012142, July 2018.

[83] Francesco Albarelli and Marco G. Genoni. A pedagogical introduction to continuously monitored quantum systems and measurement-based feedback. *Physics Letters A*, 494:129260, January 2024.

[84] Kurt Jacobs and Daniel A. Steck. A Straightforward Introduction to Continuous Quantum Measurement. *Contemporary Physics*, 47(5):279–303, September 2006.

[85] Heinz-Peter Breuer, Elsi-Mari Laine, and Jyrki Piilo. Measure for the Degree of Non-Markovian Behavior of Quantum Processes in Open Systems. *Physical Review Letters*, 103(21):210401, November 2009.

[86] Steffen Wißmann, Antti Karlsson, Elsi-Mari Laine, Jyrki Piilo, and Heinz-Peter Breuer. Optimal state pairs for non-Markovian quantum dynamics. *Physical Review A*, 86(6):062108, December 2012.

[87] Salvatore Lorenzo, Francesco Plastina, and Mauro Paternostro. Geometrical characterization of non-Markovianity. *Physical Review A*, 88(2):020102, August 2013.

[88] H. E. D. Scovil and E. O. Schulz-DuBois. Three-Level Masers as Heat Engines. *Physical Review Letters*, 2(6):262–263, March 1959.

[89] R. Alicki. The quantum open system as a model of the heat engine. *Journal of Physics A: Mathematical and General*, 12(5):L103, May 1979.

[90] Denis J. Evans, E. G. D. Cohen, and G. P. Morriss. Probability of second law violations in shearing steady states. *Physical Review Letters*, 71(15):2401–2404, October 1993.

[91] G. Gallavotti and E. G. D. Cohen. Dynamical Ensembles in Nonequilibrium Statistical Mechanics. *Physical Review Letters*, 74(14):2694–2697, April 1995.

[92] Jorge Kurchan. Fluctuation theorem for stochastic dynamics. *Journal of Physics A: Mathematical and General*, 31(16):3719, April 1998.

[93] Joel L. Lebowitz and Herbert Spohn. A Gallavotti–Cohen-Type Symmetry in the Large Deviation Functional for Stochastic Dynamics. *Journal of Statistical Physics*, 95(1):333–365, April 1999.

[94] Gavin E. Crooks. Entropy production fluctuation theorem and the nonequilibrium work relation for free energy differences. *Physical Review E*, 60(3):2721–2726, September 1999.

[95] C. Jarzynski. Nonequilibrium Equality for Free Energy Differences. *Physical Review Letters*, 78(14):2690–2693, April 1997.

[96] R. Landauer. Irreversibility and Heat Generation in the Computing Process. *IBM Journal of Research and Development*, 5(3):183–191, July 1961.

[97] Leo Szilard. On the decrease of entropy in a thermodynamic system by the intervention of intelligent beings. *Behavioral Science*, 9(4):301–310, 1964.

[98] Fernando G. S. L. Brandão, Michał Horodecki, Jonathan Oppenheim, Joseph M. Renes, and Robert W. Spekkens. Resource Theory of Quantum States Out of Thermal Equilibrium. *Physical Review Letters*, 111(25):250404, December 2013.

[99] John Goold, Marcus Huber, Arnau Riera, Lídia del Rio, and Paul Skrzypczyk. The role of quantum information in thermodynamics—a topical review. *Journal of Physics A: Mathematical and Theoretical*, 49(14):143001, February 2016.

[100] Kurt Jacobs. Quantum measurement and the first law of thermodynamics: The

energy cost of measurement is the work value of the acquired information. *Physical Review E*, 86(4):040106, October 2012.

[101] Kais Abdelkhalek, Yoshifumi Nakata, and David Reeb. Fundamental energy cost for quantum measurement, September 2018.

[102] Giulio Chiribella, Fei Meng, Renato Renner, and Man-Hong Yung. The nonequilibrium cost of accurate information processing. *Nature Communications*, 13(1):7155, November 2022.

[103] Sebastian Deffner, Juan Pablo Paz, and Wojciech H. Zurek. Quantum work and the thermodynamic cost of quantum measurements. *Physical Review E*, 94(1):010103, July 2016.

[104] Takahiro Sagawa and Masahito Ueda. Minimal Energy Cost for Thermodynamic Information Processing: Measurement and Information Erasure. *Physical Review Letters*, 102(25):250602, June 2009.

[105] Shintaro Minagawa, M. Hamed Mohammady, Kenta Sakai, Kohtaro Kato, and Francesco Buscemi. Universal validity of the second law of information thermodynamics, November 2024.

[106] Robert Alicki and Mark Fannes. Entanglement boost for extractable work from ensembles of quantum batteries. *Physical Review E*, 87(4):042123, April 2013.

[107] Felix C. Binder, Sai Vinjanampathy, Kavan Modi, and John Goold. Quantacell: Powerful charging of quantum batteries. *New Journal of Physics*, 17(7):075015, July 2015.

[108] Francesco Campaioli, Felix A. Pollock, Felix C. Binder, Lucas Céleri, John Goold, Sai Vinjanampathy, and Kavan Modi. Enhancing the Charging Power of Quantum Batteries. *Physical Review Letters*, 118(15):150601, April 2017.

[109] Dario Ferraro, Michele Campisi, Gian Marcello Andolina, Vittorio Pellegrini, and Marco Polini. High-Power Collective Charging of a Solid-State Quantum Battery. *Physical Review Letters*, 120(11):117702, March 2018.

[110] Sergi Julia-Farre, Tymoteusz Salamon, Arnau Riera, Manabendra N. Bera, and Maciej Lewenstein. Bounds on the capacity and power of quantum batteries. *Physical Review Research*, 2(2):023113, May 2020.

[111] Nicolai Friis and Marcus Huber. Precision and Work Fluctuations in Gaussian Battery Charging. *Quantum*, 2:61, April 2018.

[112] Mark T. Mitchison, John Goold, and Javier Prior. Charging a quantum battery with linear feedback control. *Quantum*, 5:500, July 2021.

[113] Tanmoy Biswas, Marcin Łobejko, Paweł Mazurek, Konrad Jałowiecki, and Michał Horodecki. Extraction of ergotropy: Free energy bound and application to open cycle engines. *Quantum*, 6:841, October 2022.

[114] Stefano Gherardini, Francesco Campaioli, Filippo Caruso, and Felix C. Binder. Stabilizing open quantum batteries by sequential measurements. *Physical Review Research*, 2(1):013095, January 2020.

[115] M. Carrega, A. Crescente, D. Ferraro, and M. Sassetti. Dissipative dynamics of an open quantum battery. *New Journal of Physics*, 22(8):083085, August 2020.

[116] F. H. Kamin, F. T. Tabesh, S. Salimi, F. Kheirandish, and Alan C. Santos. Non-Markovian effects on charging and self-discharging processes of quantum batteries. *New Journal of Physics*, 22(8):083007, August 2020.

[117] A. E. Allahverdyan, R. Balian, and Th M. Nieuwenhuizen. Maximal work extraction from finite quantum systems. *Europhysics Letters*, 67(4):565, August 2004.

[118] Gianluca Francica, Felix C. Binder, Giacomo Guarnieri, Mark T. Mitchison, John

Goold, and Francesco Plastina. Quantum Coherence and Ergotropy. *Physical Review Letters*, 125(18):180603, October 2020.

[119] Rudolf Haag, Daniel Kastler, and Ewa B. Trych-Pohlmeyer. Stability and equilibrium states. *Communications in Mathematical Physics*, 38(3):173–193, September 1974.

[120] W. Pusz and S. L. Woronowicz. Passive states and KMS states for general quantum systems. *Communications in Mathematical Physics*, 58(3):273–290, October 1978.

[121] A. Lenard. Thermodynamical proof of the Gibbs formula for elementary quantum systems. *Journal of Statistical Physics*, 19(6):575–586, December 1978.

[122] Michał Horodecki and Jonathan Oppenheim. Fundamental limitations for quantum and nanoscale thermodynamics. *Nature Communications*, 4(1):2059, June 2013.

[123] Philippe Faist, Jonathan Oppenheim, and Renato Renner. Gibbs-preserving maps outperform thermal operations in the quantum regime. *New Journal of Physics*, 17(4):043003, April 2015.

[124] Gonzalo Manzano, Francesco Plastina, and Roberta Zambrini. Optimal Work Extraction and Thermodynamics of Quantum Measurements and Correlations. *Physical Review Letters*, 121(12):120602, September 2018.

[125] André M. Timpanaro, Giacomo Guarnieri, John Goold, and Gabriel T. Landi. Thermodynamic Uncertainty Relations from Exchange Fluctuation Theorems. *Physical Review Letters*, 123(9):090604, August 2019.

[126] Patrick Pietzonka and Udo Seifert. Universal Trade-Off between Power, Efficiency, and Constancy in Steady-State Heat Engines. *Physical Review Letters*, 120(19):190602, May 2018.

[127] Patrick Pietzonka, Andre C. Barato, and Udo Seifert. Universal bounds on current fluctuations. *Physical Review E*, 93(5):052145, May 2016.

[128] Andre C. Barato and Udo Seifert. Thermodynamic Uncertainty Relation for Biomolecular Processes. *Physical Review Letters*, 114(15):158101, April 2015.

[129] Giuliano Benenti, Giulio Casati, and Jiao Wang. Power, efficiency, and fluctuations in steady-state heat engines. *Physical Review E*, 102(4):040103, October 2020.

[130] Luca Razzoli, Fabio Cavaliere, Matteo Carrega, Maura Sassetti, and Giuliano Benenti. Efficiency and thermodynamic uncertainty relations of a dynamical quantum heat engine. *The European Physical Journal Special Topics*, 233(6):1263–1274, July 2024.

[131] Luca Razzoli, Matteo Carrega, Fabio Cavaliere, Giuliano Benenti, and Maura Sassetti. Synchronization-induced violation of thermodynamic uncertainty relations. *Quantum Science and Technology*, 9(4):045032, August 2024.

[132] Alan C. Santos, Barış Çakmak, Steve Campbell, and Nikolaj T. Zinner. Stable adiabatic quantum batteries. *Physical Review E*, 100(3):032107, September 2019.

[133] Dario Rosa, Davide Rossini, Gian Marcello Andolina, Marco Polini, and Matteo Carrega. Ultra-stable charging of fast-scrambling SYK quantum batteries. *Journal of High Energy Physics*, 2020(11):67, November 2020.

[134] Francesco Campaioli, Stefano Gherardini, James Q. Quach, Marco Polini, and Gian Marcello Andolina. Colloquium: Quantum batteries. *Reviews of Modern Physics*, 96(3):031001, July 2024.

[135] Raffaele Salvia and Vittorio Giovannetti. On the distribution of the mean energy in the unitary orbit of quantum states. *Quantum*, 5:514, August 2021.

[136] Xue Yang, Yan-Han Yang, Mir Alimuddin, Raffaele Salvia, Shao-Ming Fei, Li-Ming Zhao, Stefan Nimmrichter, and Ming-Xing Luo. Battery Capacity of Energy-

Storing Quantum Systems. *Physical Review Letters*, 131(3):030402, July 2023.

[137] Felipe Barra. Dissipative Charging of a Quantum Battery. *Physical Review Letters*, 122(21):210601, May 2019.

[138] Karen V. Hovhannisyan, Martí Perarnau-Llobet, Marcus Huber, and Antonio Acín. Entanglement Generation is Not Necessary for Optimal Work Extraction. *Physical Review Letters*, 111(24):240401, December 2013.

[139] Gian Marcello Andolina, Donato Farina, Andrea Mari, Vittorio Pellegrini, Vittorio Giovannetti, and Marco Polini. Charger-mediated energy transfer in exactly-solvable models for quantum batteries. *Physical Review B*, 98(20):205423, November 2018.

[140] Gian Marcello Andolina, Maximilian Keck, Andrea Mari, Michele Campisi, Vittorio Giovannetti, and Marco Polini. Extractable work, the role of correlations, and asymptotic freedom in quantum batteries. *Physical Review Letters*, 122(4):047702, February 2019.

[141] Alba Crescente, Matteo Carrega, Maura Sassetti, and Dario Ferraro. Ultrafast charging in a two-photon Dicke quantum battery. *Physical Review B*, 102(24):245407, December 2020.

[142] Ju-Yeon Gyhm, Dario Rosa, and Dominik Šafránek. The minimal time it takes to charge a quantum system, August 2023.

[143] James Q. Quach, Kirsty E. McGhee, Lucia Ganzer, Dominic M. Rouse, Brendon W. Lovett, Erik M. Gauger, Jonathan Keeling, Giulio Cerullo, David G. Lidzey, and Tersilla Virgili. Superabsorption in an organic microcavity: Toward a quantum battery. *Science Advances*, 8(2):eabk3160, January 2022.

[144] Davide Rossini, Gian Marcello Andolina, Dario Rosa, Matteo Carrega, and Marco Polini. Quantum Advantage in the Charging Process of Sachdev-Ye-Kitaev Batteries. *Physical Review Letters*, 125(23):236402, December 2020.

[145] Ju-Yeon Gyhm, Dominik Šafránek, and Dario Rosa. Quantum Charging Advantage Cannot Be Extensive without Global Operations. *Physical Review Letters*, 128(14):140501, April 2022.

[146] Thao P. Le, Jesper Levinsen, Kavan Modi, Meera M. Parish, and Felix A. Pollock. Spin-chain model of a many-body quantum battery. *Physical Review A*, 97(2):022106, February 2018.

[147] Davide Rossini, Gian Marcello Andolina, and Marco Polini. Many-body localized quantum batteries. *Physical Review B*, 100(11):115142, September 2019.

[148] Srijon Ghosh, Titas Chanda, and Aditi Sen(De). Enhancement in the performance of a quantum battery by ordered and disordered interactions. *Physical Review A*, 101(3):032115, March 2020.

[149] Shadab Zakavati, Fatemeh T. Tabesh, and Shahriar Salimi. Bounds on charging power of open quantum batteries. *Physical Review E*, 104(5):054117, November 2021.

[150] R. R. Rodriguez, B. Ahmadi, G. Suarez, P. Mazurek, S. Barzanjeh, and P. Horodecki. Optimal Quantum Control of Charging Quantum Batteries, June 2022.

[151] Y. Yao and X. Q. Shao. Optimal charging of open spin-chain quantum batteries via homodyne-based feedback control, July 2022.

[152] Kenta Koshihara and Kazuya Yuasa. Quantum ergotropy and quantum feedback control. *Physical Review E*, 107(6):064109, June 2023.

[153] James Q. Quach and William J. Munro. Using Dark States to Charge and Stabilize Open Quantum Batteries. *Physical Review Applied*, 14(2):024092, August 2020.

[154] Srijon Ghosh, Titas Chanda, Shiladitya Mal, and Aditi Sen(De). Fast charging of a quantum battery assisted by noise. *Physical Review A*, 104(3):032207, September 2021.

[155] Gabriel T. Landi and Mauro Paternostro. Irreversible entropy production: From classical to quantum. *Reviews of Modern Physics*, 93(3):035008, September 2021.

[156] Karen V. Hovhannisyan, Felipe Barra, and Alberto Imparato. Charging assisted by thermalization. *Physical Review Research*, 2(3):033413, September 2020.

[157] Stefano Gherardini, Francesco Campaioli, Filippo Caruso, and Felix C. Binder. Stabilizing open quantum batteries by sequential measurements. *Physical Review Research*, 2(1):013095, January 2020.

[158] Stella Seah, Martí Perarnau-Llobet, Géraldine Haack, Nicolas Brunner, and Stefan Nimmrichter. Quantum speed-up in collisional battery charging. *Physical Review Letters*, 127(10):100601, August 2021.

[159] Hui-Yu Yang, Hai-Long Shi, Qing-Kun Wan, Kun Zhang, Xiao-Hui Wang, and Wen-Li Yang. Optimal energy storage in the Tavis-Cummings quantum battery. *Physical Review A*, 109(1):012204, January 2024.

[160] Chang-Kang Hu, Jiawei Qiu, Paulo J. P. Souza, Jiahao Yuan, Yuxuan Zhou, Libo Zhang, Ji Chu, Xianchuang Pan, Ling Hu, Jian Li, Yuan Xu, Youpeng Zhong, Song Liu, Fei Yan, Dian Tan, R. Bachelard, C. J. Villas-Boas, Alan C. Santos, and Dapeng Yu. Optimal charging of a superconducting quantum battery, August 2021.

[161] Giulia Gemme, Michele Grossi, Dario Ferraro, Sofia Vallecorsa, and Maura Sassetti. IBM quantum platforms: A quantum battery perspective. *arXiv:2204.10786 [cond-mat, physics:quant-ph]*, April 2022.

[162] Giulia Gemme, Michele Grossi, Sofia Vallecorsa, Maura Sassetti, and Dario Ferraro. Qutrit quantum battery: Comparing different charging protocols. *Physical Review Research*, 6(2):023091, April 2024.

[163] Seyed Navid Elyasi, Matteo A. C. Rossi, and Marco G. Genoni. Experimental simulation of daemonic work extraction in open quantum batteries on a digital quantum computer, October 2024.

[164] Daniel J. Tibben, Enrico Della Gaspera, Joel van Embden, Philipp Reineck, James Q. Quach, Francesco Campaioli, and Daniel E. Gómez. Extending the self-discharge time of Dicke quantum batteries using molecular triplets, March 2024.

[165] Andrea Camposeo, Tersilla Virgili, Floriana Lombardi, Giulio Cerullo, Dario Pisignano, and Marco Polini. Quantum Batteries: A Materials Science Perspective. *Advanced Materials*, n/a(n/a):2415073.

[166] I. Maillette de Buy Wenniger, S. E. Thomas, M. Maffei, S. C. Wein, M. Pont, A. Harouri, A. Lemaître, I. Sagnes, N. Somaschi, A. Auffèves, and P. Senellart. Coherence-powered work exchanges between a solid-state qubit and light fields, April 2022.

[167] Jitendra Joshi and T. S. Mahesh. Experimental investigation of a quantum battery using star-topology NMR spin systems. *Physical Review A*, 106(4):042601, October 2022.

[168] Charles H. Bennett. The thermodynamics of computation—a review. *International Journal of Theoretical Physics*, 21(12):905–940, December 1982.

[169] M. B. Plenio and V. Vitelli. The physics of forgetting: Landauer's erasure principle and information theory. *Contemporary Physics*, 42(1):25–60, January 2001.

[170] Koji Maruyama, Franco Nori, and Vlatko Vedral. Colloquium: The physics of Maxwell's demon and information. *Reviews of Modern Physics*, 81(1):1–23, January

2009.
[171] Takahiro Sagawa and Masahito Ueda. Information Thermodynamics: Maxwell's Demon in Nonequilibrium Dynamics. *Nonequilibrium Statistical Physics of Small Systems*, pages 181–211, February 2013.
[172] Kurt Jacobs. Second law of thermodynamics and quantum feedback control: Maxwell's demon with weak measurements. *Physical Review A*, 80(1):012322, July 2009.
[173] Gianluca Francica, John Goold, Francesco Plastina, and Mauro Paternostro. Daemonic ergotropy: Enhanced work extraction from quantum correlations. *npj Quantum Information*, 3(1):1–6, March 2017.
[174] Seth Lloyd. Quantum-mechanical Maxwell's demon. *Physical Review A*, 56(5):3374–3382, November 1997.
[175] Antoine Bérut, Artak Arakelyan, Artyom Petrosyan, Sergio Ciliberto, Raoul Dillenschneider, and Eric Lutz. Experimental verification of Landauer's principle linking information and thermodynamics. *Nature*, 483(7388):187–189, March 2012.
[176] L. L. Yan, T. P. Xiong, K. Rehan, F. Zhou, D. F. Liang, L. Chen, J. Q. Zhang, W. L. Yang, Z. H. Ma, and M. Feng. Single-Atom Demonstration of the Quantum Landauer Principle. *Physical Review Letters*, 120(21):210601, May 2018.
[177] John P. P. Silva, Roberto S. Sarthour, Alexandre M. Souza, Ivan S. Oliveira, John Goold, Kavan Modi, Diogo O. Soares-Pinto, and Lucas C. Céleri. Experimental demonstration of information to energy conversion in a quantum system at the Landauer Limit. *Proceedings of the Royal Society A: Mathematical, Physical and Engineering Sciences*, 472(2188):20150813, April 2016.
[178] Raffaele Salvia and Vittorio Giovannetti. Extracting work from correlated many-body quantum systems. *Physical Review A*, 105(1):012414, January 2022.
[179] Martí Perarnau-Llobet, Karen V. Hovhannisyan, Marcus Huber, Paul Skrzypczyk, Nicolas Brunner, and Antonio Acín. Extractable Work from Correlations. *Physical Review X*, 5(4):041011, October 2015.
[180] Jonathan Oppenheim, Michał Horodecki, Paweł Horodecki, and Ryszard Horodecki. Thermodynamical Approach to Quantifying Quantum Correlations. *Physical Review Letters*, 89(18):180402, October 2002.
[181] Wojciech Hubert Zurek. Quantum discord and Maxwell's demons. *Physical Review A*, 67(1):012320, January 2003.
[182] Koji Maruyama, Fumiaki Morikoshi, and Vlatko Vedral. Thermodynamical detection of entanglement by Maxwell's demons. *Physical Review A*, 71(1):012108, January 2005.
[183] Sang Wook Kim, Takahiro Sagawa, Simone De Liberato, and Masahito Ueda. Quantum Szilard Engine. *Physical Review Letters*, 106(7):070401, February 2011.
[184] Eric G. Brown, Nicolai Friis, and Marcus Huber. Passivity and practical work extraction using Gaussian operations. *New Journal of Physics*, 18(11):113028, November 2016.
[185] Mario A. Ciampini, Luca Mancino, Adeline Orieux, Caterina Vigliar, Paolo Mataloni, Mauro Paternostro, and Marco Barbieri. Experimental extractable work-based multipartite separability criteria. *npj Quantum Information*, 3(1):1–6, March 2017.
[186] Matteo Brunelli, Marco G. Genoni, Marco Barbieri, and Mauro Paternostro. Detecting Gaussian entanglement via extractable work. *Physical Review A*, 96(6):062311, December 2017.

[187] Dominik Šafránek, Dario Rosa, and Felix C. Binder. Work Extraction from Unknown Quantum Sources. *Physical Review Letters*, 130(21):210401, May 2023.

[188] Harold Ollivier and Wojciech H. Zurek. Quantum Discord: A Measure of the Quantumness of Correlations. *Physical Review Letters*, 88(1):017901, December 2001.

[189] Fabian Bernards, Matthias Kleinmann, Otfried Gühne, and Mauro Paternostro. Daemonic Ergotropy: Generalised Measurements and Multipartite Settings. *Entropy*, 21(8):771, August 2019.

[190] Sebastian Deffner and Steve Campbell. *Quantum Thermodynamics*. 2053-2571. 2019.

[191] H. J. Groenewold. A problem of information gain by quantal measurements. *International Journal of Theoretical Physics*, 4(5):327–338, September 1971.

[192] Masanao Ozawa. On information gain by quantum measurements of continuous observables. *Journal of Mathematical Physics*, 27(3):759–763, March 1986.

[193] Michael Horodecki, Peter W. Shor, and Mary Beth Ruskai. Entanglement Breaking Channels. *Reviews in Mathematical Physics*, 15(06):629–641, August 2003.

[194] Raffaele Salvia, Martí Perarnau-Llobet, Géraldine Haack, Nicolas Brunner, and Stefan Nimmrichter. Quantum advantage in charging cavity and spin batteries by repeated interactions. *arXiv:2205.00026 [quant-ph]*, April 2022.

[195] Gabriel T. Landi. Battery charging in collision models with Bayesian risk strategies. *Entropy*, 23(12):1627, December 2021.

[196] Franco Mayo and Augusto J. Roncaglia. Collective effects and quantum coherence in dissipative charging of quantum batteries. *Physical Review A*, 105(6):062203, June 2022.

[197] Felipe Barra. Efficiency fluctuations in a quantum battery charged by a repeated interaction process. *Entropy*, 24(6):820, June 2022.

[198] Vahid Shaghaghi, Varinder Singh, Giuliano Benenti, and Dario Rosa. Micromasers as Quantum Batteries. *arXiv:2204.09995 [cond-mat, physics:quant-ph]*, April 2022.

[199] Vahid Shaghaghi, Varinder Singh, Matteo Carrega, Dario Rosa, and Giuliano Benenti. Lossy Micromaser Battery: Almost Pure States in the Jaynes–Cummings Regime. *Entropy*, 25(3):430, March 2023.

[200] Gianluca Francica, Felix C. Binder, Giacomo Guarnieri, Mark T. Mitchison, John Goold, and Francesco Plastina. Quantum Coherence and Ergotropy. *Physical Review Letters*, 125(18):180603, October 2020.

[201] Elsi-Mari Laine, Heinz-Peter Breuer, Jyrki Piilo, Chuan-Feng Li, and Guang-Can Guo. Nonlocal Memory Effects in the Dynamics of Open Quantum Systems. *Physical Review Letters*, 108(21):210402, May 2012.

[202] Elsi-Mari Laine, Heinz-Peter Breuer, and Jyrki Piilo. Nonlocal memory effects allow perfect teleportation with mixed states. *Scientific Reports*, 4(1):4620, April 2014.

[203] Álvaro Cuevas, Andrea Geraldi, Carlo Liorni, Luís Diego Bonavena, Antonella De Pasquale, Fabio Sciarrino, Vittorio Giovannetti, and Paolo Mataloni. All-optical implementation of collision-based evolutions of open quantum systems. *Scientific Reports*, 9(1):3205, March 2019.

[204] Guillermo García-Pérez, Matteo A. C. Rossi, and Sabrina Maniscalco. IBM Q Experience as a versatile experimental testbed for simulating open quantum systems. *npj Quantum Information*, 6(1):1–10, January 2020.

[205] Marco Cattaneo, Matteo A.C. Rossi, Guillermo García-Pérez, Roberta Zambrini, and Sabrina Maniscalco. Quantum Simulation of Dissipative Collective Effects on Noisy Quantum Computers. *PRX Quantum*, 4(1):010324, March 2023.

[206] Maria Popovic, Mark T. Mitchison, and John Goold. Thermodynamics of decoherence. *Proceedings of the Royal Society A: Mathematical, Physical and Engineering Sciences*, 479(2272):20230040, April 2023.

[207] Ruari McCloskey and Mauro Paternostro. Non-Markovianity and system-environment correlations in a microscopic collision model. *Physical Review A*, 89(5):052120, May 2014.

[208] Hüseyin T. Şenyaşa, Şahinde Kesgin, Göktuğ Karpat, and Barış Çakmak. Entropy Production in Non-Markovian Collision Models: Information Backflow vs. System-Environment Correlations. *Entropy*, 24(6):824, June 2022.

[209] J. R. Johansson, P. D. Nation, and Franco Nori. QuTiP: An open-source Python framework for the dynamics of open quantum systems. *Computer Physics Communications*, 183(8):1760–1772, August 2012.

[210] J. R. Johansson, P. D. Nation, and Franco Nori. QuTiP 2: A Python framework for the dynamics of open quantum systems. *Computer Physics Communications*, 184(4):1234–1240, April 2013.

[211] Kurt Jacobs. How to project qubits faster using quantum feedback. *Physical Review A*, 67(3):030301, March 2003.

[212] Joshua Combes and Kurt Jacobs. Rapid State Reduction of Quantum Systems Using Feedback Control. *Physical Review Letters*, 96(1):010504, January 2006.

[213] H. M. Wiseman and J. F. Ralph. Reconsidering rapid qubit purification by feedback. *New Journal of Physics*, 8(6):90, June 2006.

[214] Andrew N. Jordan and Alexander N. Korotkov. Qubit feedback and control with kicked quantum nondemolition measurements: A quantum Bayesian analysis. *Physical Review B*, 74(8):085307, August 2006.

[215] Howard M. Wiseman and Luc Bouten. Optimality of Feedback Control Strategies for Qubit Purification. *Quantum Information Processing*, 7(2):71–83, June 2008.

[216] Rusko Ruskov, Joshua Combes, Klaus Mølmer, and Howard M. Wiseman. Qubit purification speed-up for three complementary continuous measurements. *Philosophical Transactions of the Royal Society A: Mathematical, Physical and Engineering Sciences*, 370(1979):5291–5307, November 2012.

[217] Yu-Yu Zhang, Tian-Ran Yang, Libin Fu, and Xiaoguang Wang. Powerful harmonic charging in a quantum battery. *Physical Review E*, 99(5):052106, May 2019.

[218] A. Crescente, M. Carrega, M. Sassetti, and D. Ferraro. Charging and energy fluctuations of a driven quantum battery. *New Journal of Physics*, 22(6):063057, June 2020.

[219] Lajos Diósi. Non-Markovian Continuous Quantum Measurement of Retarded Observables. *Physical Review Letters*, 100(8):080401, February 2008.

[220] Howard M. Wiseman and J. M. Gambetta. Pure-State Quantum Trajectories for General Non-Markovian Systems Do Not Exist. *Physical Review Letters*, 101(14):140401, September 2008.

[221] Jyrki Piilo, Sabrina Maniscalco, Kari Härkönen, and Kalle-Antti Suominen. Non-Markovian Quantum Jumps. *Physical Review Letters*, 100(18):180402, May 2008.

[222] A. Barchielli, C. Pellegrini, and F. Petruccione. Stochastic Schrödinger equations with coloured noise. *Europhysics Letters*, 91(2):24001, August 2010.

[223] Andrea Smirne, Matteo Caiaffa, and Jyrki Piilo. Rate Operator Unraveling for Open Quantum System Dynamics. *Physical Review Letters*, 124(19):190402, May 2020.

[224] Takahiro Sagawa and Masahito Ueda. Second Law of Thermodynamics with Dis-

crete Quantum Feedback Control. *Physical Review Letters*, 100(8):080403, February 2008.

[225] Joan A. Vaccaro and Stephen M. Barnett. Information erasure without an energy cost. *Proceedings of the Royal Society A: Mathematical, Physical and Engineering Sciences*, 467(2130):1770–1778, January 2011.

[226] Nicole Yunger Halpern. Toward physical realizations of thermodynamic resource theories. In Ian T. Durham and Dean Rickles, editors, *Information and Interaction: Eddington, Wheeler, and the Limits of Knowledge*, pages 135–166. Springer International Publishing, Cham, 2017.

[227] M. Born and V. Fock. Beweis des Adiabatensatzes. *Zeitschrift für Physik*, 51(3):165–180, March 1928.

[228] Matteo Lostaglio, Álvaro M. Alhambra, and Christopher Perry. Elementary Thermal Operations. *Quantum*, 2:52, February 2018.

[229] A. T. Rezakhani, W.-J. Kuo, A. Hamma, D. A. Lidar, and P. Zanardi. Quantum Adiabatic Brachistochrone. *Physical Review Letters*, 103(8):080502, August 2009.